Supporting Information

Bicyclic Sulfonium Pincer Ligand with a Thiatriptycenium Backbone - Synthesis and Applications in π-Acid Catalysis

Mohammad Zafar,[a] Donia Shamali,[a] Nitsan Barel,[a] David Danovich[a] and Yuri Tulchinsky*

[a] Institute of Chemistry, Hebrew University of Jerusalem, Israel

*Corresponding author: yuri.tulchinsky@mail.huji.ac.il

Table of Contents

Experimental Procedures

1. Synthetic procedures and characterization

1.1. General information

All air sensitive reactions were carried out under an atmosphere of purified nitrogen in a glovebox equipped with an inert gas purifier. Toluene, acetonitrile (MeCN), diethyl ether (Et_2O), dichloromethane (DCM) and methanol (MeOH), were purified by passing through a column of activated alumina under inert atmosphere. Anhydrous hexane, dimethoxyethane (DME), 1,2-dichloroethane (DCE) and pentane packed under inert gas over molecular sieves were used as purchased. 2,7-di-tert-butyl-4,5-bis(diphenylphosphoryl)-9H-thioxanthen-9-one (compound **1**),[1] 2-ethynyl-1,1'-binaphthalene,[2] 2-ethynyl-1-(2,3,4-trimethoxyphenyl)naphthalene,[3] $[Pt(CH_3CN)_4](OTf)_2$,[4] $[Pt(CH_3CN)_4](BF_4)_2$,[4] $[Pt(CH_3CN)_4](PF_6)_2$,[5] 2-(2-ethynylnaphthalen-1-yl)thiophene,[6] 2-ethynyl-1-(4-fluorophenyl)naphthalene,[2] dimethyl 2-(but-3-en-1-yl)-2-(prop-2-yn-1-yl)malonate,[7] 4-methyl-N-(3-methylbut-2-en-1-yl)-N-(prop-2-yn-1-yl)benzenesulfonamide, 4-methyl-N-(2-methylallyl)-N-(prop-2-yn-1-yl)benzenesulfonamide[8] were prepared according to literatures procedures. $Pt(COD)Cl_2$, 2-(trimethylsilyl)phenyl trifluoromethanesulfonate, tetrabutylammonium fluoride solution (1.0 M in THF), potassium hydride (KH), methyl triflate, phenyl silane and triflic acid (TfOH) were purchased from STREM. Chemicals and used without purification. All chromatographic purifications were performed with prepacked SiO_2 columns on CombiFlash EZ-Prep instrument. High resolution mass spectra (HRMS) were recorded on HR Q-TOF-MS mass instrument, using an electrospray ionization (ESI+) technique (MeCN/H_2O 80%, flow: 0.2 ml/min). NMR spectra were measured using Bruker 500 MHz Avance II and Neo spectrometers. Residual solvent peaks were used as internal standards for ^1H and ^{13}C respectively ($CDCl_3$: δ 7.26/77.0 ppm; CD_2Cl_2: δ 5.31/53.8 ppm, and CD_3CN: δ 1.94/0.3 ppm and $C_2D_4Cl_2$: δ 3.74 / 43.2 ppm. Other nuclei were referenced to the ^1H reference frequency multiplied by the standard ratios:[7] ^{11}B 0.32083974, ^{13}C 0.25145020, ^{19}F 0.94094011, ^{31}P 0.40480742, and ^{195}Pt 0.21496784. NMR data are reported as follows: chemical shift, multiplicity (s = singlet, d = doublet, t = triplet, q = quartet, m = multiplet, br = broad, v = virtual), coupling constant(s), and integration. FT-IR spectra were measure using Bruker AlPHA II compact spectrometer. The NMR spectra were measured at 25 °C, unless stated otherwise. All reactions involving the preparation of sulfonium complexes were performed in degassed dry solvents under the atmosphere of purified nitrogen inside glovebox.

1.2. Synthesis of the thiatriptycenium-based ligands

2,7-di-tert-butyl-4,5-bis(diphenylphosphoryl)-9-hydroxy-9H-9,10-[1,2]benzenothioxanthen-10-ium trifluoromethane-sulfonate [2](OTf)

Under an inert atmosphere 2,7-di-*tert*-butyl-4,5-bis(diphenylphosphoryl)-9H-thioxanthen-9-one (compound **1**) (0.3 g, 0.414 mmol) and TBAF (0.35 mL, 1.24 mmol) were added in 6 mL of acetonitrile and the reaction mixture was stirred for 15 min at room temperature. A solution of 2-(trimethylsilyl)phenyl trifluoromethane sulfonate (0.3 g, 1.24 mmol) in 2 mL acetonitrile was slowly added to the reaction mixture over 1h and stirred for 2 days at room temperature. Then, the reaction mixture was diluted with 150 mL of ethyl acetate and the organic layer was washed 5 times with 2M aqueous HCl (30 mL each time). The organic layer was then separated and the extracted with ethyl acetate five times. The combined organic layers were washed with water, 10% $NaHCO_3$, and water, then dried over Na_2SO_4. After evaporation of the solvents, the crude products were washed three times with Et_2O (5 mL of each time), affording 0.295 g of a pure **[2]**OTf, as a white powder (295 mg, 77%).

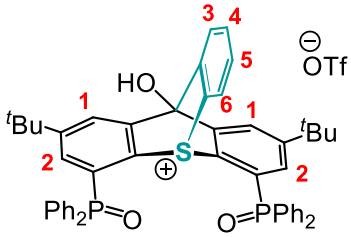

^1H NMR (400 MHz, $CDCl_3$): δ 8.57 (s, 2H, $_{Thiatrip}$-H1), 8.36 (d, $^4J_{HH}$ = 6.6 Hz, 1H $_{Thiatrip}$-H3), 7.73 – 7.69 (m, 4H$_{Ph}$), 7.63 – 7.59 (m, 5H$_{Ph}$), 7.57 – 7.52 (m, 7H$_{Ph}$), 7.50 – 7.46 (m, 4H$_{Ph}$, 1H $_{Thiatrip}$-H4), 7.15 (t, *J* = 14.7 Hz,1H $_{Thiatrip}$-H5), 7.04 (d, *J* = 13.1 Hz, 2H, $_{Thiatrip}$-H2), 6.89 (d, *J* = 6.8 Hz, 1H $_{Thiatrip}$-H6), 1.18 (s, 18H $^t{}_{Bu}$)

$^{13}C\{^1H\}$ NMR (101 MHz, $CDCl_3$): δ 157.6 (d, *J* = 9.6 Hz, Ar<u>C</u>-^{t}Bu), 148.9 (d, J_{PC} = 8.2 Hz, Ar<u>C</u>$_{Thiatrip}$), 146.6 (d, J_{PC} = 2.2 Hz, Ar<u>C</u>$_{Thiatrip}$), 133.5 (s, Ph), 132.2-132.0 (m, Ph), 129.7 (d, *J* = 12.0 Hz, Ar<u>C</u>$_{Thiatrip}$), 129.5 (d, J_{PC} = 12.1 Hz, Ph), 129.2 (J_{PC} = 12.5 Hz, Ph), 81.0 (s, <u>C</u>-OH), 35.8(s, <u>C</u>$(CH_3)_3$), 30.7(s, C(<u>C</u>$H_3)_3$);

$^{19}F\{^1H\}$ NMR (376 MHz, $CDCl_3$): δ -78.3 (s, OTf)

$^{31}P\{^1H\}$ NMR (162 MHz, $CDCl_3$): δ 29.6 ppm.

FTIR: v = 1118 cm^{-1} (P=O) cm^{-1}.

MS (ESI$^+$): *m/z* calculated for $[C_{51}H_{47}O_3P_2S]^+$: 801.2710, found 801.2715.

2,7-di-tert-butyl-4,5-bis(diphenylphosphoryl)-9-methoxy-9H-9,10-[1,2]benzenothioxanthen-10-ium trifluoromethanesulfonate [3](OTf)

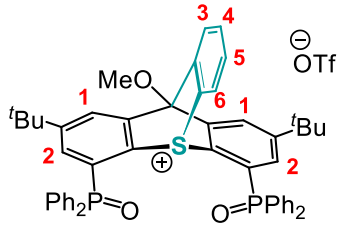

Inside glovebox, a 25 mL Schlenk tube was loaded with compound **[2]**OTf (0.3 g, 0.32 mmol) and KH (0.045 g, 1.12 mmol) in 4 mL of 1,2-dimethoxyethane (DME) and the reaction mixture was stirred overnight at room temperature. A solution of methyl triflate (MeOTf) (0.1 mL, 0.98 mmol) in 1 mL of DME was added slowly to the reaction mixture and stirred for 1h at room temperature. The reaction mixture was then quenched with 15 mL of aqueous NH_4Cl at 0°C. The organic material was extracted three times with ethyl acetate (3 × 20mL). The organic phase was washed with saturated $NaHCO_3$ and dried with Na_2SO_4. The organic phase was evaporated, affording the crude product as an orange solid. This was then purified by an automatic flash chromatography on silica-gel eluting with a DCM/MeOH (3%) mixture to afford the pure product, as a light yellow (192 mg, 63% yield).

^{1}H NMR (400 MHz, $CDCl_3$): δ 8.22 (d, $^4J_{HH}$ = 1.2 Hz, 2H $_{Thiatrip}$-H1), 8.12 (d, $^2J_{HH}$ = 8.4 Hz, 1H $_{Thiatrip}$-H3), 7.80 – 7.73 (m, 4H$_{Ph}$), 7.68 (d, $^3J_{HP}$ = 1.7 Hz, 3H$_{Ph}$), 7.61 – 7.56 (m, 5H$_{Ph}$), 7.51 – 7.45 (m, 7H$_{Ph}$, 1H $_{Thiatrip}$-H6), 7.37 – 7.32 (m, 1H1H $_{Thiatrip}$-H4), 7.19 (d, $^3J_{HH}$ = 1.1 Hz, 1H1H $_{Thiatrip}$-H5), 7.03 (dd, $^4J_{HH}$ = 13.1, 2.0 Hz, 2H1H $_{Thiatrip}$-H2), 4.45 (s, 3H$_{OMe}$), 1.17 (s, 18H ^{t}$_{Bu}$)

^{13}C{^{1}H} NMR (101 MHz, $CDCl_3$): δ 156.8 (d, *J* = 9.6 Hz, Ar<u>C</u>-^{t}Bu), 148.9 (d, J_{PC} = 8.2 Hz, Ar<u>C</u>$_{Thiatrip}$), 146.6 (d, J_{PC} = 2.2 Hz, Ar<u>C</u>$_{Thiatrip}$), 133.1-133.0 (m, Ph) 132.1 (dd, J_{PC} = 16.4, 10.2 Hz, Ph), 131.0 (s, Ar<u>C</u>$_{Thiatrip}$), 129.8 (d, *J* = 8.0 Hz, Ph), 129.5 – 128.6 (m, Ph), 127.8 (m, Ar<u>C</u>$_{Thiatrip}$), 83.7 (s, <u>C</u>-OMe), 59.2 (OMe), 35.8 (s, <u>C</u>$(CH_3)_3$), 30.8(s, C(<u>C</u>$H_3)_3$).

^{19}F{^{1}H} NMR (376 MHz, $CDCl_3$): δ −78.1 (s, OTf) ppm

^{31}P{^{1}H} NMR (162 MHz, $CDCl_3$): δ 28.1 ppm.

FTIR: v = 1117 (P=O) cm^{-1}.

MS (ESI$^+$): *m/z* calculated for $[C_{52}H_{49}O_3P_2S]^+$: 815.2873, found 819.2879.

2,7-di-tert-butyl-4,5-bis(diphenylphosphanyl)-9-methoxy-9H-9,10-[1,2]benzenothioxanthen-10-ium trifluoromethanesulfonate [4](OTf).

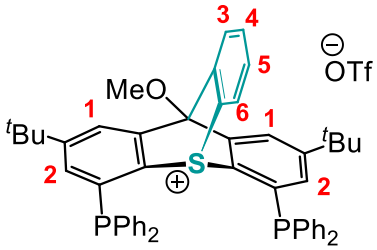

Inside glovebox, compound **[3]**(OTf) (0.3 g, 0.321 mmol) was loaded into an oven-dried Schlenk tube and suspended in 12 ml of a 1:2 DCE/Toluene mixture. Then 8.5 µL (0.3 eq.) of triflic acid were added and the reaction mixture was stirred for 10 minutes. Next, 0.55 mL (16 eq.) of $PhSiH_3$ were added, the tube was sealed and placed in a preheated oil bath at 90°C. During the reaction, the suspension turned into a clear orange solution. The reaction progress was monitored by ^{31}P NMR which showed a complete conversion after 12 h. After cooling down to room temperature, the solvent was evaporated, affording the crude product as an orange solid. This was then purified by passing through a short silica plug, as follows. The crude product was dissolved in a minimum amount of DCM and applied on a silica-gel plug that was first quickly washed with hexane and DCM, followed by eluting the yellow-colored product with a 3% MeOH/DCM mixture. The collected fractions were evaporated, affording the product, as a light brown solid (260 mg, 88% yield). Crystals of **[3]**(OTf) suitable for XRD were grown by a slow diffusion of hexane into its toluene solution.

^{1}H NMR (400 MHz, CD_2Cl_2): δ 8.02 (dd, $^2J_{HH}$ = 1.1 Hz, 7.9 Hz, 1H $_{Thiatrip}$-H3), 7.99 (d, $^4J_{HH}$ = 1.9 Hz, 1H $_{Thiatrip}$-H1), 7.58 (dt, $^2J_{HH}$ = 1.17 Hz, 15.41 1H $_{Thiatrip}$-H4), 7.53-7.48 (m, 9H$_{Ph}$), 7.53-7.48 (m, 9H$_{Ph}$), 7.47-7.34 (m, 8H$_{Ph}$), 7.32 – 7.27 (m, 4H$_{Ph}$), 7.09 (t, *J* = 7.7 Hz, $_{Thiatrip}$-H5), 6.76 (dd, *J* = 3.6, 1.9 Hz, $_{Thiatrip}$-H2), 6.05 (dd, $^2J_{HH}$ = 1.2 Hz, 7.9 Hz, 1H $_{Thiatrip}$-H6), 4.39 (s, 3H$_{OMe}$), 1.15 (s, 18H ^{t}$_{Bu}$)

^{13}C{^{1}H} NMR (101 MHz, CD_2Cl_2): δ 157.2 (s, Ar<u>C</u>-^{t}Bu), 145.9 (s, Ar<u>C</u>$_{Thiatrip}$), 144.7 (s, Ar<u>C</u>$_{Thiatrip}$), 141.83 (d, $J_{C\text{-}P}$ = 21.1 Hz, Ar<u>C</u>$_{Thiatrip}$), 135.4 – 134.4 (m, Ph), 133.4 (m, Ar<u>C</u>$_{Thiatrip}$), 132.3 (s, Ar<u>C</u>$_{Thiatrip}$), 131.03 (d, $J_{C\text{-}P}$ = 9.4 Hz, Ph), 130.1 (t, $J_{C\text{-}P}$ = 8.2 Hz, Ph), 129.9 (t, $J_{C\text{-}P}$ = 8.1 Hz, Ph), 128.7 (s, Ar<u>C</u>$_{Thiatrip}$), 128.6 (s, Ar<u>C</u>$_{Thiatrip}$), 127.9 (s, Ar<u>C</u>$_{Thiatrip}$), 124.0 128.7 (s, Ar<u>C</u>$_{Thiatrip}$), 88.4 (s, <u>C</u>-OMe), 58.9 (s, O<u>C</u>H3), 36.0 (s, <u>C</u>$(CH_3)_3$), 30.8 (s, C(<u>C</u>$H_3)_3$)

^{19}F{^{1}H} NMR (376 MHz, CD_2Cl_2): δ −78.1 (s, OTf) ppm

^{31}P{^{1}H} NMR (162 MHz, CD_2Cl_2): δ −7.2 (s) ppm.

MS (ESI$^+$): *m/z* calculated for $[C_{52}H_{49}OP_2S]^+$: 783.2974, found 783.2984.

2,7-di-tert-butyl-4,5-bis(diphenylphosphanyl)-10-(2-fluorophenyl)-9-oxo-9,10-dihydrothioxanthylium tetrafluoroborate [4](BF$_4$) and hexafluorophosphate [4](PF$_6$)

These compounds were prepared by a double anion exchange, as follows:

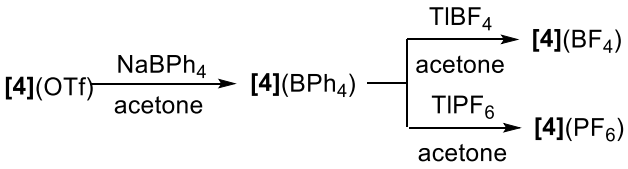

Compound **[4]**(OTf) (100 mg, 0.12 mmol) was dissolved in 3 mL of dry acetone. Separately, $NaBPh_4$ (52 mg, 1.2 eq.) was dissolved in additional 2 mL of dry acetone and added to the solution of **[4]**(OTf). The reaction mixture was stirred at room temperature for 15 min. Then the solvent was removed under vacuum, the residue was extracted into DCM and filtered through the Celite. The solvent was removed under vacuum yielding **[4]**(BPh_4) as a yellow solid (109 mg, 92%). Next, **[4]**(BPh_4) (100mg, 0.9 mmol) was dissolved in 2 mL of dry acetone. Separately $TlBF_4$ (26.3 mg 1 eq.) was dissolved in additional 2 mL of dry acetone and added to the solution of **[4]**(BPh_4). Immediately, a white precipitate ($TlBPh_4$) formed and was filtered out. The filtrate was then evaporated, and the residue dissolved in $CHCl_3$, and filtered through the celite, affording **[4]**(BF_4) as yellowish solid (72 mg, 92%). In cases, when the obtained **[4]**(BF_4) was not pure by NMR, it was additionally purified by passing it through a short silica plug as follows. Inside glovebox, the crude product was dissolved in a minimum amount of dry DCM and applied on a silica-gel plug that was first quickly washed with dry DCM, followed by eluting the product with a 3% MeOH/DCM mixture. Using $TlPF_6$ instead of $TlBF_4$ in an analogous manner afforded compound **[4]**(PF_6) in (74 mg, 88%) yield.

^{1}H NMR (400 MHz, CD_2Cl_2): δ 8.06 (d, $^3J_{HH}$ = 7.2 Hz, 1H $_{Thiatrip}$-H3), 7.99 (d, $^4J_{HH}$ = 1.9 Hz, 2H $_{Thiatrip}$-H1), 7.63 (t, $^3J_{HH}$ = 14.2 Hz, 1H $_{Thiatrip}$-H4), 7.53-7.44 (m, 8H$_{Ph}$), 7.39-7.35 (m, 8H$_{Ph}$), 7.31-7.28 (m, 4H$_{Ph}$), 7.10 (t, $^3J_{HH}$ = 15.5 Hz, 1H $_{Thiatrip}$-H5), 6.75 (dd, J_{HH} = 8.8 Hz, 1.9Hz, 2H $_{Thiatrip}$-H2), 6.04 (d, $^3J_{HH}$ = 7.6 Hz, 1H $_{Thiatrip}$-H6), 4.39 (s, 3H$_{OMe}$), 1.14 (s, 18H ^{t}$_{Bu}$).

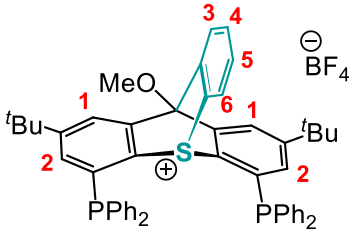

^{13}C{^{1}H} NMR (126 MHz, CD_2Cl_2): δ 156.8(s, Ar$\underline{C}$-^{t}Bu), 145.5 (s, Ar$\underline{C}_{Thiatrip}$), 144.1(s, Ar$\underline{C}_{Thiatrip}$) 135.2 (s, Ph), 134.4 (s, Ph), 133.2 (s, Ar$\underline{C}_{Thiatrip}$), 130.59 (d, J_{PC} = 11.5 Hz, Ph), 129.7 (s, Ar$\underline{C}_{Thiatrip}$) 129.6 (t, J_{PC} = 8.3 Hz, Ph), 129.3 (t, J_{PC} = 8.2 Hz, Ph), 128.3 (s, (s, Ar$\underline{C}_{Thiatrip}$) 128.2 (s, Ar$\underline{C}_{Thiatrip}$), 127.5 (s, Ar$\underline{C}_{Thiatrip}$), 126.8 (s, Ar$\underline{C}_{Thiatrip}$), 123.6 (s, Ar$\underline{C}_{Thiatrip}$), 88.0 (s, $\underline{C}$-OMe), 58.7 (s, O$\underline{C}$H$_3$), 35.6 (s, $\underline{C}$(CH$_3$)$_3$), 30.4(s, C($\underline{C}$H$_3$)$_3$).

^{19}F{^{1}H} NMR (376 MHz, CD_2Cl_2): δ -153.9 ($^{10}BF_4$), -154.0 ($^{11}BF_4$) ppm.

^{31}P{^{1}H} NMR (162 MHz, CD_2Cl_2): δ -7.1 ppm.

HRMS (ESI$^+$): *m/z* calculated for $[C_{52}H_{49}OP_2S]^+$: 783.2774, found 787.2984.

^{1}H NMR (400 MHz, $CDCl_3$): δ 8.03 (d, $^3J_{HH}$ = 7.2 Hz, 1H $_{Thiatrip}$-H3), 7.96 (d, $^4J_{HH}$ = 1.9 Hz, 2H $_{Thiatrip}$-H1), 7.61 (t, $^3J_{HH}$ = 14.2 Hz, 1H $_{Thiatrip}$-H4), 7.54-7.44 (m, 8H$_{Ph}$), 7.39-7.35 (m, 8H$_{Ph}$), 7.31-7.28 (m, 4H$_{Ph}$), 7.10 (t, $^3J_{HH}$ = 15.5 Hz, 1H $_{Thiatrip}$-H5), 6.70 (dd, J_{HH} = 8.8 Hz, 1.9Hz, 2H $_{Thiatrip}$-H2), 5.92 (d, $^3J_{HH}$ = 7.6 Hz, 1H $_{Thiatrip}$-H6), 4.38 (s, 3H$_{OMe}$), 1.14 (s, 18H ^{t}$_{Bu}$).

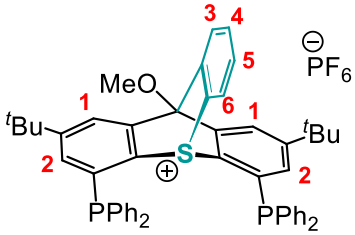

^{13}C{^{1}H} NMR (126 MHz, CD_2Cl_2, 25 °C): δ 156.8(s, Ar$\underline{C}$-^{t}Bu), 145.5 (s, Ar$\underline{C}_{Thiatrip}$), 134.8 (s, Ph), 134.9-134.7 (m, Ph), 133.2 (s, Ar$\underline{C}_{Thiatrip}$), 130.6 (d, J_{PC} = 11.5 Hz, Ph), 129.7 (s, Ar$\underline{C}_{Thiatrip}$) 129.6 (t, J_{PC} = 8.3 Hz, Ph), 129.3 (t, J_{PC} = 8.2 Hz, Ph), 128.4 (s, (s, Ar$\underline{C}_{Thiatrip}$) 128.2 (s, Ar$\underline{C}_{Thiatrip}$), 127.6 (s, Ar$\underline{C}_{Thiatrip}$), 126.8 (s, Ar$\underline{C}_{Thiatrip}$), 123.7 (s, Ar$\underline{C}_{Thiatrip}$), 88.0 (s, $\underline{C}$-OMe), 58.7 (s, O$\underline{C}$H$_3$), 35.6 (s, $\underline{C}$(CH$_3$)$_3$), 30.5 (s, C($\underline{C}$H$_3$)$_3$).

^{19}F{^{1}H} NMR (376 MHz, $CDCl_3$): δ -73.3, (d,$^1J_{P-F}$ = 707 Hz) ppm.

^{31}P{^{1}H} NMR (162 MHz, $CDCl_3$): δ –6.8, –144.3 (septet,$^1J_{P-F}$ = 707 Hz).

HRMS (ESI$^+$): *m/z* calculated for $[C_{52}H_{49}OP_2S]^+$: 783.2774, found 787.2984.

1.3. Synthesis of the Pt(II) complexes

Tris-cationic thiatripticenium Pt-acetonitrile complexes [6](OTf)$_3$.

Inside glovebox, ligand **[4]**(OTf) (0.045g, 0.05 mmol) was dissolved in dry MeCN (2 mL) and added slowly to a solution of $Pt(CH_3CN)_4(OTf)_2$ (0.027g, 0.05 mmol) in MeCN (2 mL). The resulting mixture was stirred for 30 min at room temperature. The solvent was then removed under vacuum and the residue was washed several times with diethyl ether. The volatiles were again removed under vacuum yielding **[5]**(OTf)$_3$, as a white solid (52 mg, 93% yield). Under similar reaction condition, the analogues *tris*-cationic Pt complexes with BF_4 or PF_6, as a counter anions, were prepared by reacting ligands **[4]**(X) with $Pt(CH_3CN)_4(X)_2$ (X = BF_4 or PF_6, (51 mg) 89% and (53 mg) 94%, respectively).

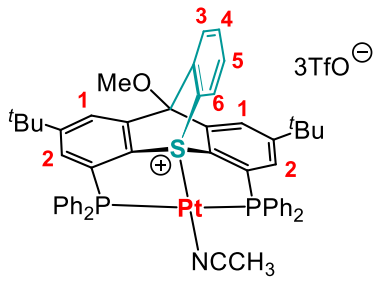

^{1}H NMR (400 MHz, CD_3CN): δ 8.41 (dd, ^2J = 1.2 Hz, 8.1 Hz, 1H $_{Thiatrip}$H3), 8.38 (d, ^4J = 1.9 Hz, 2H $_{Thiatrip}$H1), 8.09 (dd, J = 7.8, 1.1, 7.1 Hz, 1H $_{Thiatrip}$H6), 8.02 (td, J = 7.7, 1.2 Hz, 1H $_{Thiatrip}$H4), 7.95 – 7.91 (m, 4H$_{Ph}$), 7.81 (d, J = 1.3 Hz, 4H$_{Ph}$), 7.75-7.68 (m, 3H$_{Ph,}$ 1H $_{Thiatrip}$H5), 7.60 (d, J = 1.8 Hz, 5H$_{Ph}$), 7.41– 7.37 (m, 4H$_{Ph}$), 7.12 – 7.08 (m, 2H $_{Thiatrip}$H2), 4.54 (s, 3H$_{OMe}$), 1.15 (s, 18H ^{t}$_{Bu}$)

^{13}C{^{1}H} NMR (126 MHz, CD_3CN): δ = ^{13}C{^{1}H} NMR (126 MHz, CD_3CN, 25 °C): δ = 158.7 (s, Ar<u>C</u>-^{t}Bu), 148.9 (s, Ar<u>C</u>$_{Thiatrip}$), 145.4 (s, Ar<u>C</u>$_{Thiatrip}$),137.3 (t, J_{P-C} = 16.9 Hz, Ph), 136.1 (s, Ar<u>C</u>$_{Thiatrip}$),135.8 (s, Ar<u>C</u>$_{Thiatrip}$), 134.8 (s, Ar<u>C</u>$_{Thiatrip}$), 134.5 (s, Ar<u>C</u>$_{Thiatrip}$), 133.3 (t, J_{P-C} = 12.5 Hz, Ph). 131.6-131.4 (m, Ph), 131.3 (t, J_{P-C} = 12.1 Hz, Ph), 130.7 (s, Ar<u>C</u>$_{Thiatrip}$), 130.5 (s, Ph), 129.5 (s, Ar<u>C</u>$_{Thiatrip}$),128.8-127.6 (m, Ar<u>C</u>$_{Thiatrip}$),125.2 (s, Ar<u>C</u>$_{Thiatrip}$), 122.94 (s, Ar<u>C</u>$_{Thiatrip}$),124.5 (s, SO_3-<u>C</u>F_3), 89.2 (s, <u>C</u>-OMe), 59.8 (s, O<u>C</u>H_3), 36.7 (s, <u>C</u>$(CH_3)_3$), 30.8 (s, C(<u>C</u>$H_3)_3$).

^{19}F{^{1}H} NMR (376 MHz, CD_3CN): δ -78.0 (OTf) ppm

^{31}P{^{1}H} NMR (202 MHz, CD_3CN): δ 18.1 (s, Pt satellites, J_{Pt-P} = 2198.0 Hz) ppm

HRMS (ESI$^+$): *m/z* calculated for $[C_{52}H_{49}OP_2PtS]^{2+}$ and $[C_{52}H_{49}OP_2PtS]^+$ ([M - MeCN]$^{2+}$ and ([M – MeCN]$^+$, respectively): 489.1311 and 978.2627, found 489.0568 and 978.2630 (presumably, single and double electron reduction, concomitant with a loss of a weakly bound MeCN ligand, occurs upon the ionization of this *tris*-cationic complex).

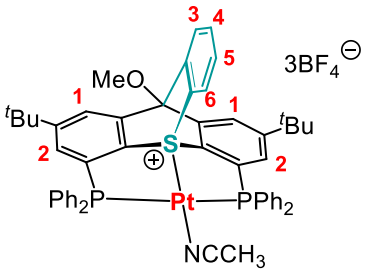

^{1}H NMR (400 MHz, CD_3CN): δ 8.41 (d, J = 8.1 Hz, 1H $_{Thiatrip}$H3), 8.38 (d, J = 1.9 Hz, 2H $_{Thiatrip}$H1), 8.09 (dd, J = 7.8, 1.1, Hz, 1H $_{Thiatrip}$H6), 8.00 (td, J = 7.7, 1.2 Hz, 1H $_{Thiatrip}$H4), 7.95 – 7.91 (m, 4H$_{Ph}$), 7.81 (d, J = 1.3 Hz, 4H$_{Ph}$), 7.72 (s, 4H$_{Ph}$), 7.60 (d, J = 1.8 Hz, 5H$_{Ph}$), 7.40 – 7.37 (m, 4H$_{Ph}$), 7.12 – 7.08 (m, 2H $_{Thiatrip}$H1), 4.54 (s, 3H$_{OMe}$), 1.15 (s, 18H ^{t}$_{Bu}$)

^{13}C{^{1}H} NMR (126 MHz, CD_3CN): δ = ^{13}C{^{1}H} NMR (126 MHz, CD_3CN, 25 °C): δ = 158.8 (s, Ar<u>C</u>-^{t}Bu), 148.9 (s, Ar<u>C</u>$_{Thiatrip}$), 145.4 (s, Ar<u>C</u>$_{Thiatrip}$),137.3 (t, J_{P-C} = 16.9 Hz, Ph), 135.9 (s, Ar<u>C</u>$_{Thiatrip}$),134.9 (s, Ar<u>C</u>$_{Thiatrip}$), 133.4 (s, Ar<u>C</u>$_{Thiatrip}$), 131.5 (t, J_{P-C} = 12.5 Hz, Ph). 131.3 (t, J_{P-C} = 13.1 Hz, Ph), 130.8 (s, Ar<u>C</u>$_{Thiatrip}$), 130.5 (t, J_{P-C} = 11.6 Hz, Ph), 129.6 (m, Ar<u>C</u>$_{Thiatrip}$), 128.2 (s, Ar<u>C</u>$_{Thiatrip}$), 125.3 (s, Ar<u>C</u>$_{Thiatrip}$), 89.2 (s, <u>C</u>-OMe), 59.8 (s, O<u>C</u>H_3), 36.7 (s, <u>C</u>$(CH_3)_3$), 30.4 (s, C(<u>C</u>$H_3)_3$).

^{19}F{^{1}H} NMR (376 MHz, CD_3CN): δ –151.46 ($^{10}BF_4$), –151.51 ($^{11}BF_4$) ppm

^{31}P{^{1}H} NMR (202 MHz, CD_3CN): δ 18.6 (s, Pt satellites, J_{Pt-P} = 2198.0 Hz) ppm

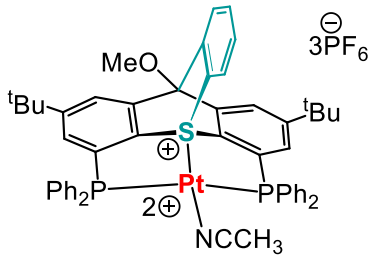

^{1}H NMR (400 MHz, CD_3CN): δ 8.41 (d, J = 7.58 Hz, 1H $_{Thiatrip}$H3), 8.38 (d, J = 1.9 Hz, 2H$_{Thiatrip}$H3), 8.09 (dd, J = 7.81, 0.82 Hz, 1H $_{Thiatrip}$H6), 8.00 (td, J = 15.53, 1.18 Hz, 1H $_{Thiatrip}$H4), 7.93 – 7.89 (m, 4H$_{Ar}$), 7.83 – 7.79 (m, 4H$_{Ar}$), 7.74 (m, 4H$_{Ar}$), 7.70 (s, 4H$_{Ar}$), 7.59 (m, 5H$_{Ar}$), 7.40 – 7.37 (m, 4H$_{Ar}$), 7.12 – 7.08 (m, 2H $_{Thiatrip}$H1), 4.55 (s, 3H$_{OMe}$), 1.15 (s, 18H ^{t}$_{Bu}$)

^{13}C{^{1}H} NMR (126 MHz, CD_3CN): δ = ^{13}C{^{1}H} NMR (126 MHz, CD_3CN, 25 °C): δ = 158.0 (s, Ar<u>C</u>-^{t}Bu), 148.1 (s, Ar<u>C</u>$_{Thiatrip}$), 144.5 (s, Ar<u>C</u>$_{Thiatrip}$),136.4 (t, J_{P-C} = 16.9 Hz, Ph), 135.3 (s, Ar<u>C</u>$_{Thiatrip}$),135.1 (s, Ar<u>C</u>$_{Thiatrip}$), 134.1 (s, Ar<u>C</u>$_{Thiatrip}$), 133.0 (s, Ar<u>C</u>$_{Thiatrip}$), 132.6 (t, J_{P-C} = 12.5 Hz, Ph). 130.7 (t, J_{P-C} = 13.1 Hz, Ph), 130.6 (s, Ar<u>C</u>$_{Thiatrip}$), 130.4 (t, J_{P-C} = 11.6 Hz, Ph), 129.7 (m, Ar<u>C</u>$_{Thiatrip}$),128.8 (s, Ar<u>C</u>$_{Thiatrip}$),128.3 (s, Ar<u>C</u>$_{Thiatrip}$), 127.4 (s, Ar<u>C</u>$_{Thiatrip}$),, 126.9 (s, Ar<u>C</u>$_{Thiatrip}$), 88.4 (s, <u>C</u>-OMe), 59.0 (s, O<u>C</u>H_3), 35.9 (s, <u>C</u>$(CH_3)_3$), 29.7 (s, C(<u>C</u>$H_3)_3$).

^{19}F{^{1}H} NMR (376 MHz, CD_3CN): –73.4 (d, $^1J_{P-F}$ = 707 Hz) ppm.

^{31}P{^{1}H} NMR (202 MHz, CD_3CN): δ 18.4 (s, Pt satellites, J_{Pt-P} = 2198.0 Hz), 144.6 (septet, $^1J_{P-F}$ = 707 Hz).

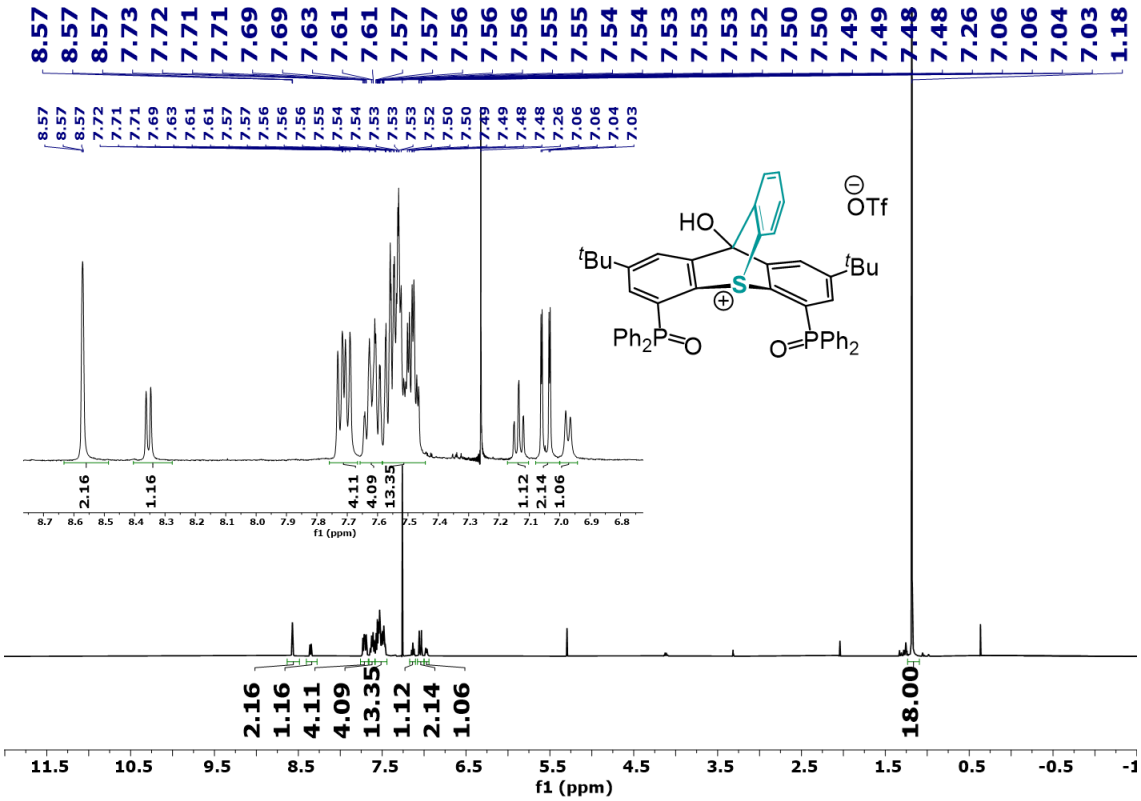

Figure S1. ^{1}H NMR spectrum of **2**(OTf) in $CDCl_3$ (400 MHz).

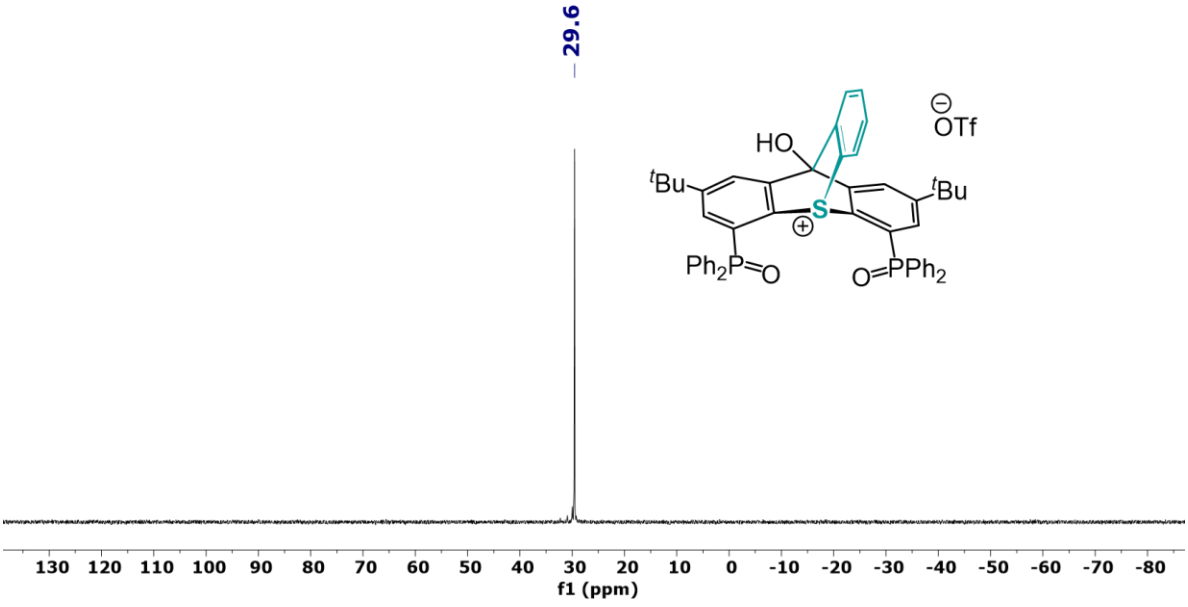

Figure S2. ^{31}P NMR spectrum of **[2]**(OTf) in $CDCl_3$ (162 MHz).

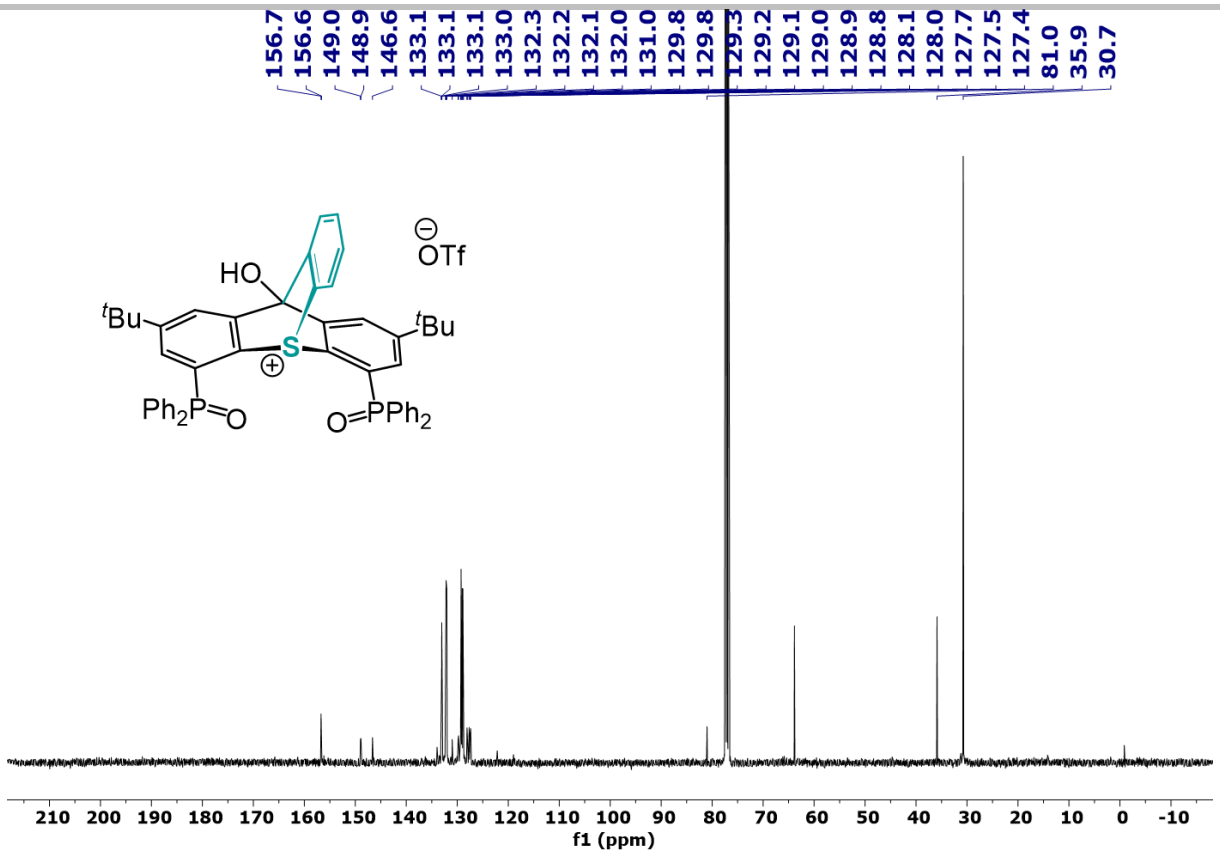

Figure S3. $^{13}C\{^{1}H\}$ NMR spectrum of **[2]**(OTf) in $CDCl_3$ (101 MHz).

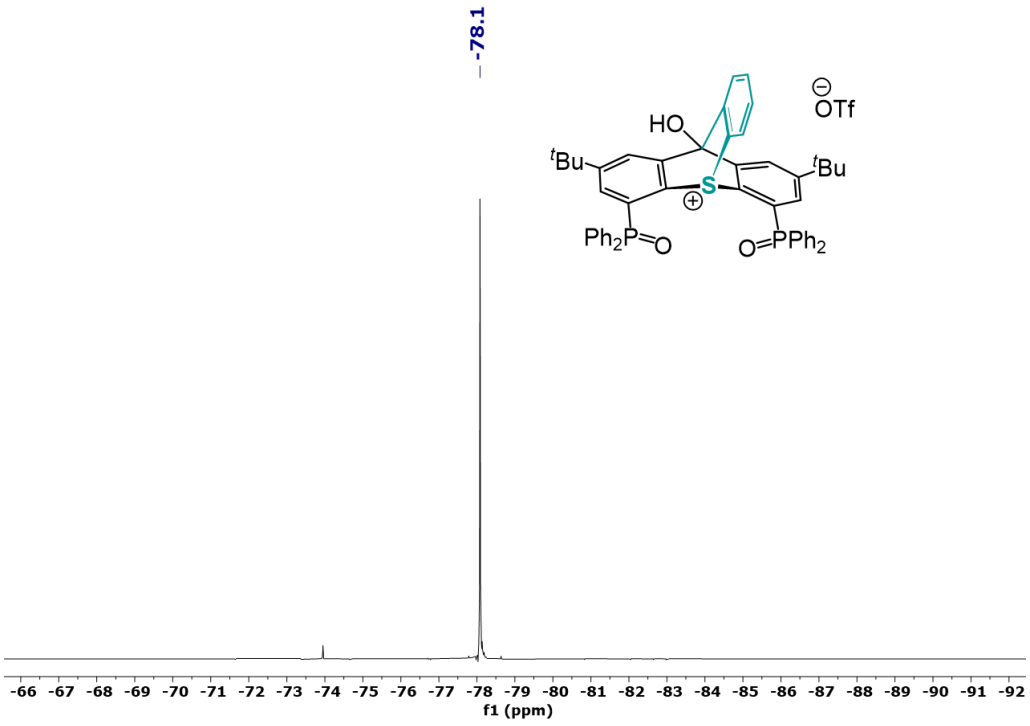

Figure S4. $^{19}F\{^{1}H\}$ NMR spectrum of **[2]**(OTf) in $CDCl_3$ (376 MHz).

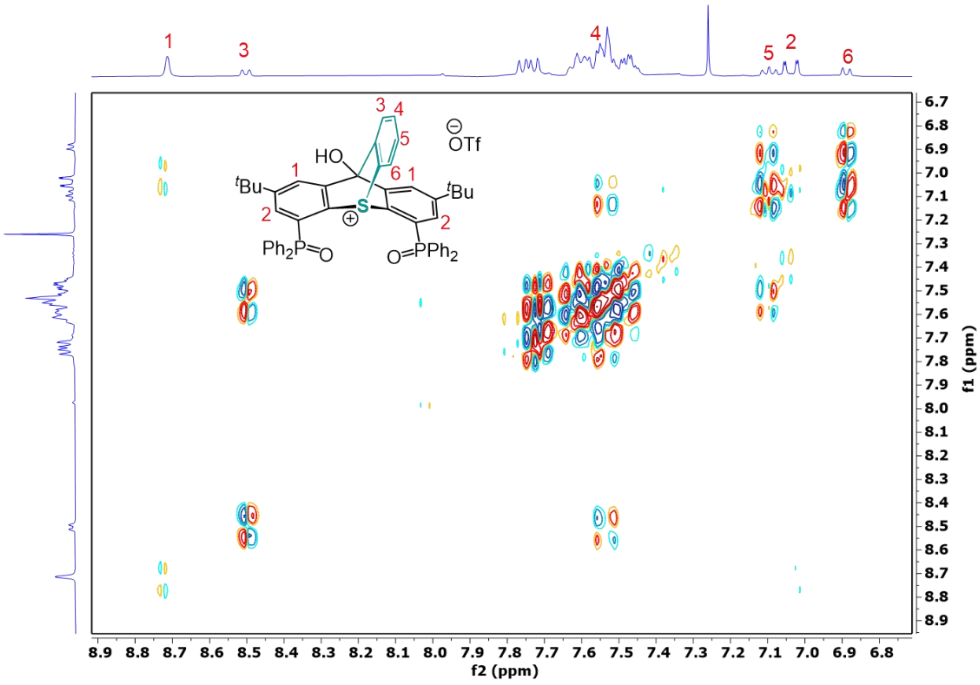

Figure S5. $^{1}H–^{1}H$ COSY NMR (400 MHz) of **[2]**(OTf) in $CDCl_3$.

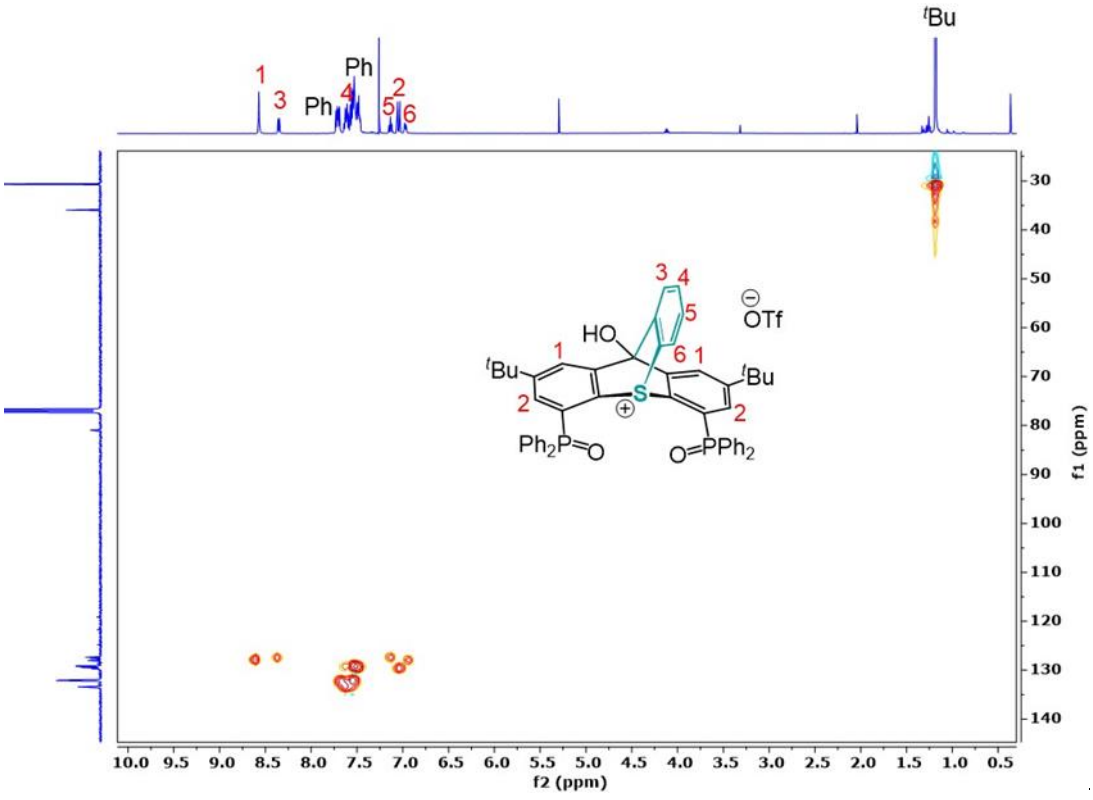

Figure S6. $^{1}H–^{13}C$ HSQC NMR (400 MHz) of **[2]**(OTf) in $CDCl_3$.

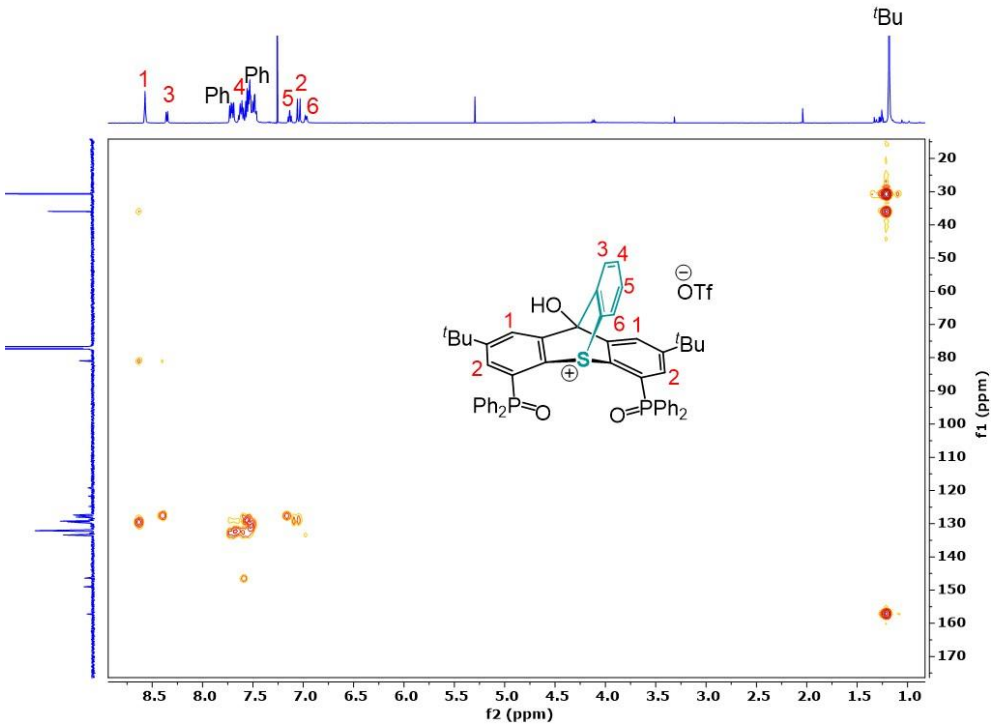

Figure S7. ^{1}H–^{13}C HMBC NMR (400 MHz) of **[2]**(OTf) in $CDCl_3$.

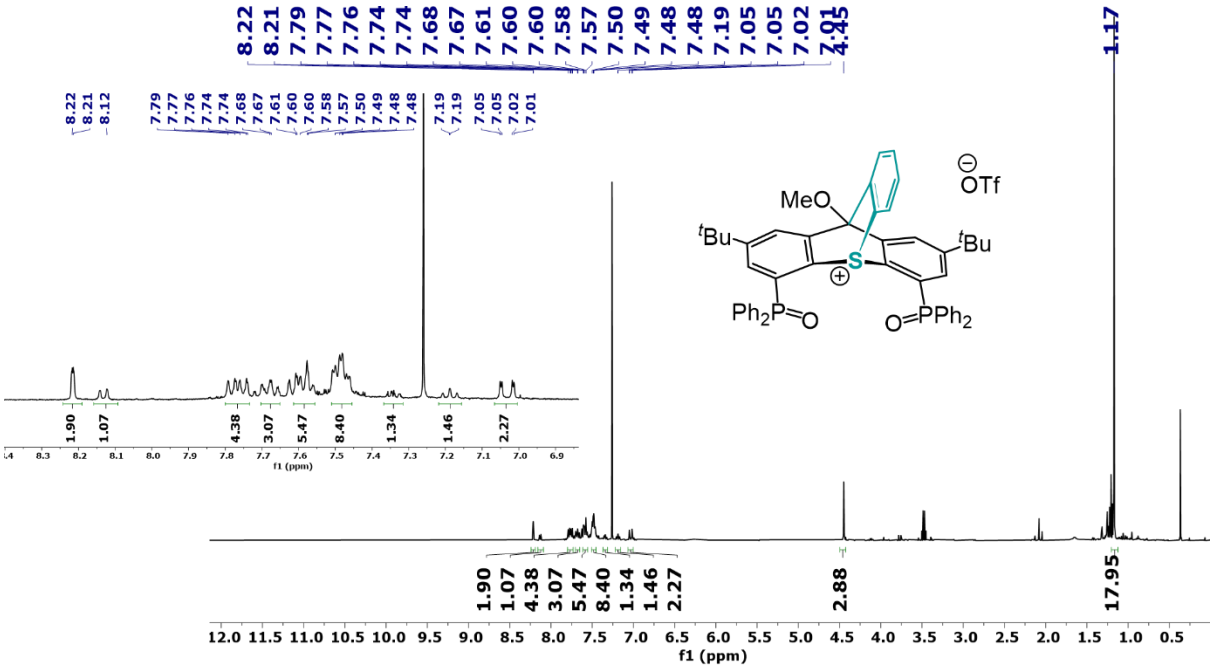

Figure S8. ^{1}H NMR spectrum of the **[3]**(OTf) in $CDCl_3$ (500 MHz).

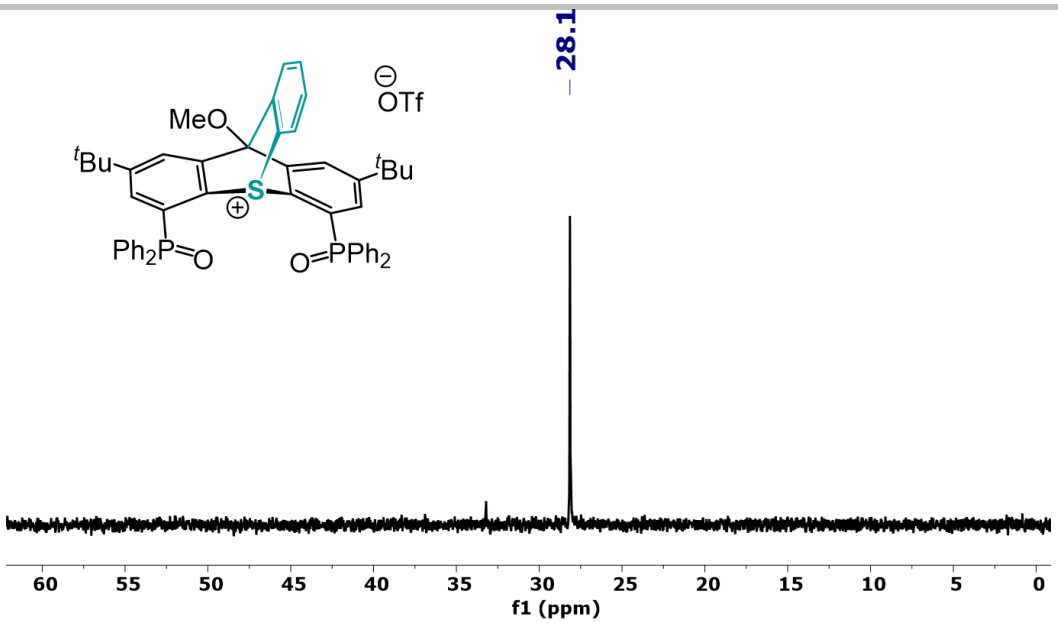

Figure S9. $^{31}P\{^{1}H\}$ NMR spectrum of the **[3]**(OTf) in $CDCl_3$ (162 MHz).

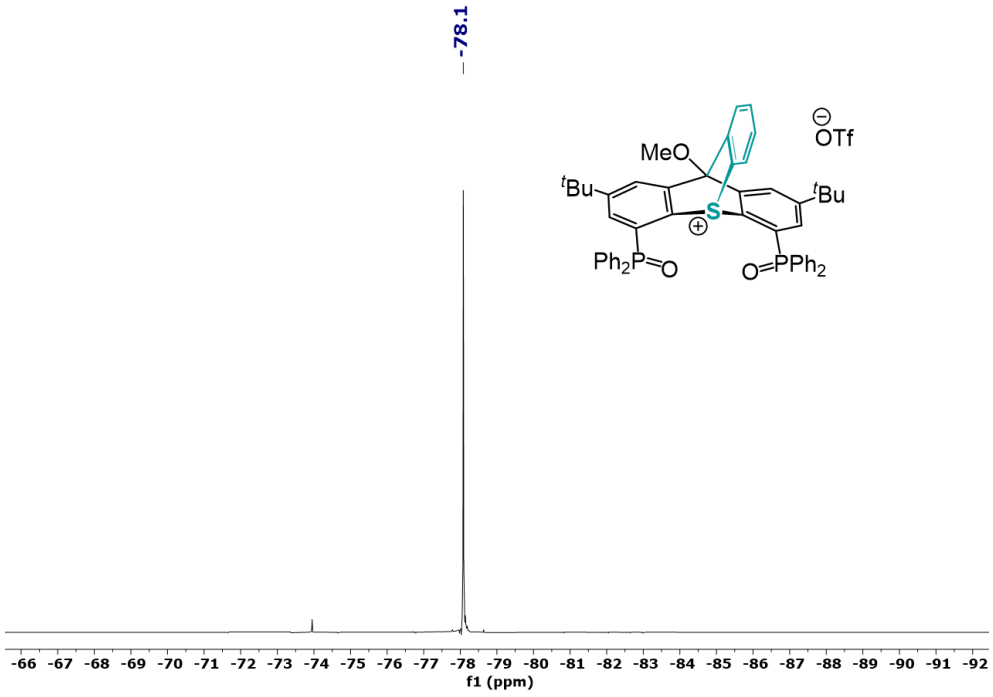

Figure S10. $^{19}F\{^{1}H\}$ NMR spectrum of **[3]**(OTf) in $CDCl_3$ (376 MHz).

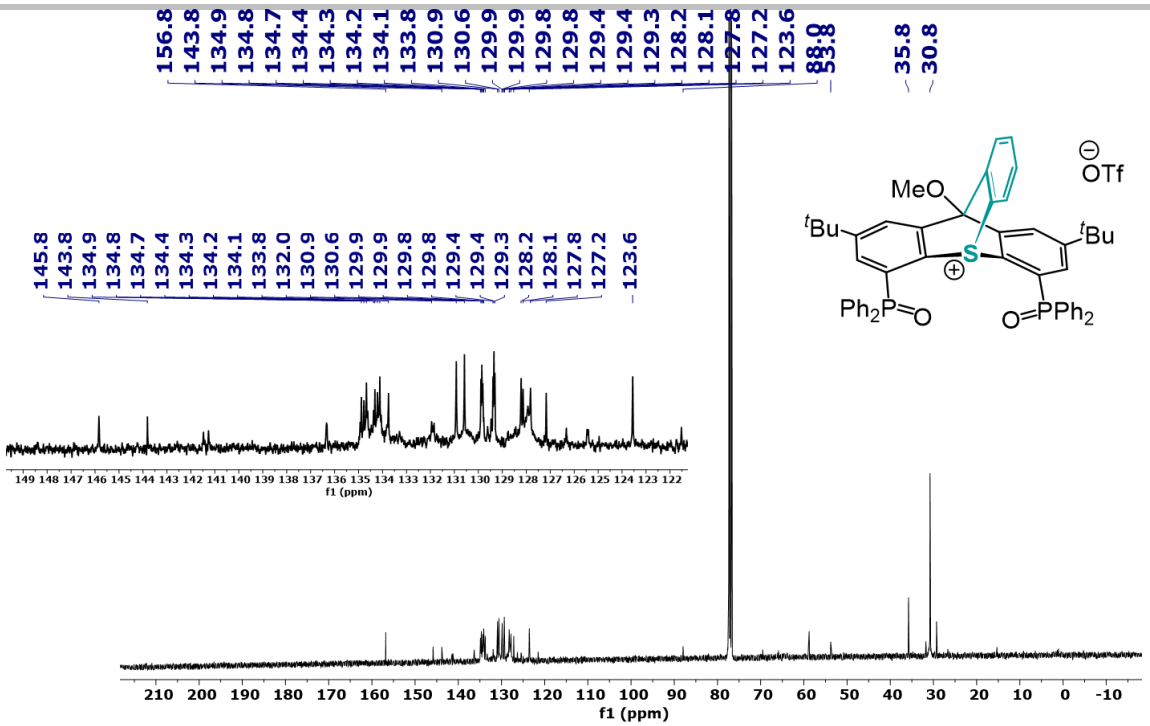

Figure S11. $^{13}C\{^{1}H\}$ NMR spectrum of **[3]**(OTf) in $CDCl_3$ (101 MHz).

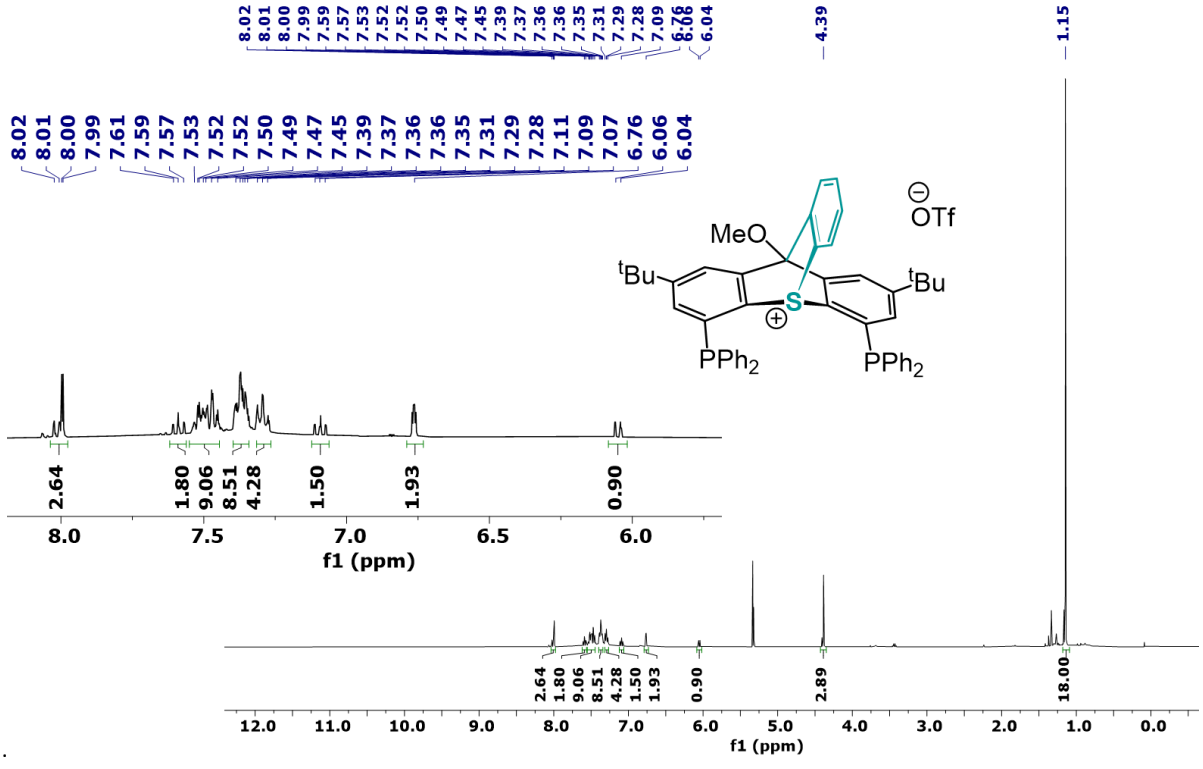

Figure S12. ^{1}H NMR spectrum of **[4]**(OTf) in CD_2Cl_2 (400 MHz).

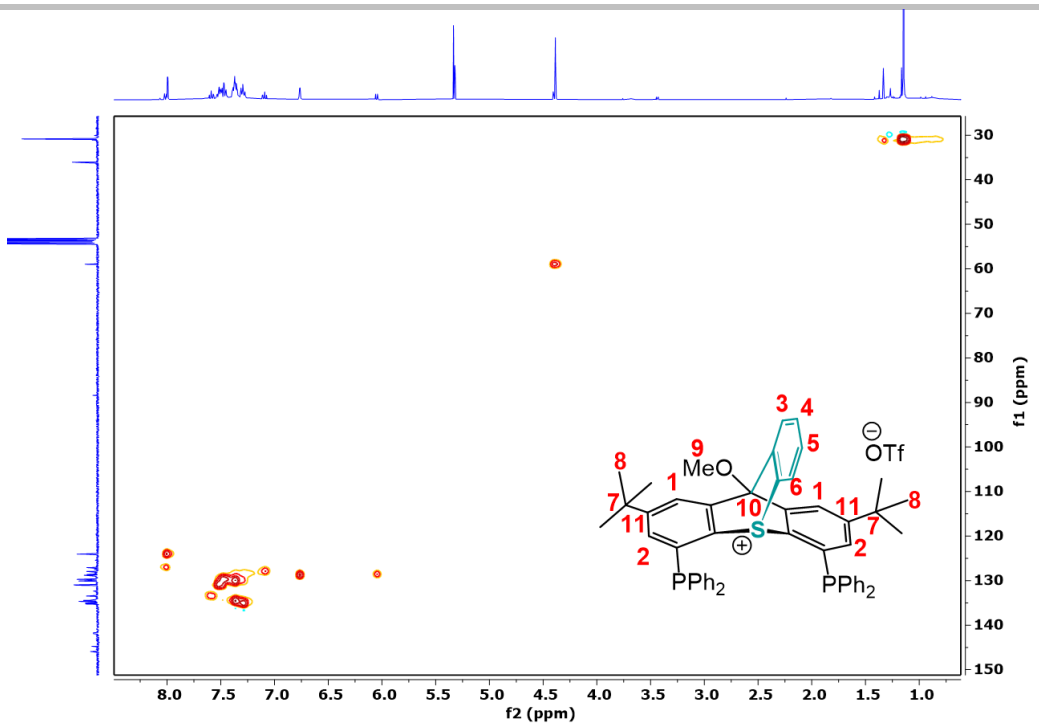

Figure S13. $^{1}H–^{13}C$ HSQC NMR (400 MHz) of **[4]**(OTf) in CD_2Cl_2.

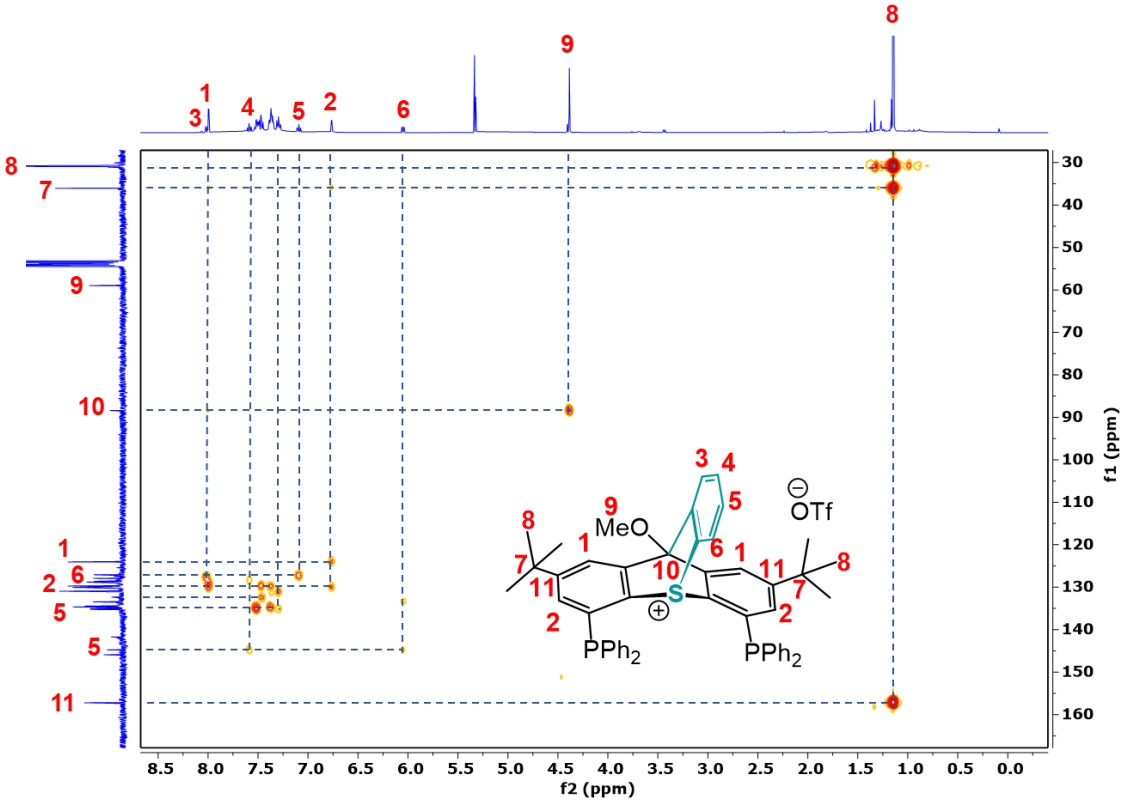

Figure S14. $^{1}H–^{13}C$ HMBC NMR (400 MHz) of **[4]**(OTf) in CD_2Cl_2.

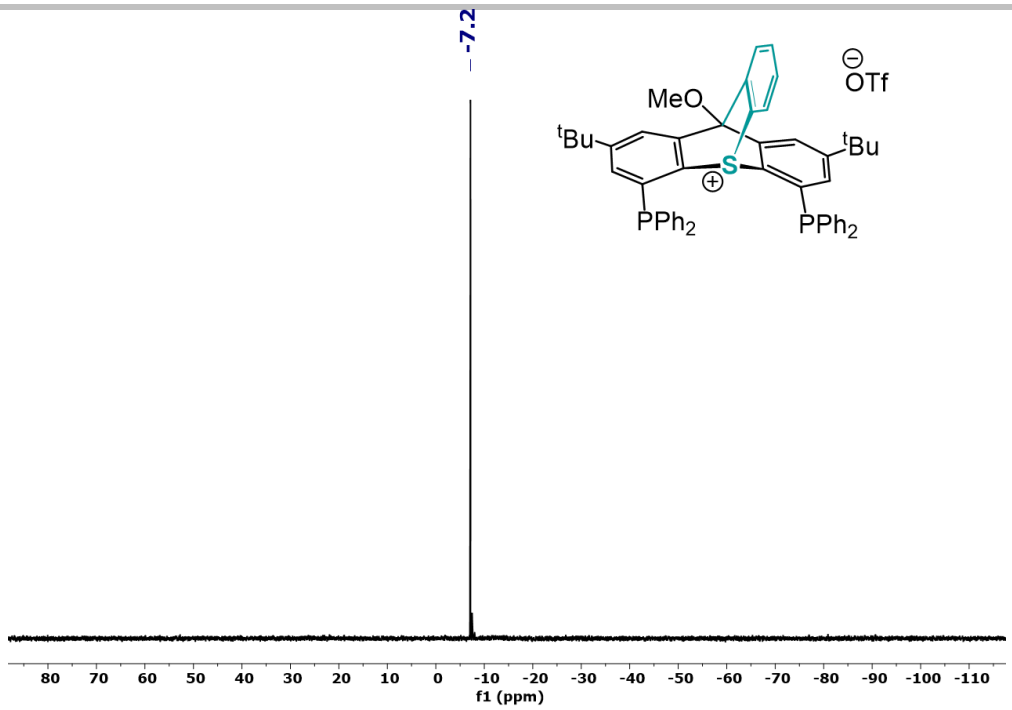

Figure S15. $^{31}P\{^{1}H\}$ NMR spectrum of **[4]**(OTf) in CD_2Cl_2 (162 MHz).

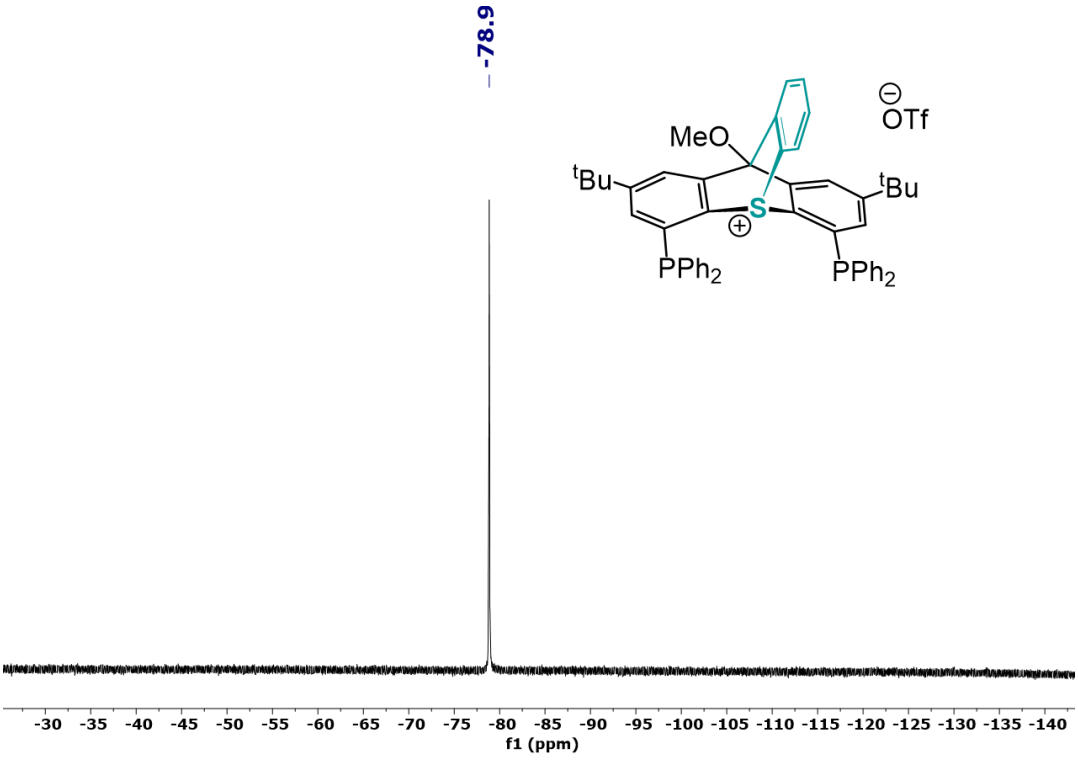

Figure S16. $^{19}F\{^{1}H\}$ NMR spectrum of **[4]**(OTf) in CD_2Cl_2 (376 MHz).

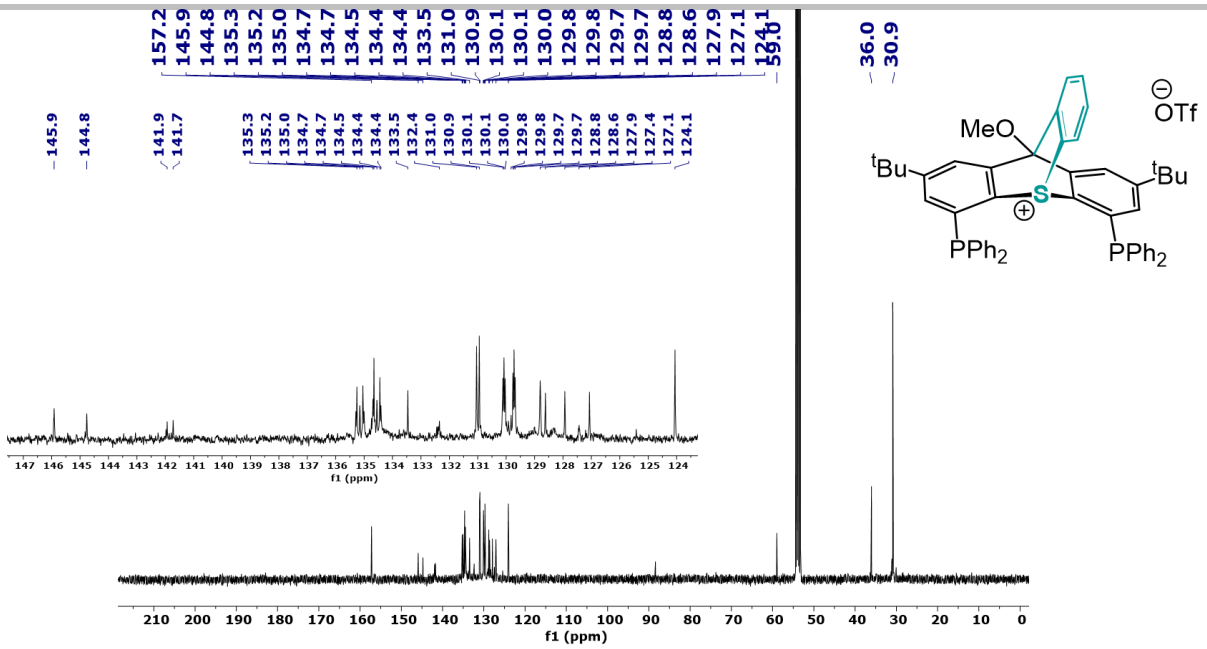

Figure S17. $^{13}C\{^{1}H\}$ NMR spectrum of **[4]**(OTf) in CD_2Cl_2 (101 MHz).

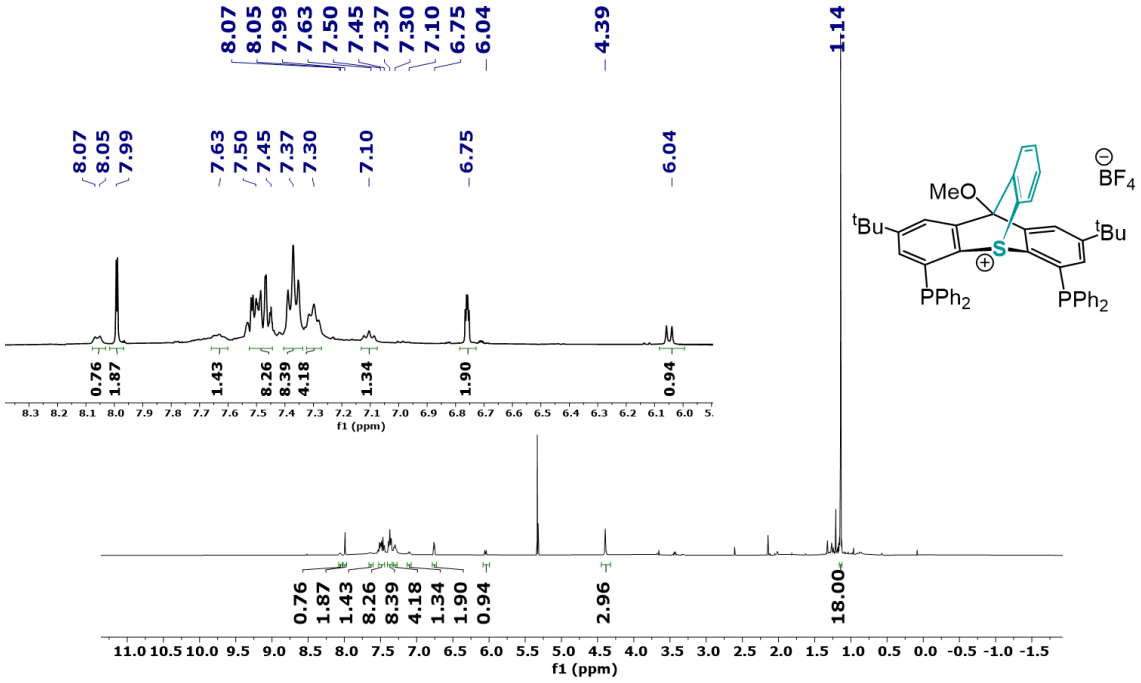

Figure S18. ^{1}H NMR spectrum of **[4]**(BF_4) in CD_2Cl_2 (400 MHz).

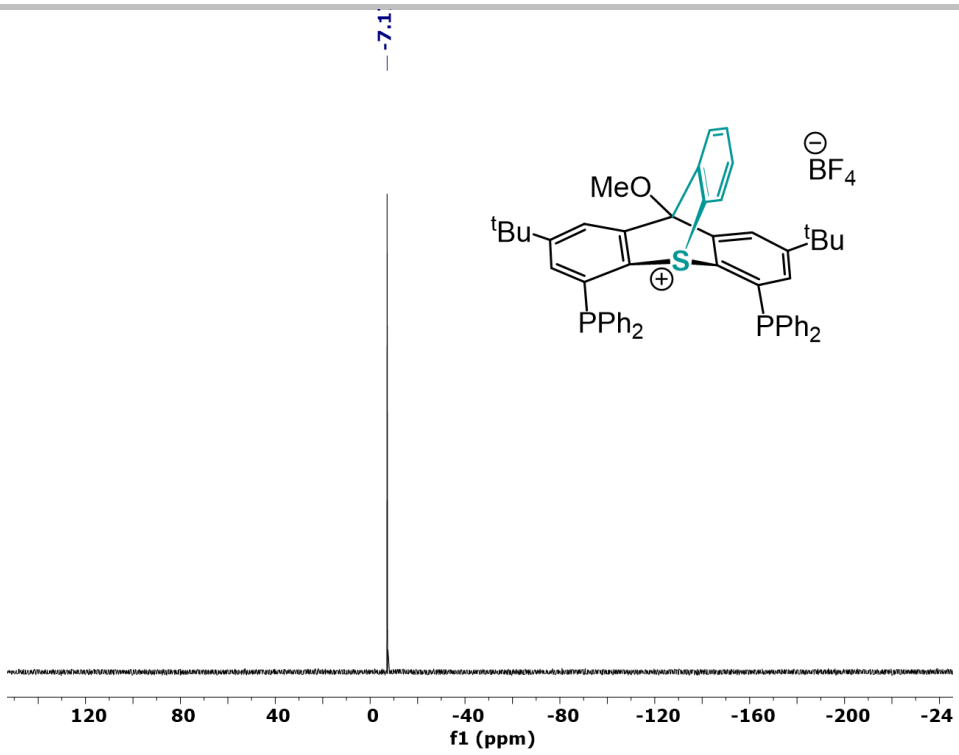

Figure S19. $^{31}P\{^{1}H\}$ NMR spectrum of **[4]**(BF_4) in CD_2Cl_2 (162 MHz).

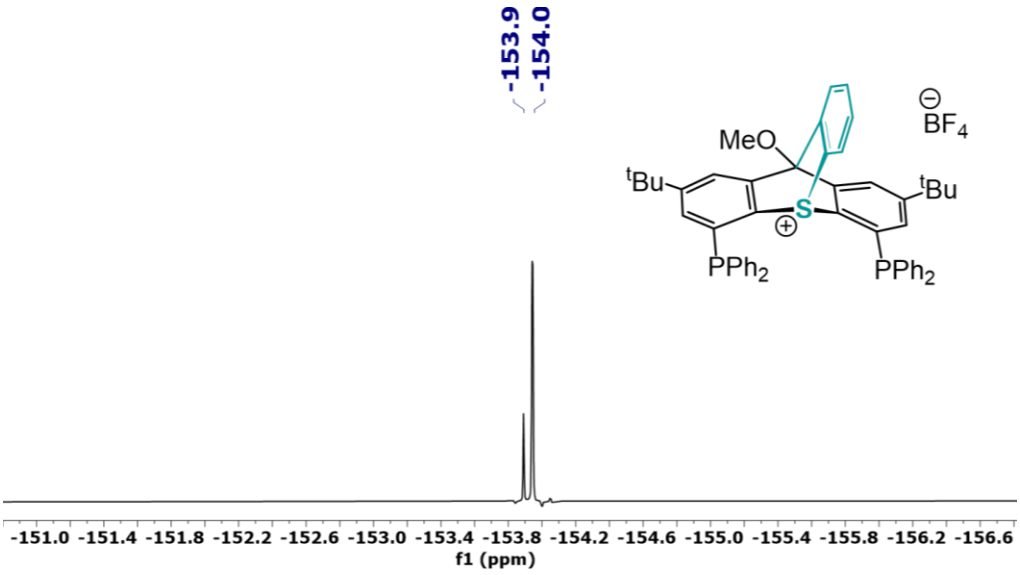

Figure S20. $^{19}F\{^{1}H\}$ NMR spectrum of **[4]**(BF_4) in CD_2Cl_2 (376 MHz).

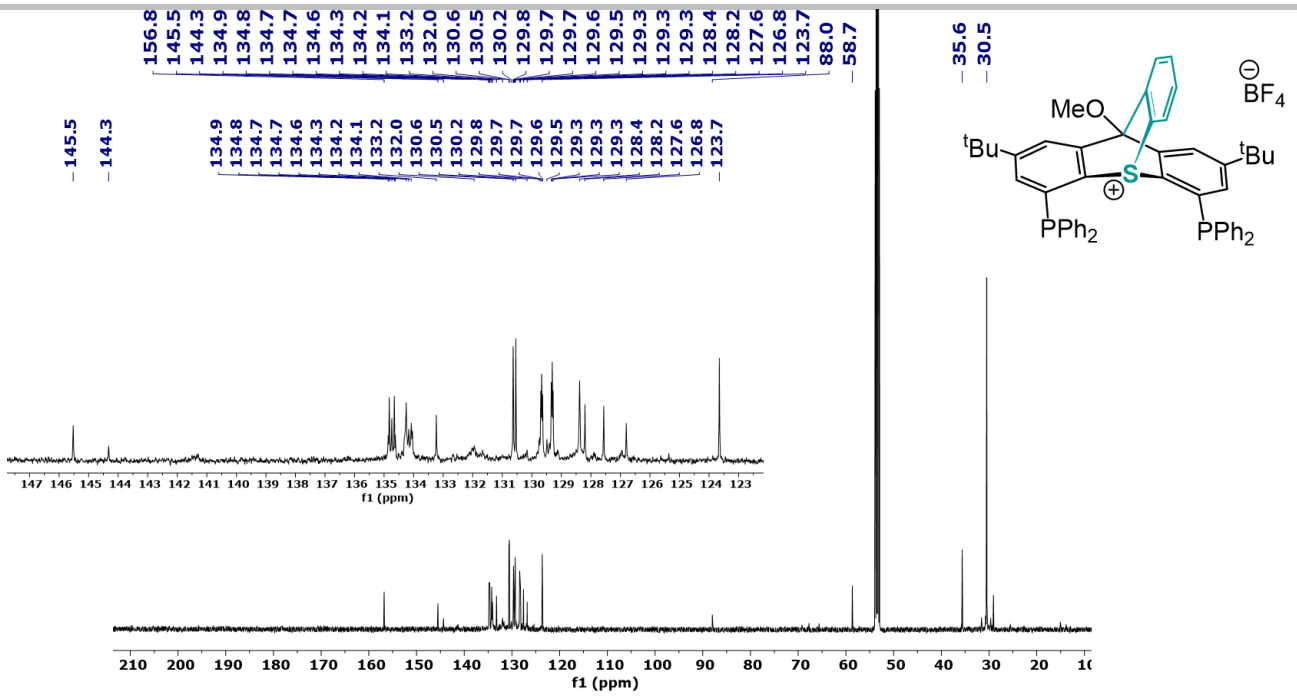

Figure S21. $^{13}C\{^{1}H\}$ NMR spectrum of the **[4]**(BF_4) in CD_2Cl_2 (101 MHz).

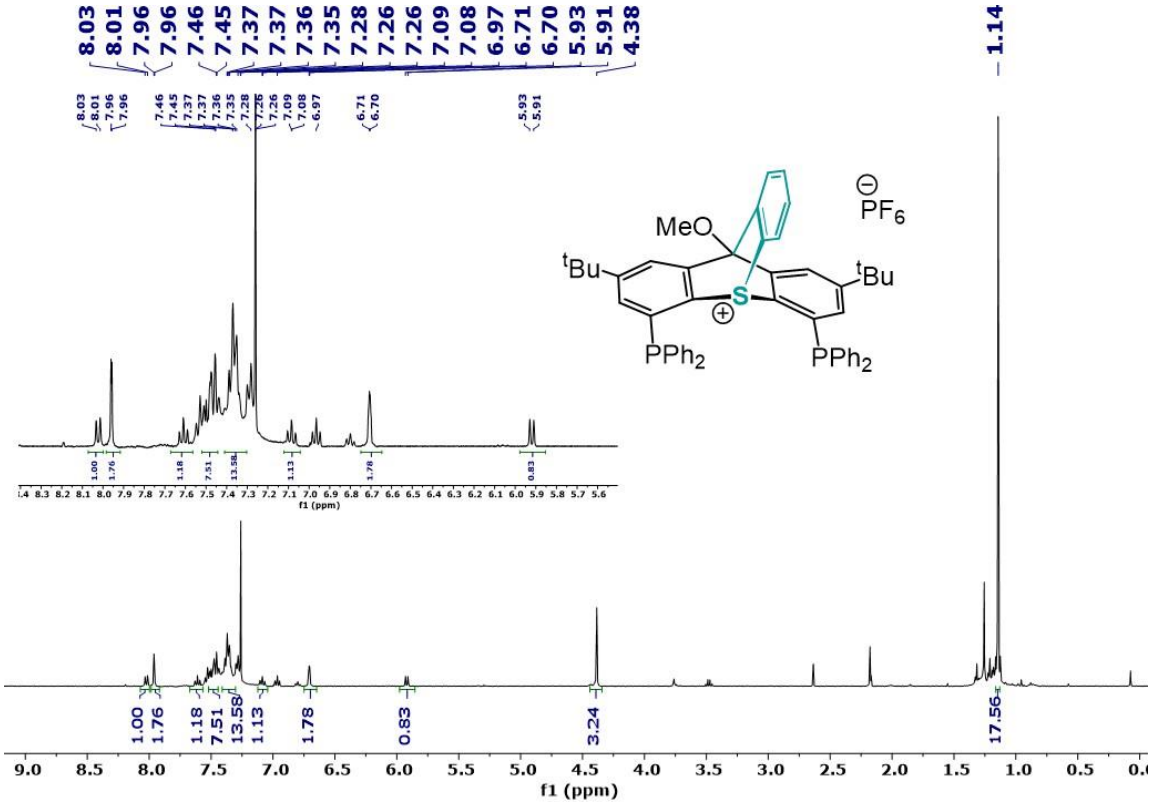

Figure S22. ^{1}H NMR spectrum of **[4]**(PF_6) in $CDCl_3$ (400 MHz).

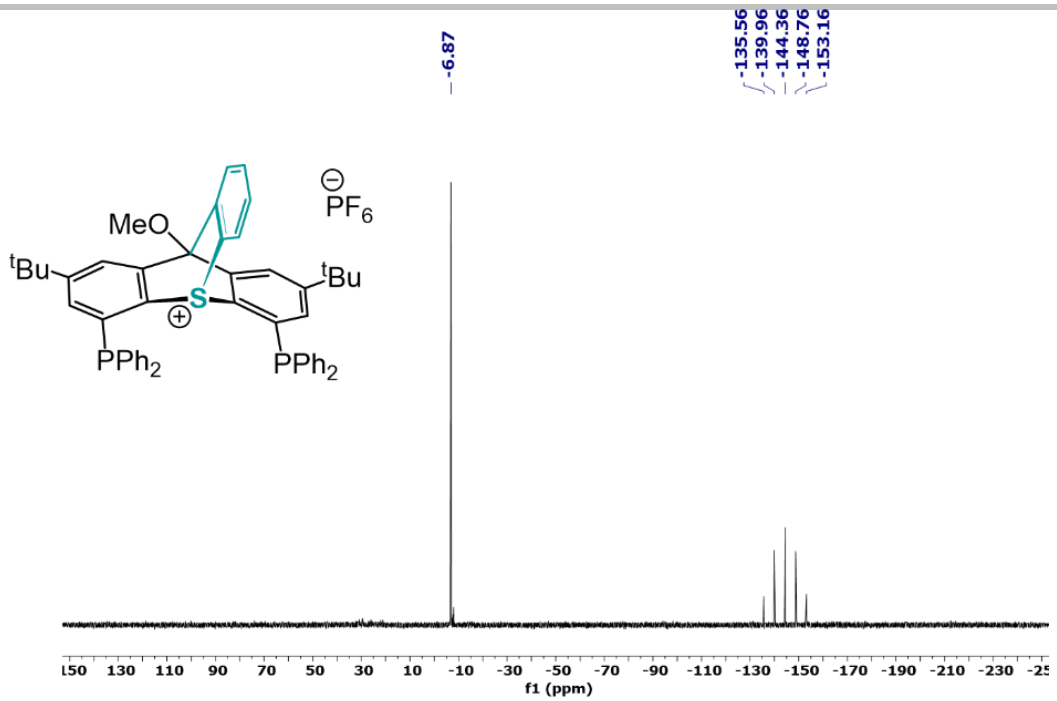

Figure S23. $^{31}P\{^{1}H\}$ NMR spectrum of **[4]**(PF_6) in $CDCl_3$ (162 MHz).

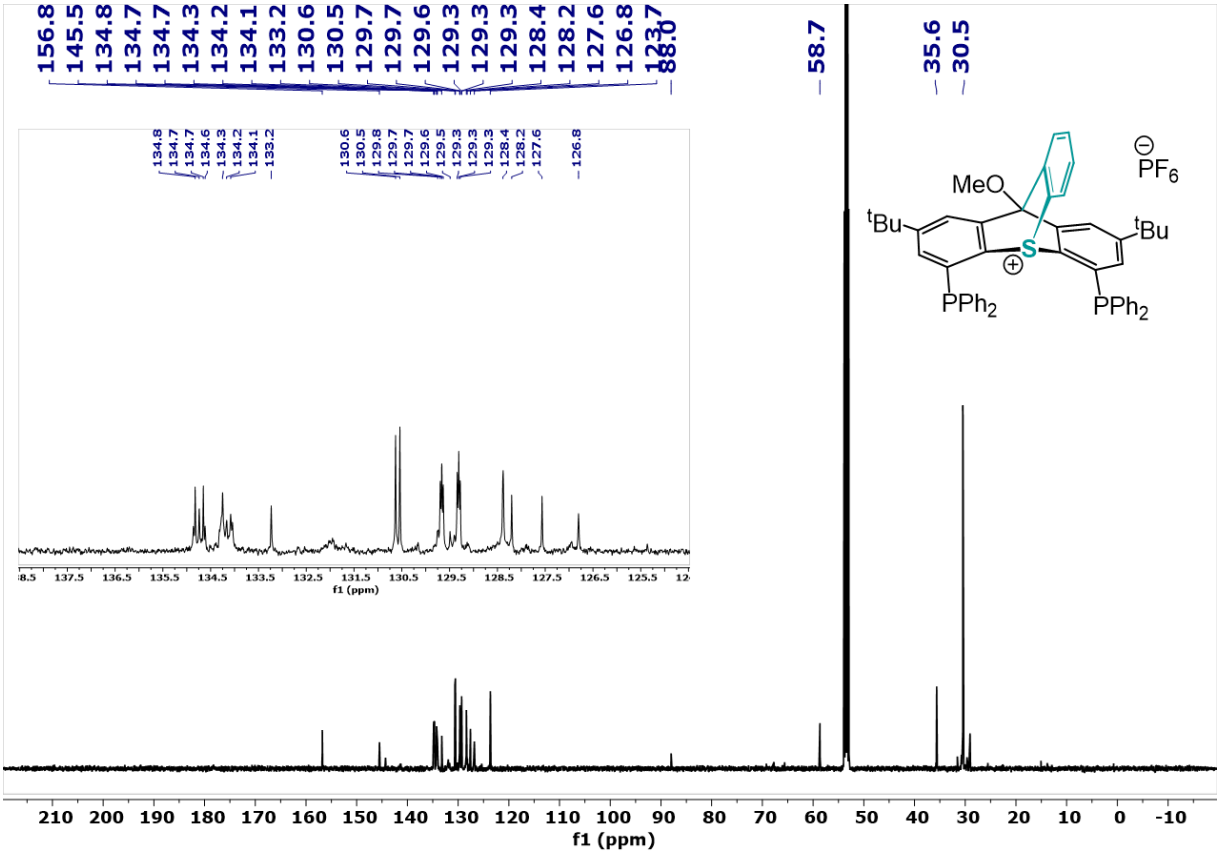

Figure S24. $^{13}C\{^{1}H\}$ NMR spectrum of the **[4]**(PF_6) in CD_2Cl_2 (101 MHz).

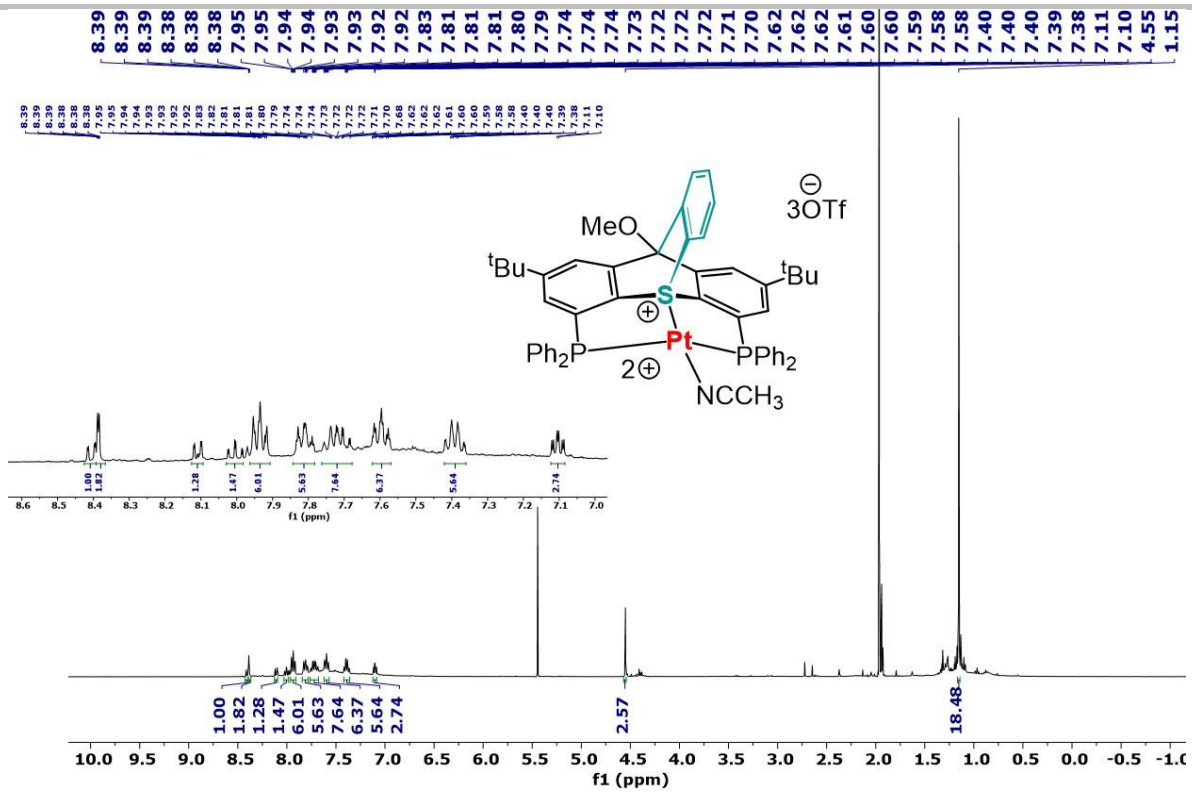

Figure S25. ^{1}H NMR spectrum of **[5]**$(OTf)_3$ in CD_3CN (400 MHz).

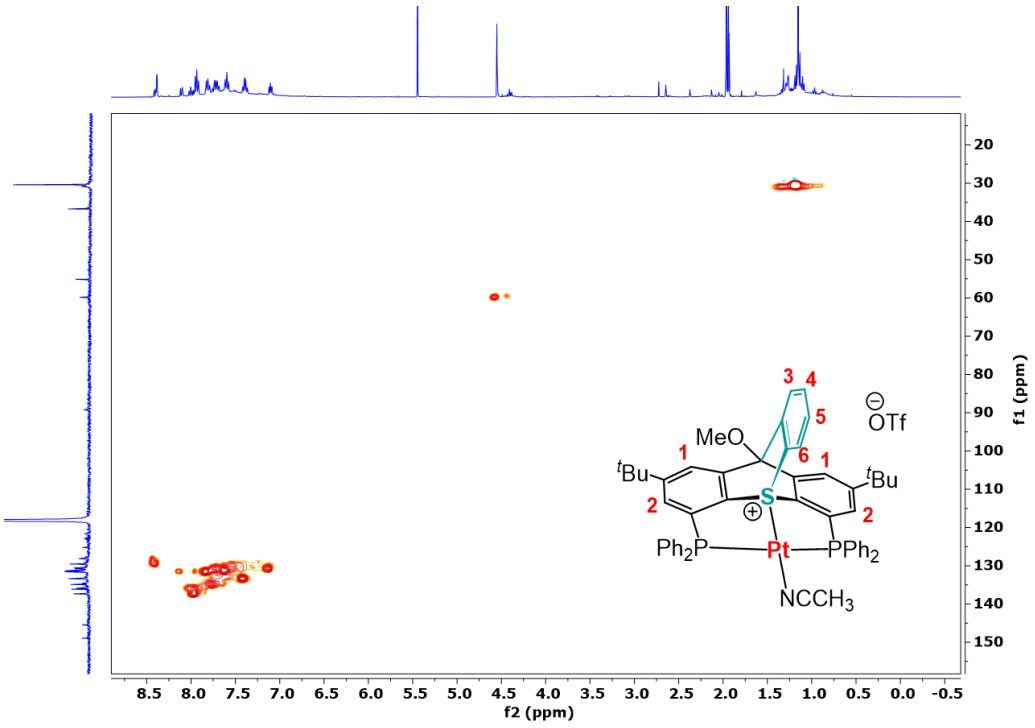

Figure S26. ^{1}H–^{13}C HSQC NMR (400 MHz) of **[5]**$(OTf)_3$ in CD_3CN.

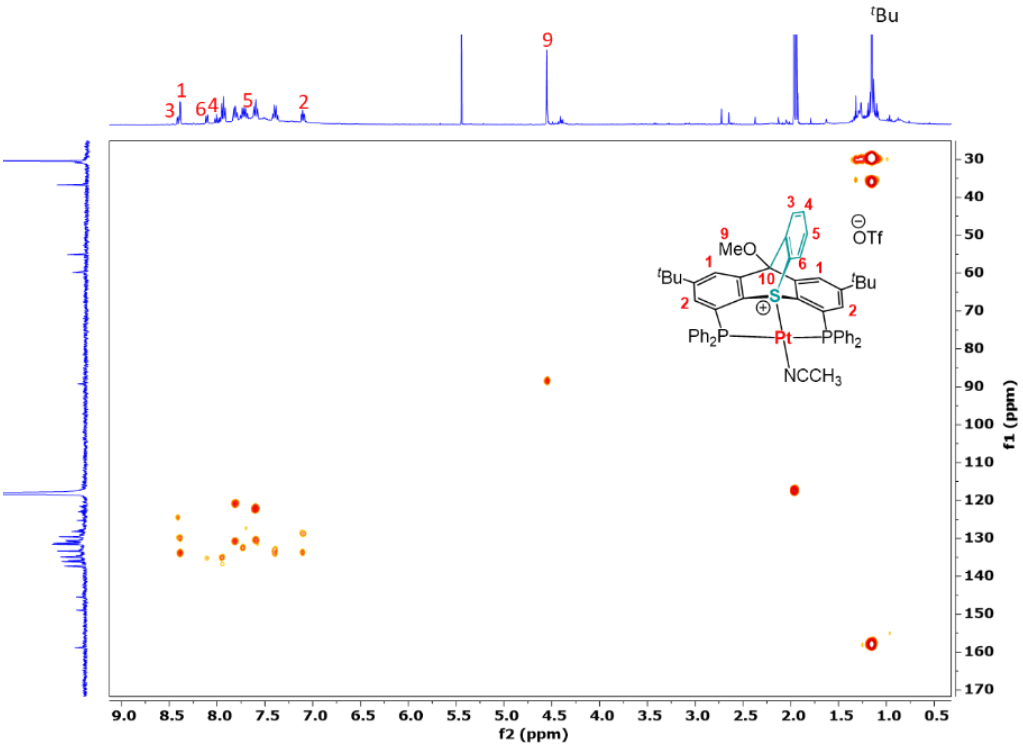

Figure S27. $^{1}H–^{13}C$ HMBC NMR (400 MHz) of **[5]**$(OTf)_3$ in CD_3CN.

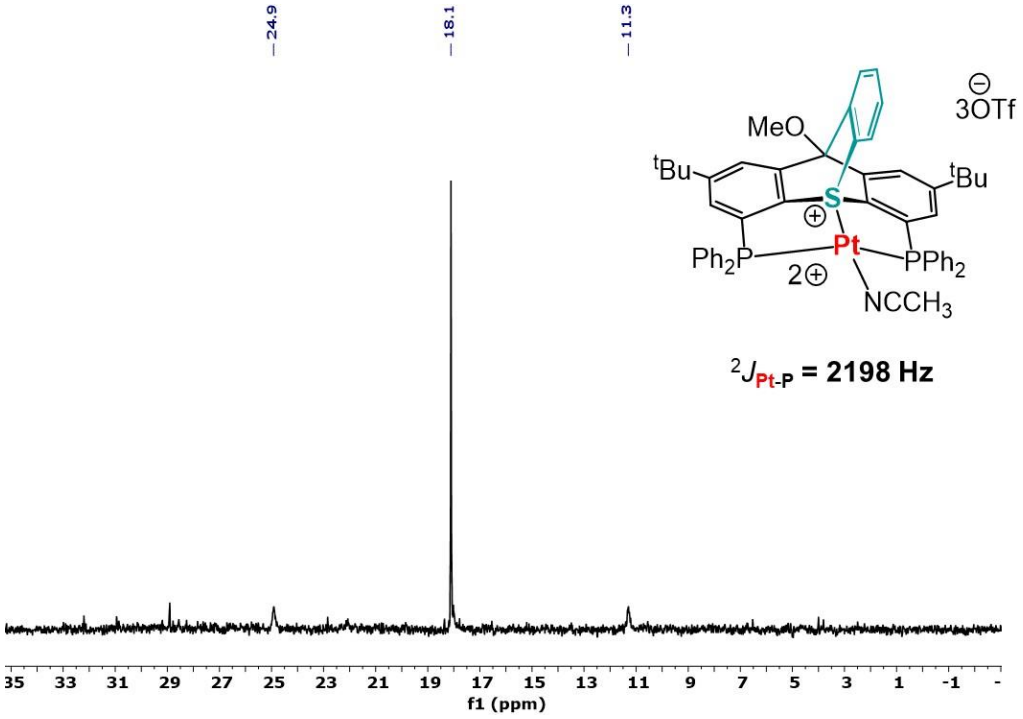

Figure S28. $^{31}P\{^{1}H\}$ NMR spectrum of **[5]**$(OTf)_3$ in CD_3CN (162 MHz).

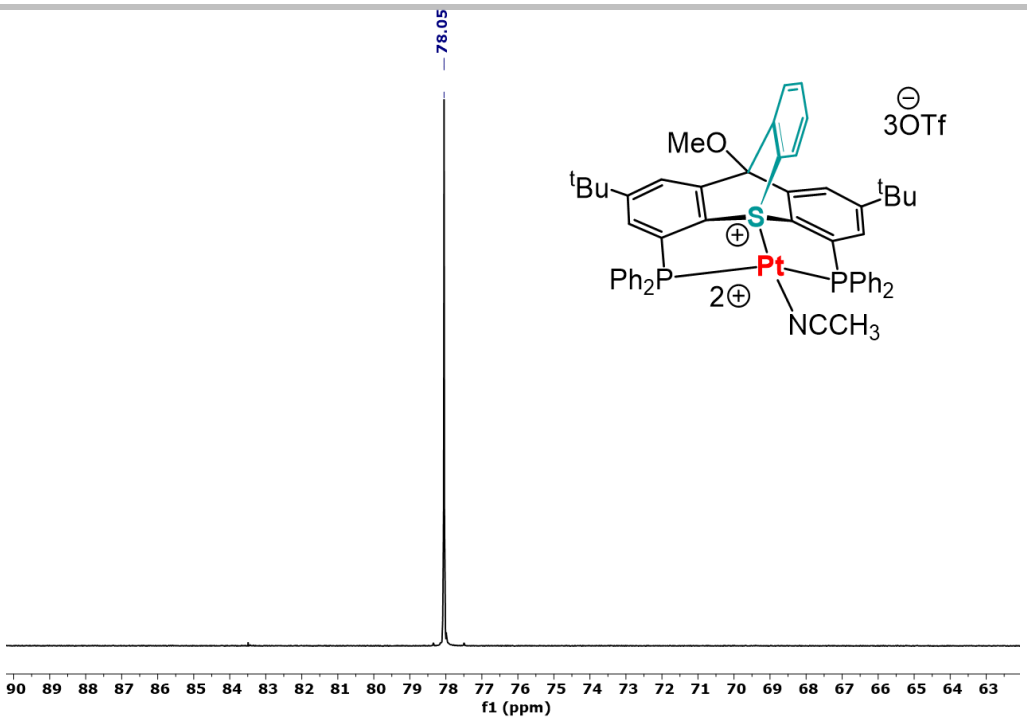

Figure S29. $^{19}F\{^{1}H\}$ NMR spectrum of the **[5]**$(OTf)_3$ in CD_3CN (376 MHz).

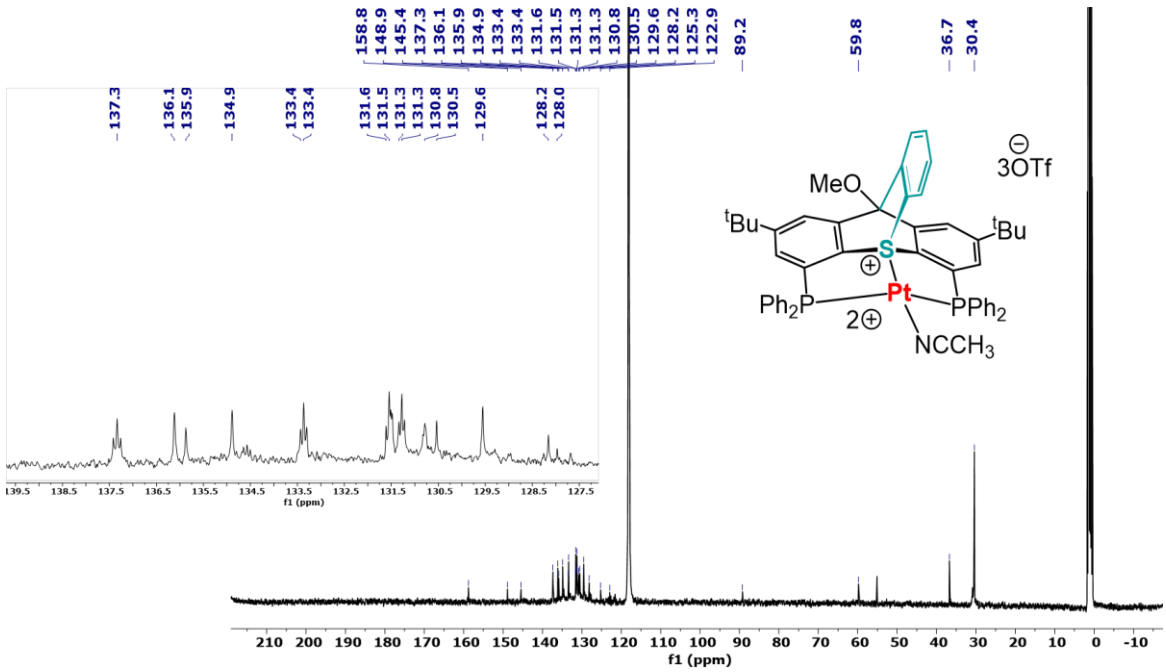

Figure S30. $^{13}C\{^{1}H\}$ NMR spectrum of the **[5]**$(OTf)_3$ in CD_3CN (101 MHz).

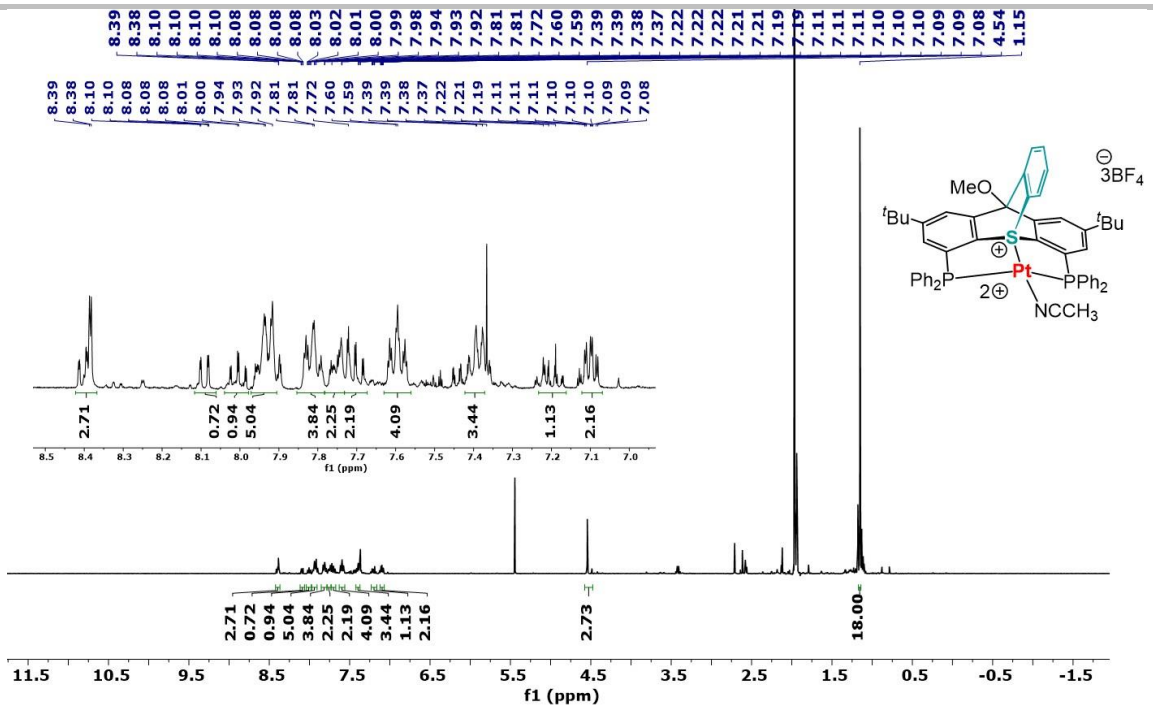

Figure S31. ^{1}H NMR spectrum of **[5]**$(BF_4)_3$ in CD_3CN (400 MHz).

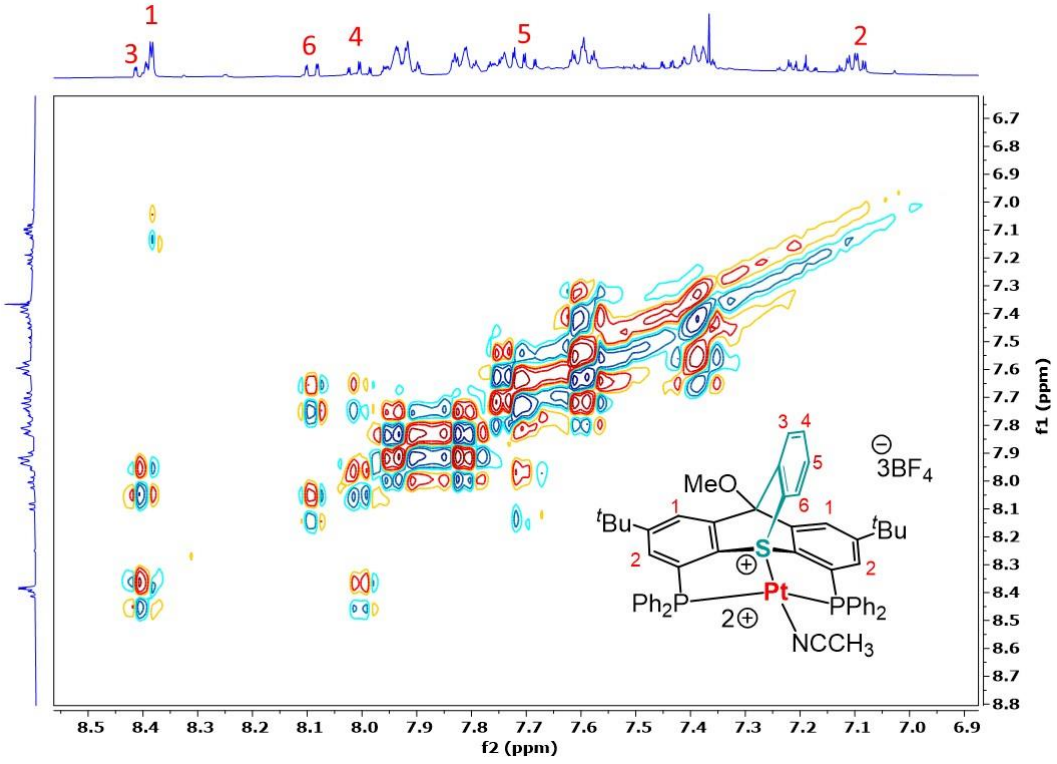

Figure S32. ^{1}H–^{1}H COSY NMR (400 MHz) of **[5]**$(BF_4)_3$ in CD_3CN.

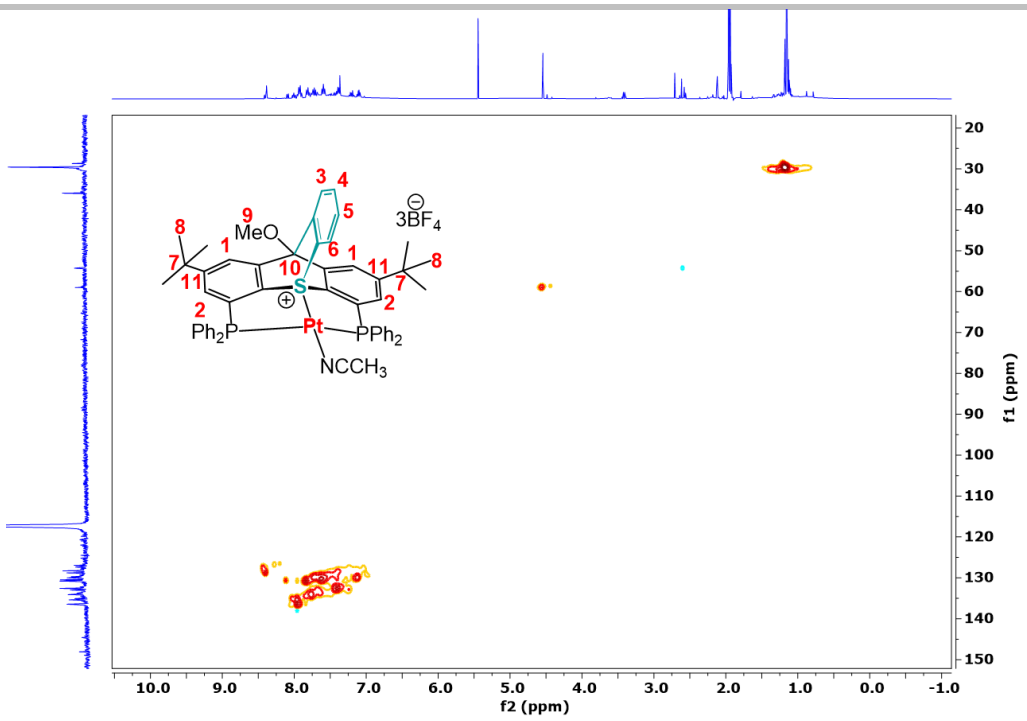

Figure S33. ^{1}H–^{13}C HSQC NMR (400 MHz) of **[5]**$(BF_4)_3$ in CD_3CN.

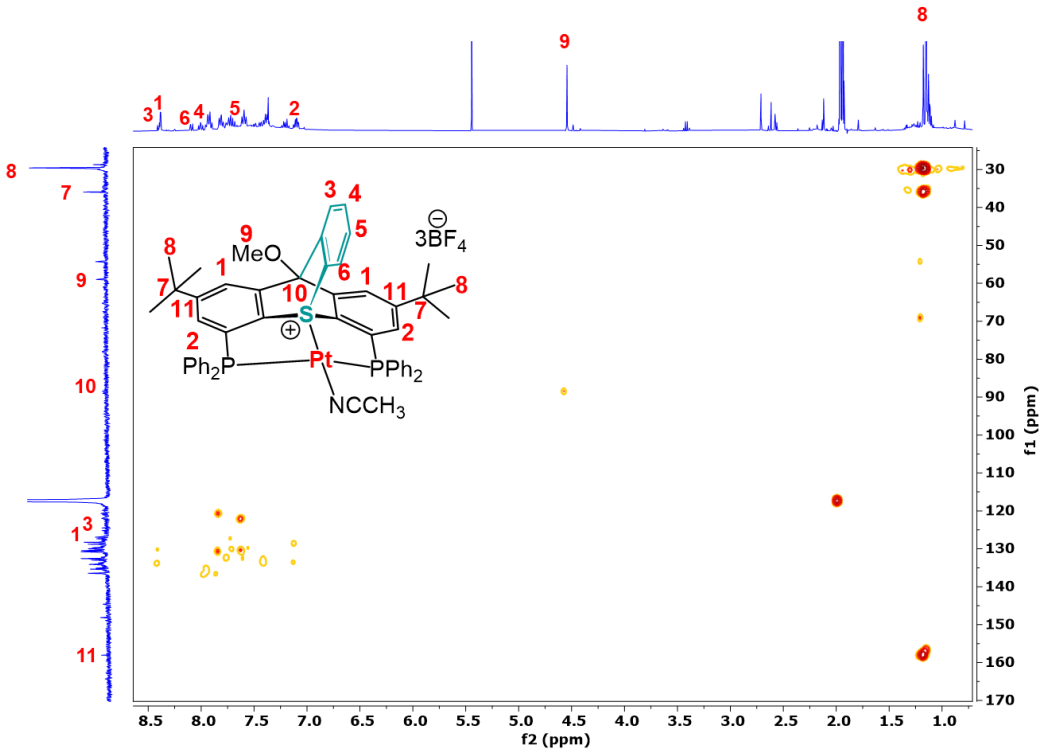

Figure S34. ^{1}H–^{13}C HMBC NMR (400 MHz) of **[5]**$(BF_4)_3$ in CD_3CN.

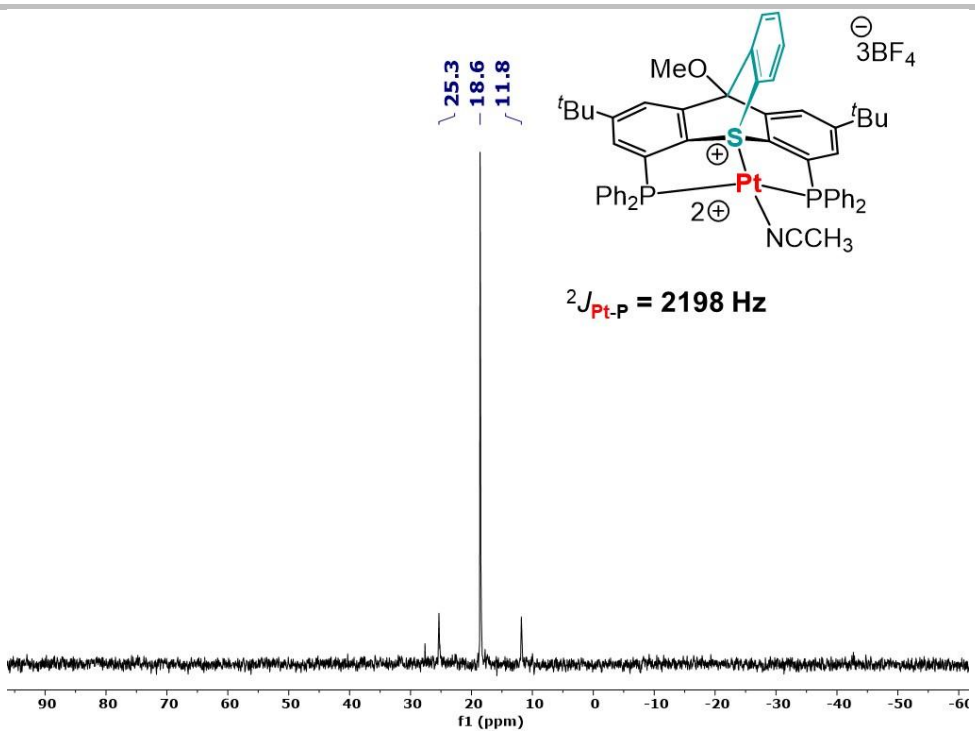

Figure S35. $^{31}P\{^{1}H\}$ NMR spectrum of **[5]**$(BF_4)_3$ in CD_3CN (162 MHz).

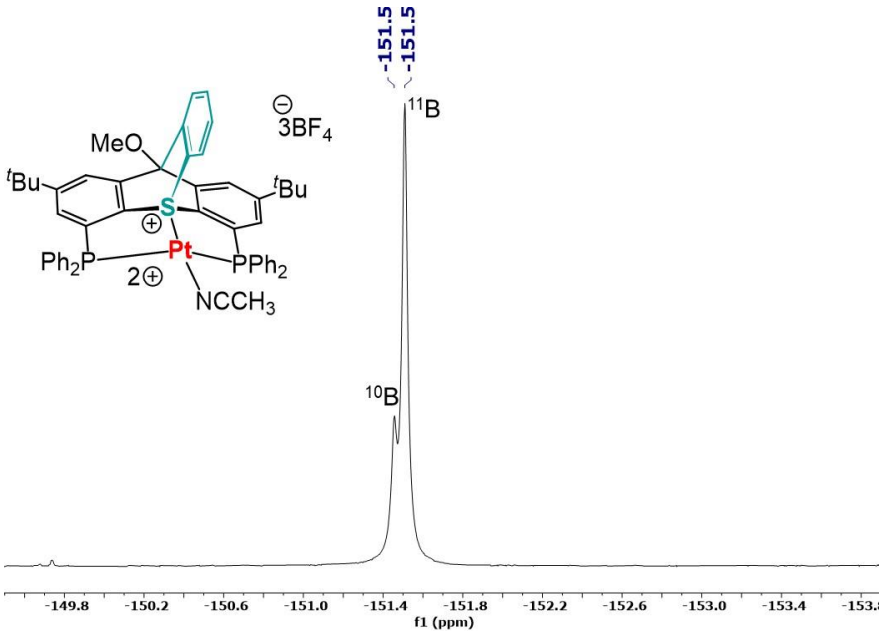

Figure S36. $^{19}F\{^{1}H\}$ NMR spectrum of the **[5]**$(BF_4)_3$ in CD_3CN (376 MHz).

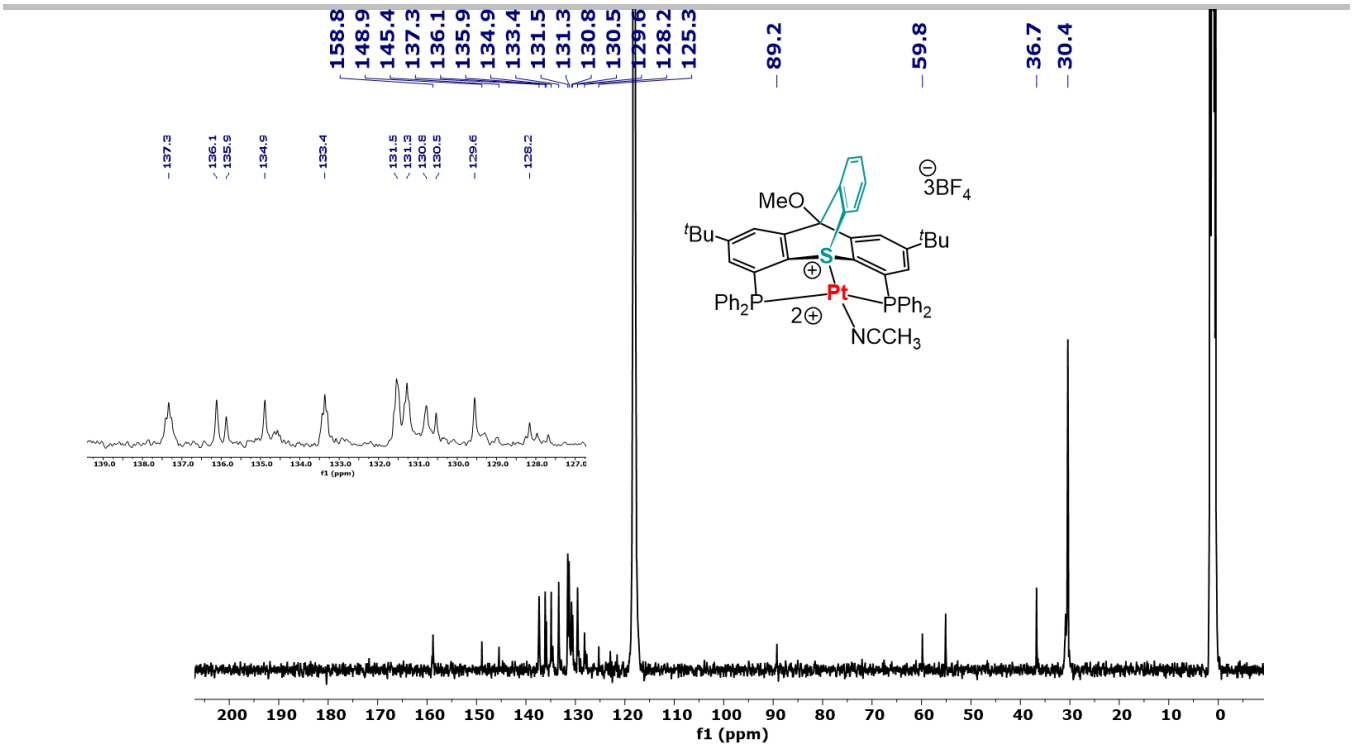

Figure S37. $^{13}C\{^{1}H\}$ NMR spectrum of the **[5]**$(BF_4)_3$ in CD_3CN (101 MHz).

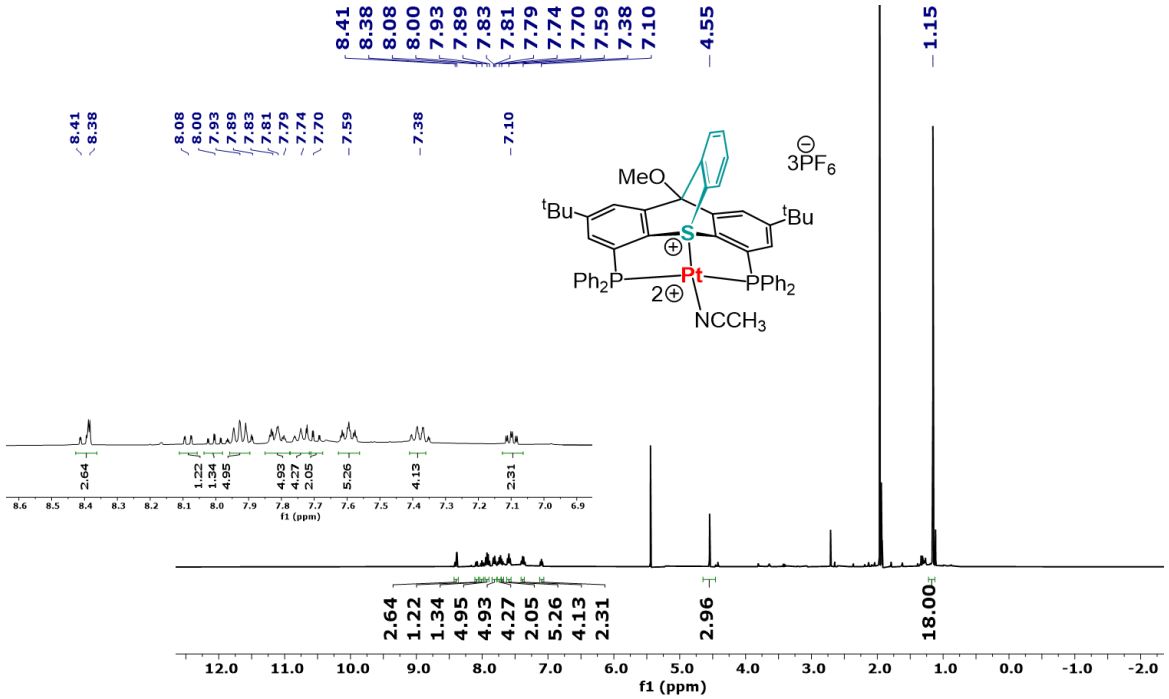

Figure S38. ^{1}H NMR spectrum of **[5]**$(PF_6)_3$ in CD_3CN (400 MHz).

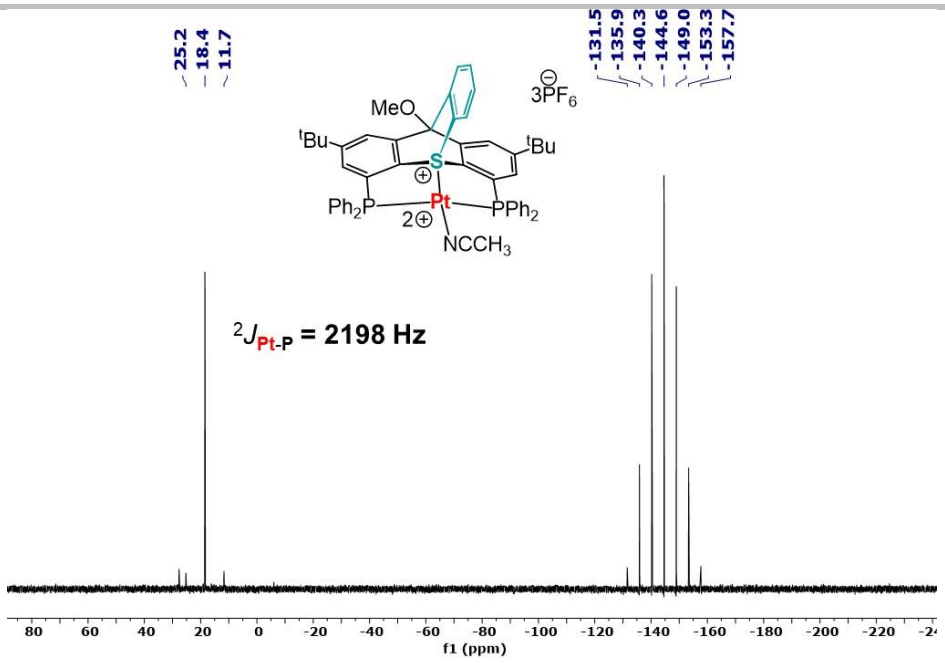

Figure S39. $^{31}P\{^{1}H\}$ NMR spectrum of **[5]**$(PF_6)_3$ in CD_3CN (162 MHz).

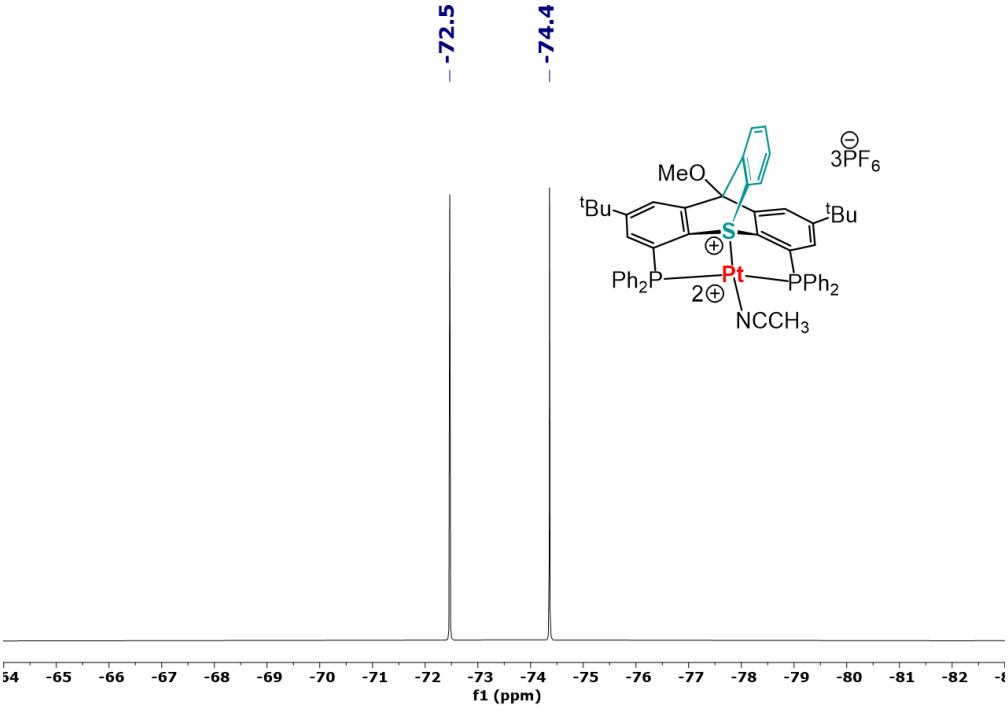

Figure S40. $^{19}F\{^{1}H\}$ NMR spectrum of the **[5]**$(PF_6)_3$ in CD_3CN (376 MHz).

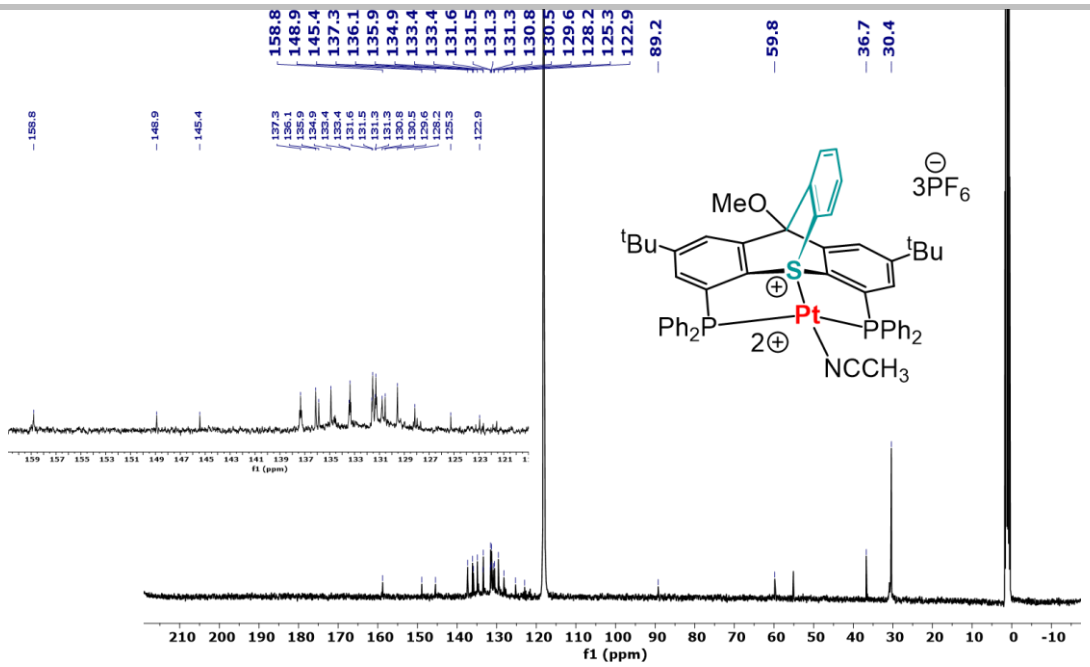

Figure S41. $^{13}C\{^{1}H\}$ NMR spectrum of the **[5]**$(PF_6)_3$ in CD_3CN (101 MHz).

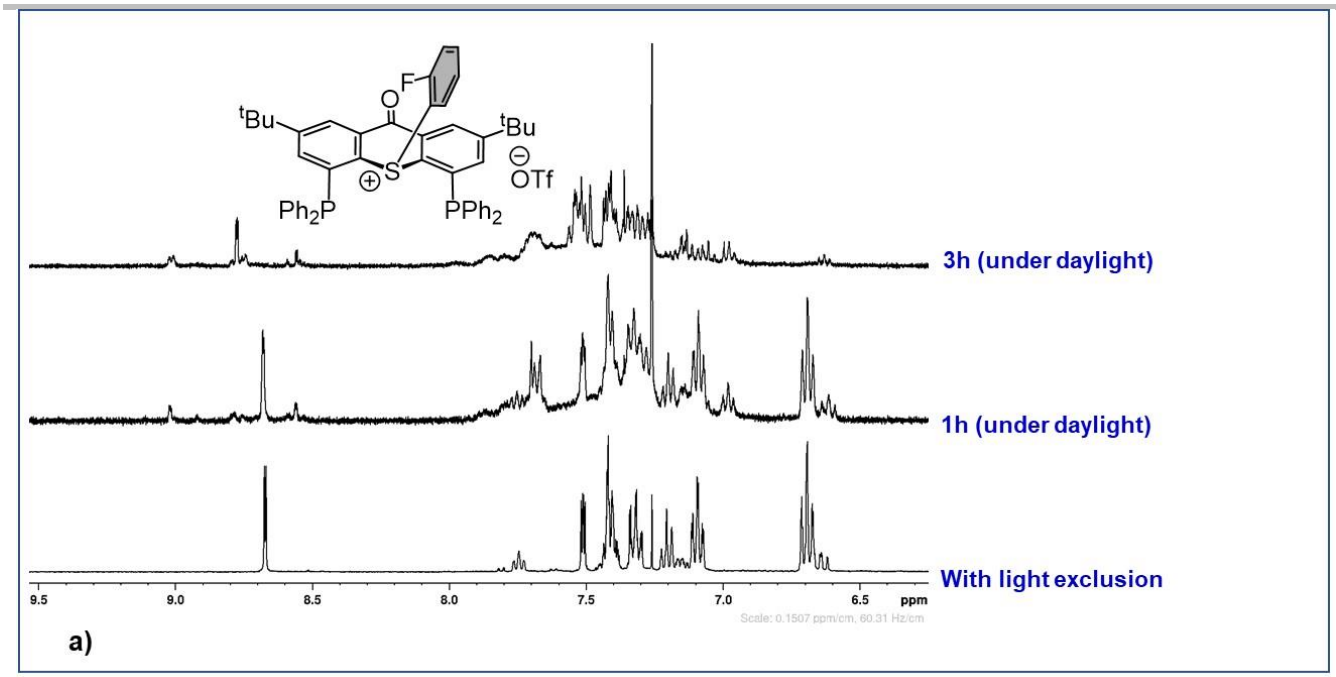

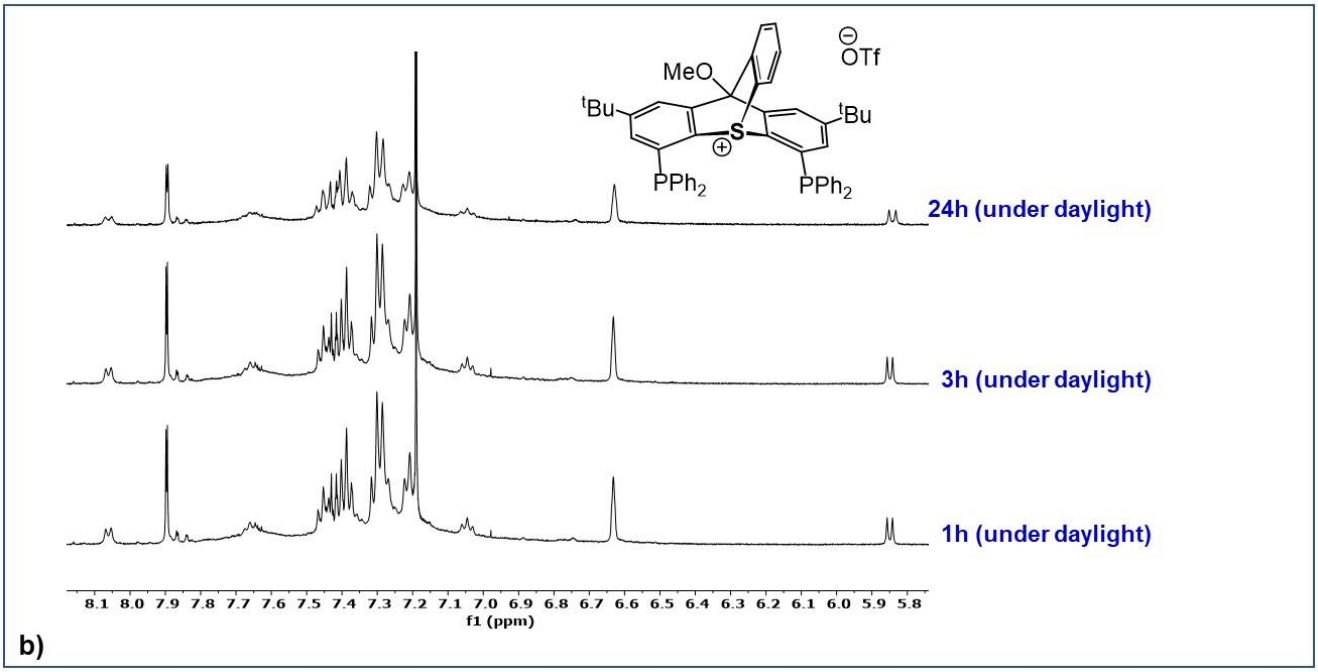

Figure S42. ^{1}H NMR spectra recorded after different timed of light exposure of the sulfonium ligand **L2** (**a**) and the thiatripticenium ligand **L3** (**b**) in $CDCl_3$.

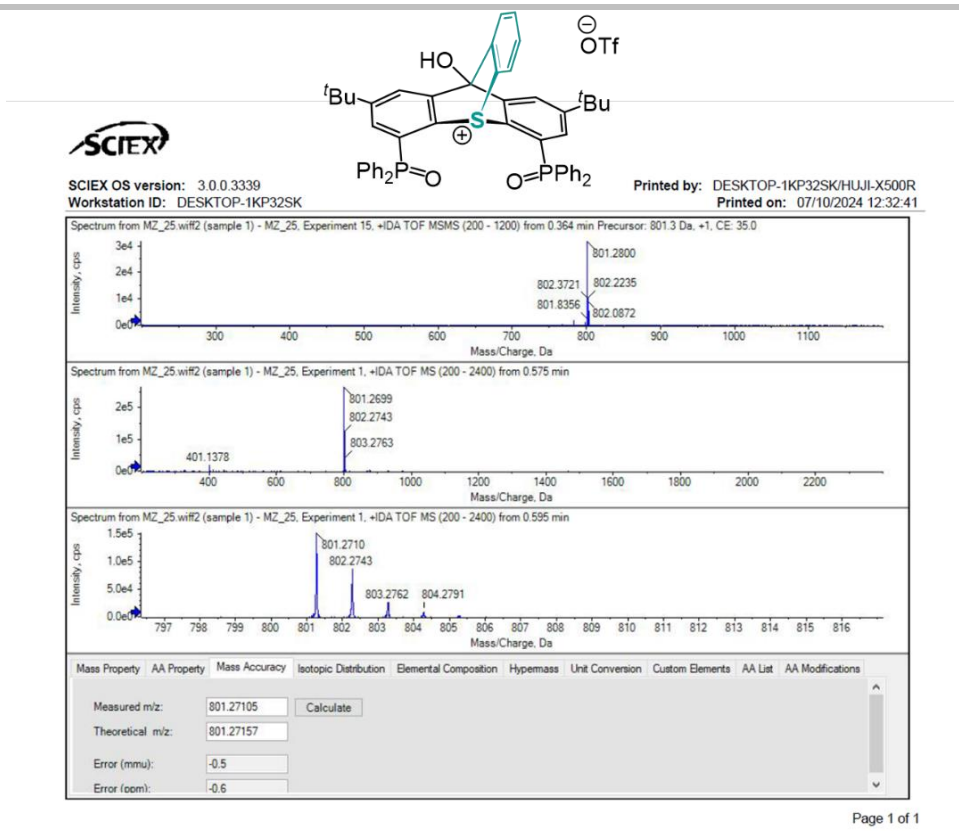

Figure S43. HRMS mass spectra of compound **[2]**(OTf).

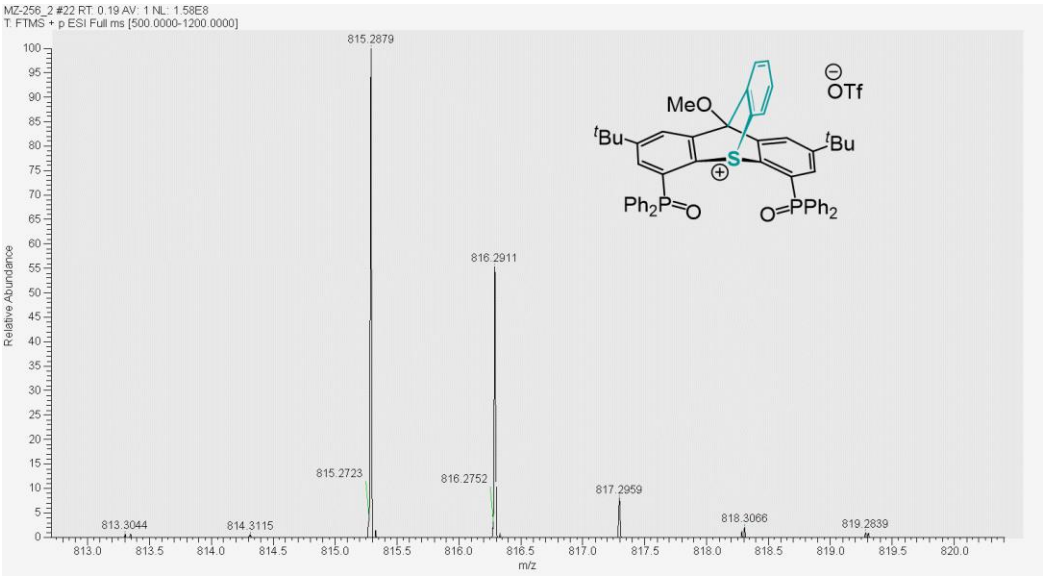

Figure S44. Mass spectra of compound **[3]**(OTf).

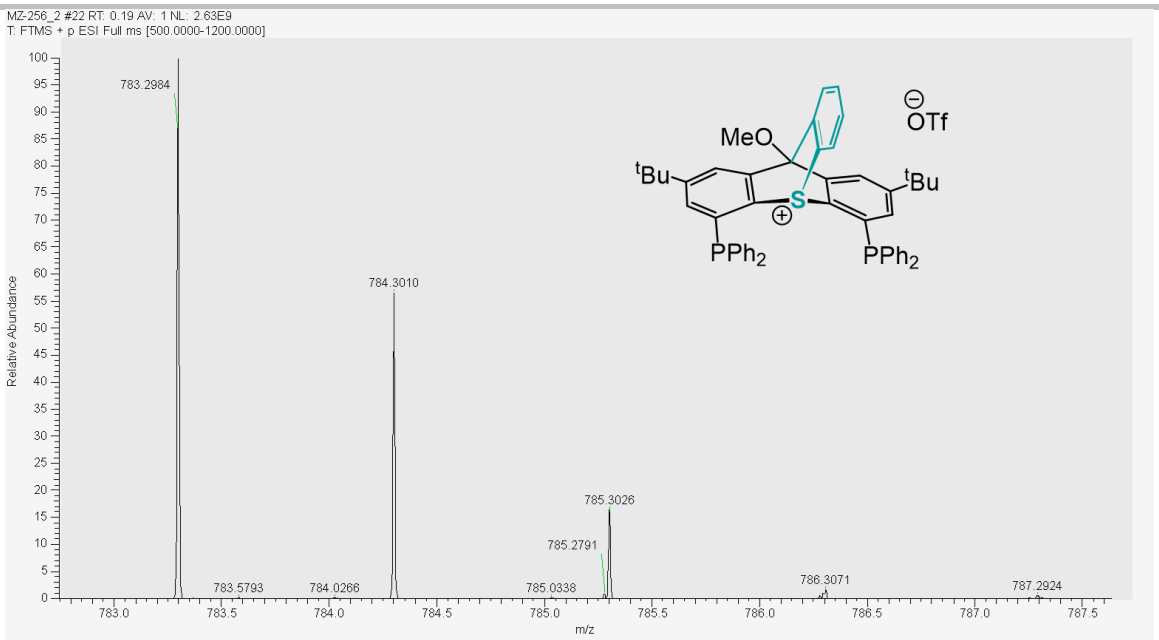

Figure S45. Mass spectra of compound **[4]**(OTf).

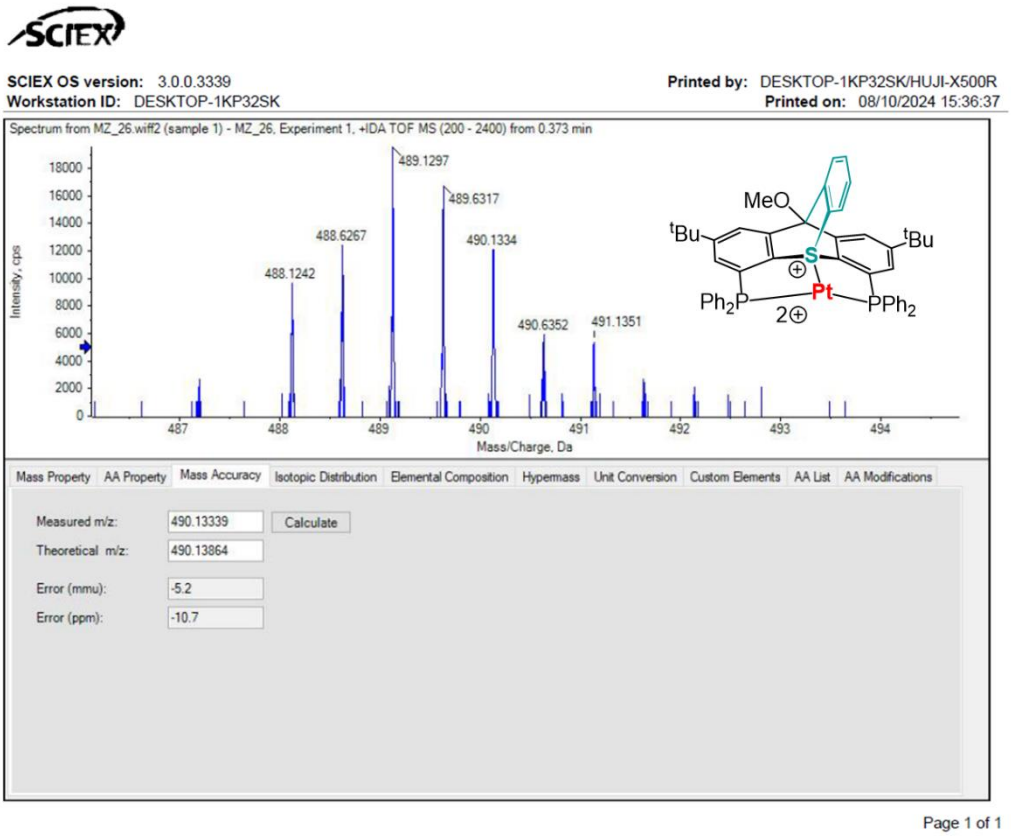

Figure S46. HRMS mass spectra of compound **[5]**(OTf).

2. Catalytic reactions

2.1. General procedures

The general procedure for the Pt catalyzed cycloisomerization reactions

Catalytic reactions were carried out under N_2. In a typical reaction, an alkyne (1 eq.) was mixed with catalyst (5% mmol) in 0.5 ml dichloroethane-d_4 (50 mM) in a J-Young tube that was heated to 80°C. The reaction progress was monitored by ^{1}H NMR. Once full conversion of the starting material was observed, the solvent was evaporated and the products were extracted into hexane. The yield was calculated after evaporation of the solvent or purification of the product(s) by flash chromatography. The products **13a-c, 15**, **17a,b** and **19a,b** were identified according to the literature.[9-12]

2.2. Cycloisomerization of o-ethynyl biaryl substrates

Loading: **2-Ethynyl-1,1'-binaphthalene** (70 mg, 0.2 mmol), catalyst (14 mg, 5 mol%) in DCE (5 mL). Conversion: 100%, yield(%) of **9:10** = 92% (100:0).

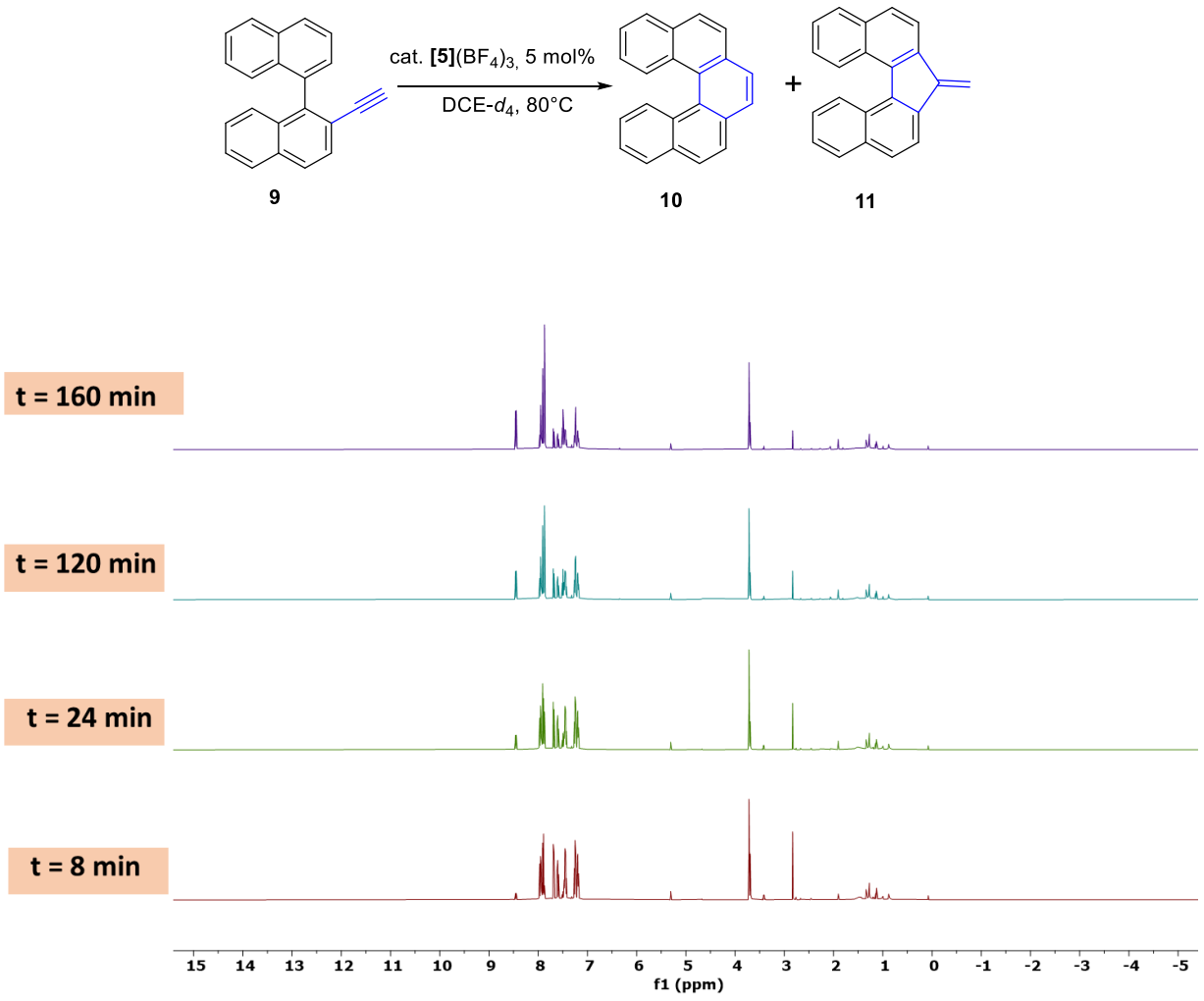

Figure S47. ^{1}H NMR spectra collected during cycloisomerization of alkyne **9**.

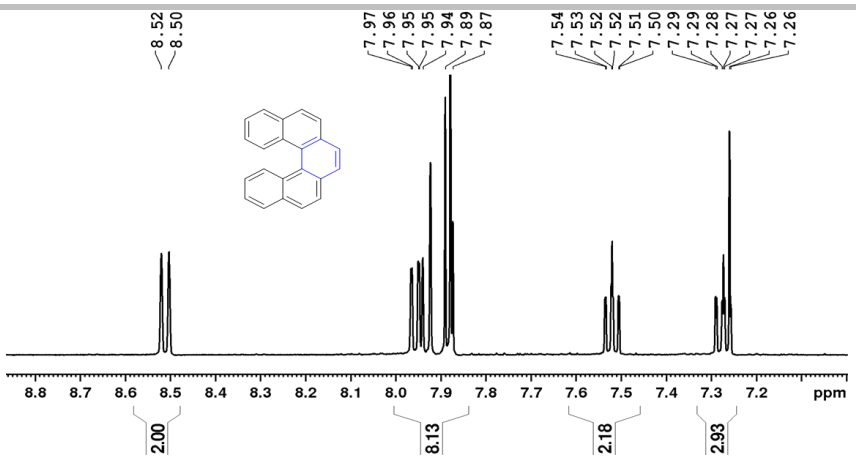

Figure S48. ^{1}H NMR of pure pentahelicene **10** in $CDCl_3$.

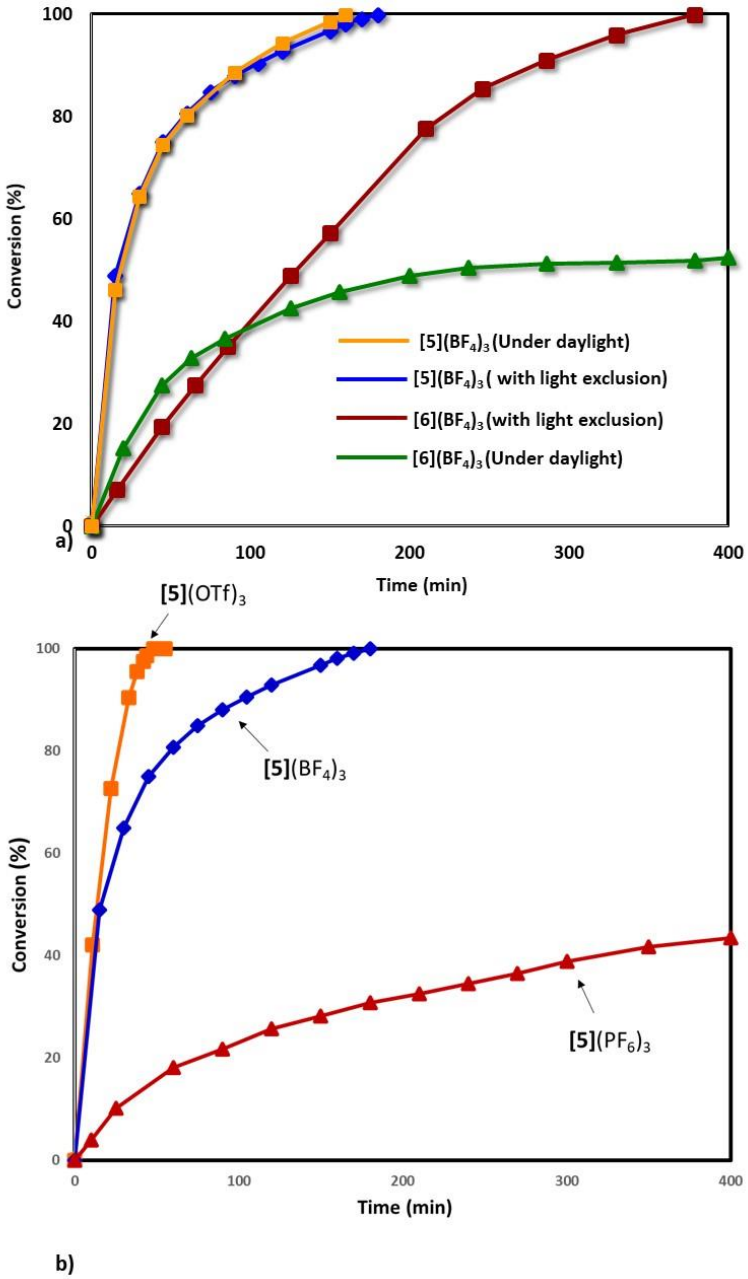

Figure S49. Influence of ambient daylight (**a**) and counter anion effect (**b**) on Pt-catalyzed cycloisomerization of **9**. Conditions: Pt catalyst (5 mol %), **9** (0.05 M), DCE, 80°C.

Loading: **2-ethynyl-1-(2,3,4-trimethoxyphenyl)naphthalene** (70 mg, 0.22 mmol), catalyst (14 mg, 5 mol%) in DCE (5 mL). Conversion: 100%, yield(%) of **13a** = 92%

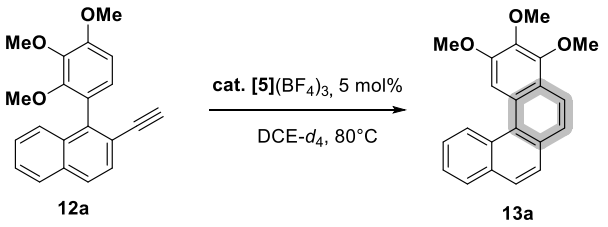

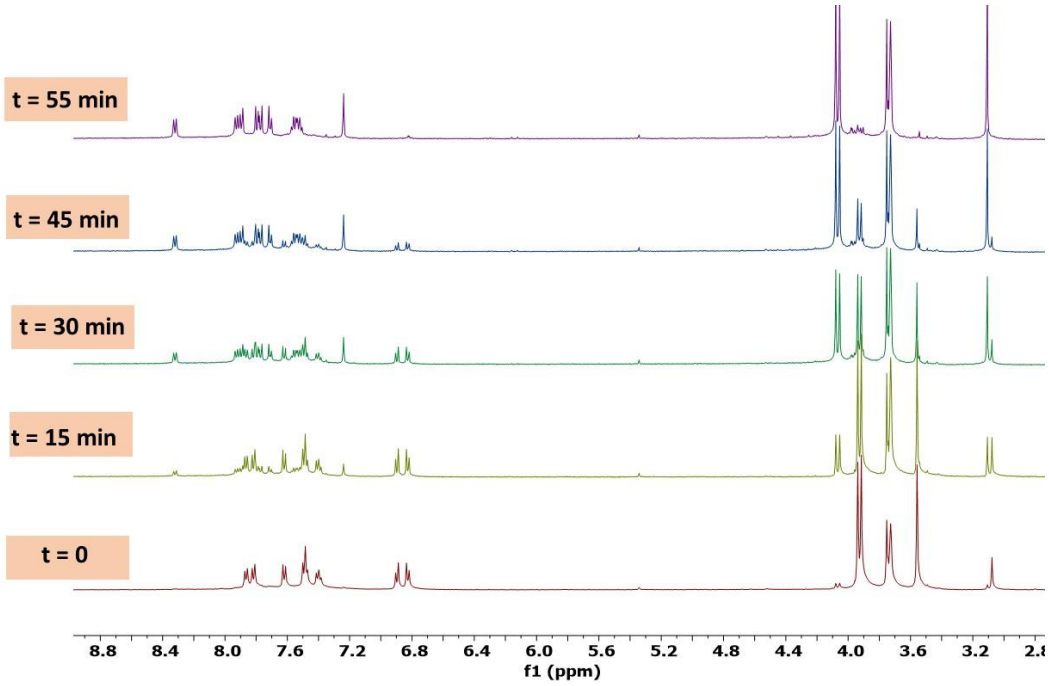

Figure S50. ^{1}H NMR spectra collected during cycloisomerization of alkyne **12a**.

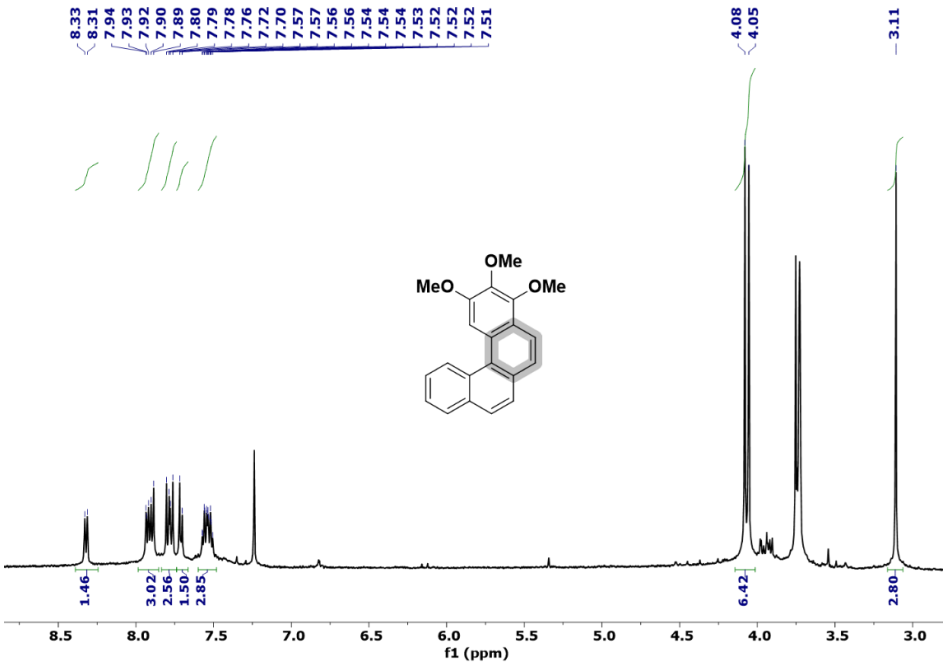

Figure S51. ^{1}H NMR of pure pentahelicene **13a** in $CDCl_3$.[9a]

Cycloisomerization of 2-(2-ethynylnaphthalen-1-yl)thiophene.

Loading: **2-(2-ethynylnaphthalen-1-yl)thiophene** (70 mg, 0.3 mmol), catalyst (19 mg, 5 mol%) in DCE (5 mL). Conversion: 100%, yield(%) of **13b** = 82%

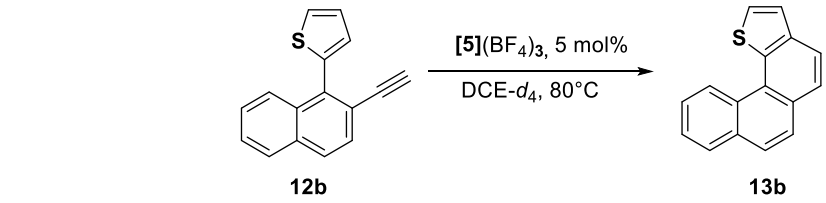

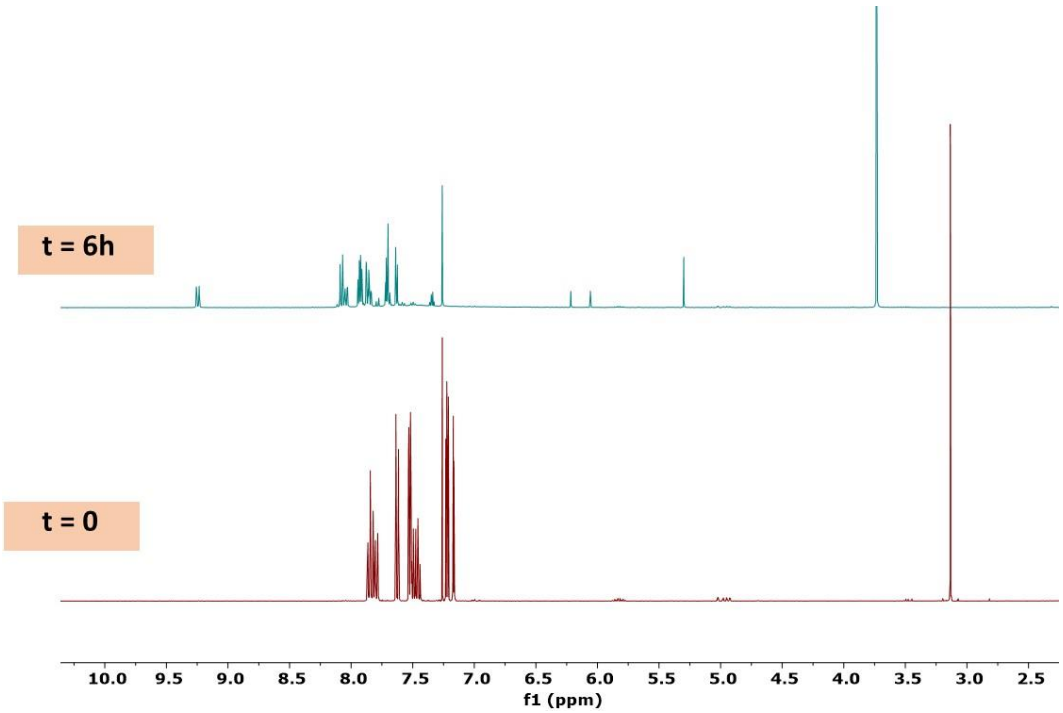

Figure S52. ^{1}H NMR spectra collected during cycloisomerization of alkyne **12b**.

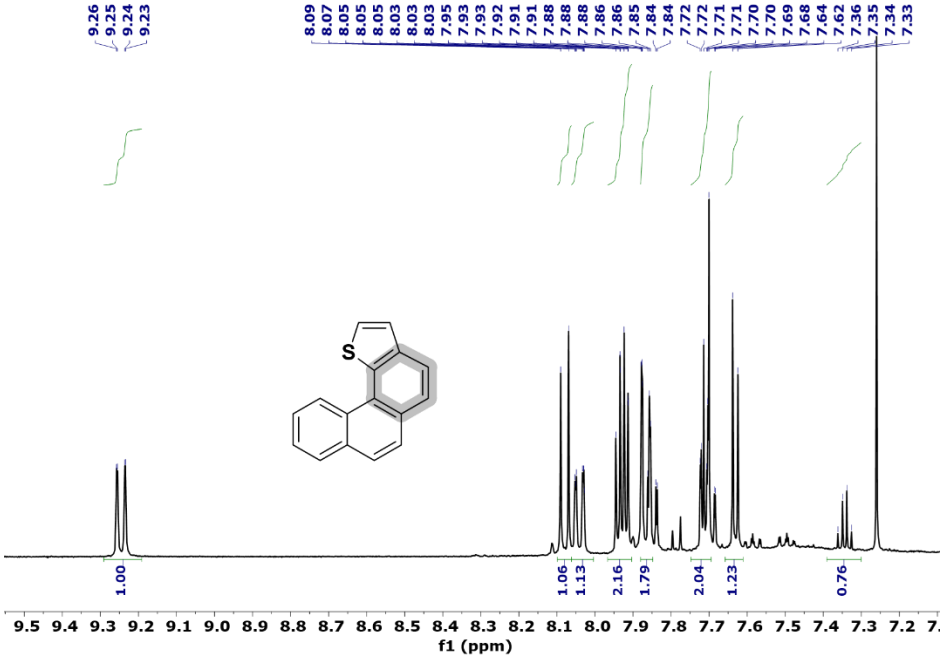

Figure S53. ^{1}H NMR of helicene **13b** in $CDCl_3$.[9b]

Loading: **2-ethynyl-1-(4-fluorophenyl)naphthalene** (70 mg, 0.28 mmol), catalyst (18 mg, 5 mol%) in DCE (5 mL). Conversion: 40%, of **13c**

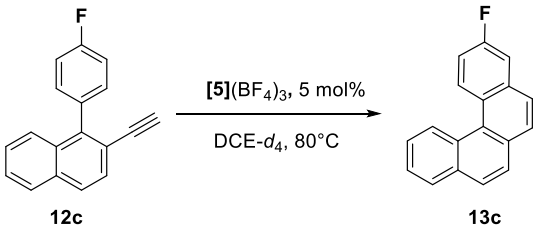

12c **13c**

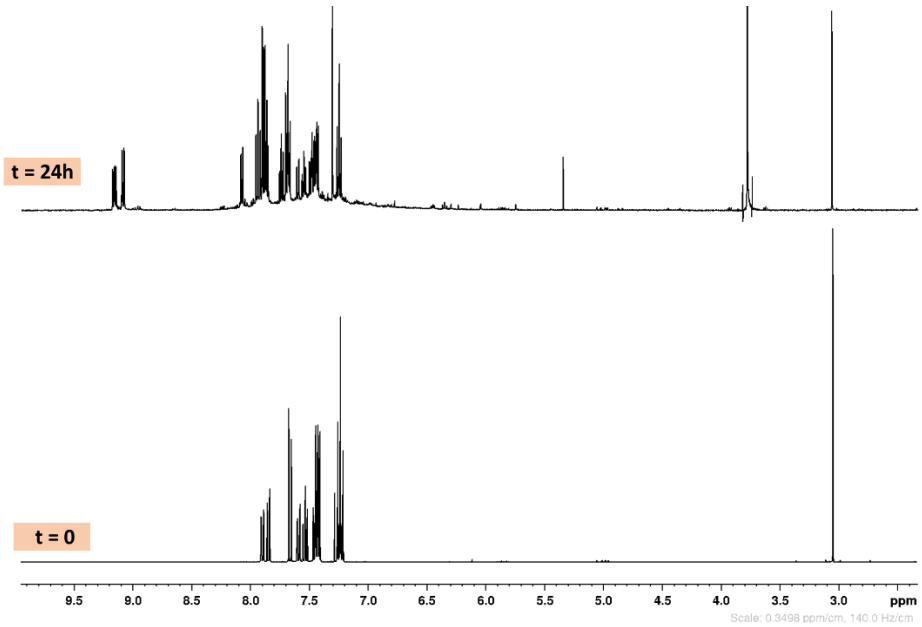

Figure S54. ^{1}H NMR spectra collected during cycloisomerization of alkyne **12c**.

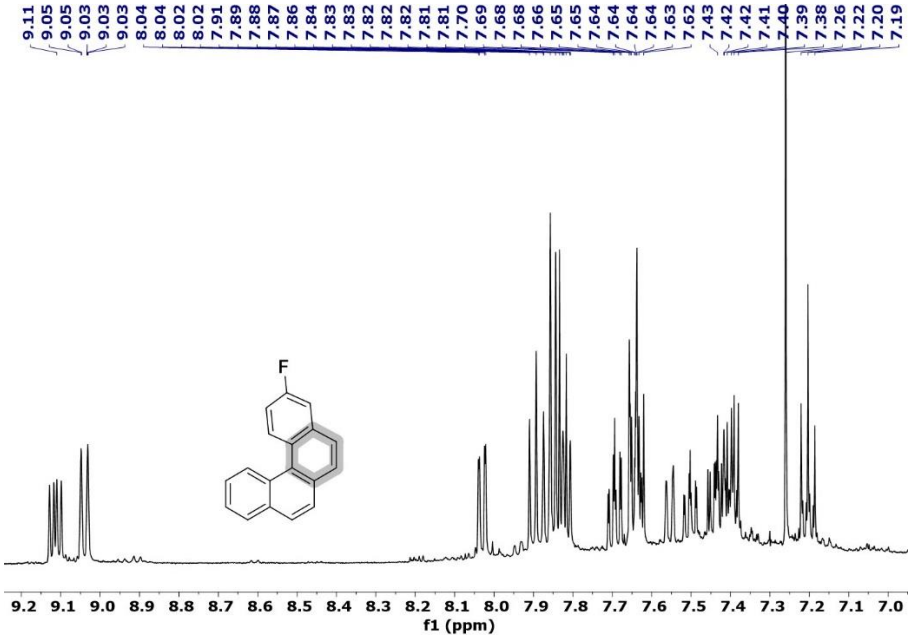

Figure S55. Mixture ^{1}H NMR of helicene **13c** in $CDCl_3$.[9a]

2.1. Cycloisomerization of enyne substrates

Loading: **dimethyl 2-(but-3-en-1-yl)-2-(prop-2-yn-1-yl)malonate** (70 mg, 0.31 mmol), catalyst (20 mg, 5 mol%) in DCE (5 mL). Conversion: 100%, yield(%) of **15** = 92%

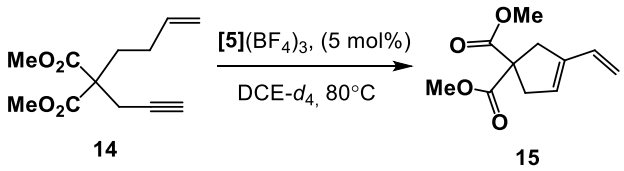

14 15

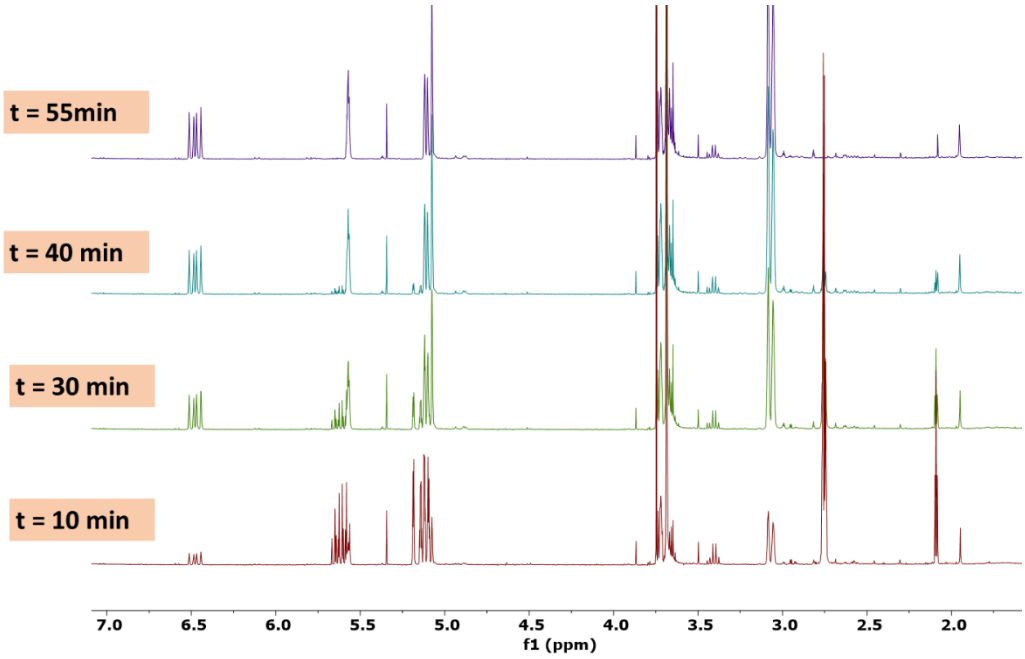

Figure S56. ^{1}H NMR spectra collected during cycloisomerization of enyne **14**.

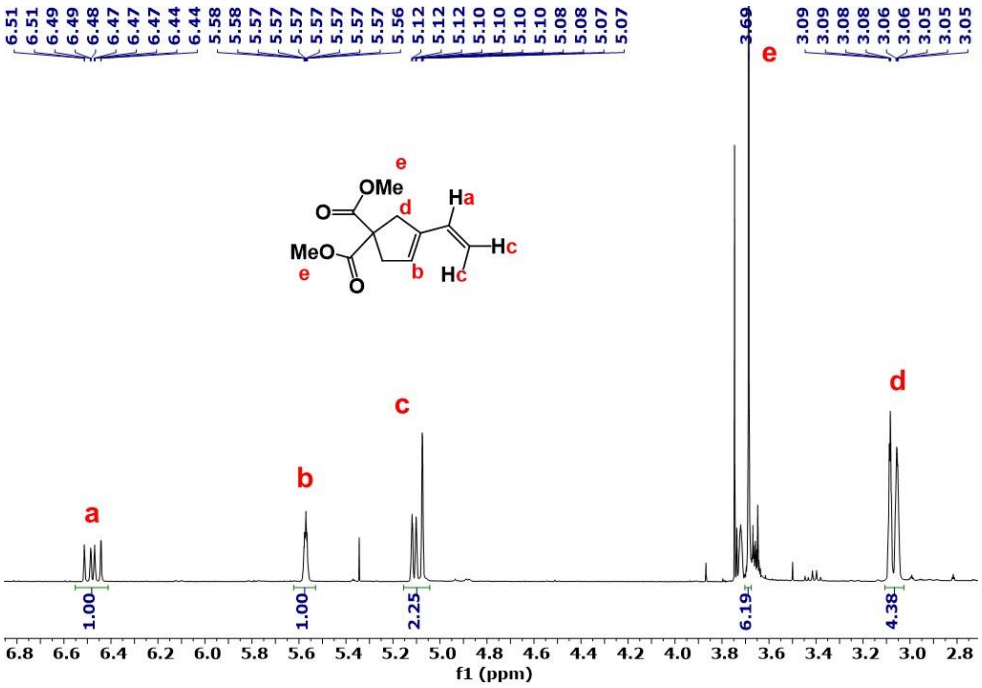

Figure S57. ^{1}H NMR of compound **15** in $CDCl_3$.[10]

Loading: **4-methyl-N-(2-methylallyl)-N-(prop-2-yn-1-yl)benzenesulfonamide** (70 mg, 0.26 mmol), catalyst (18 mg, 5 mol%) in DCE (5 mL). Conversion: 100%, yield(%) of **17a:17b** = 44:56

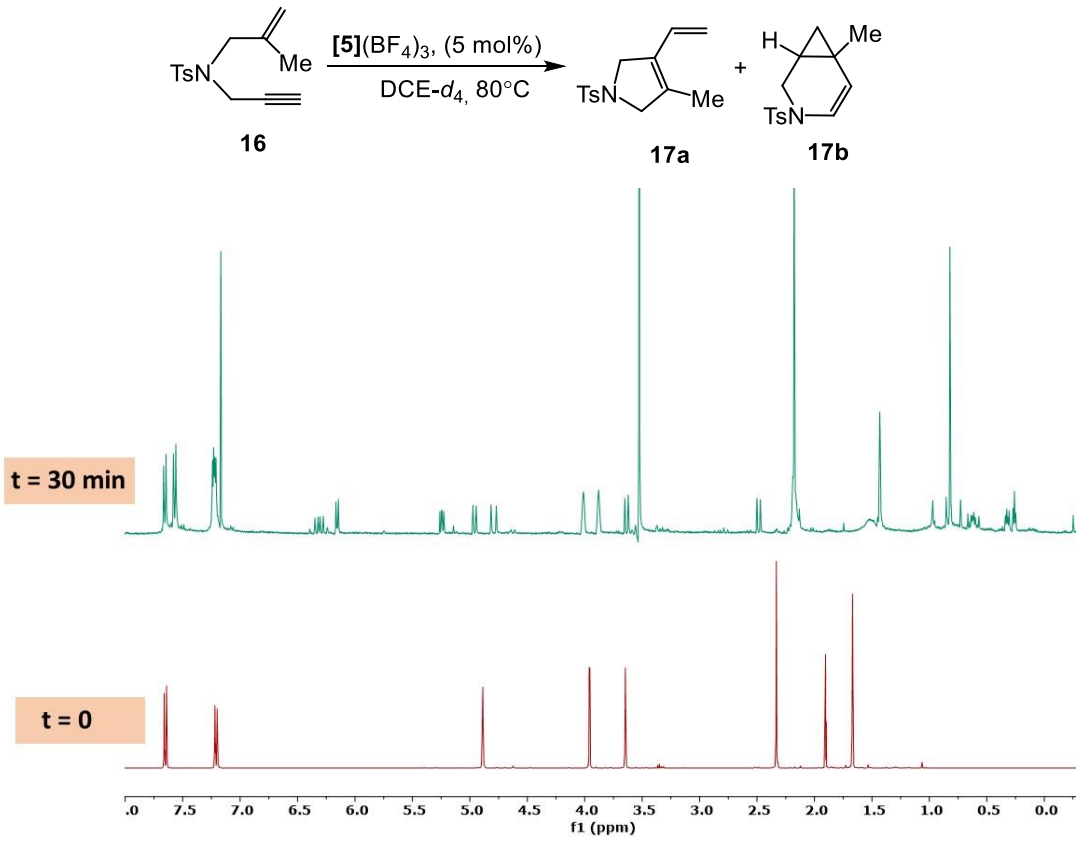

Figure S58. ^{1}H NMR spectra collected during cycloisomerization of enyne **16**.

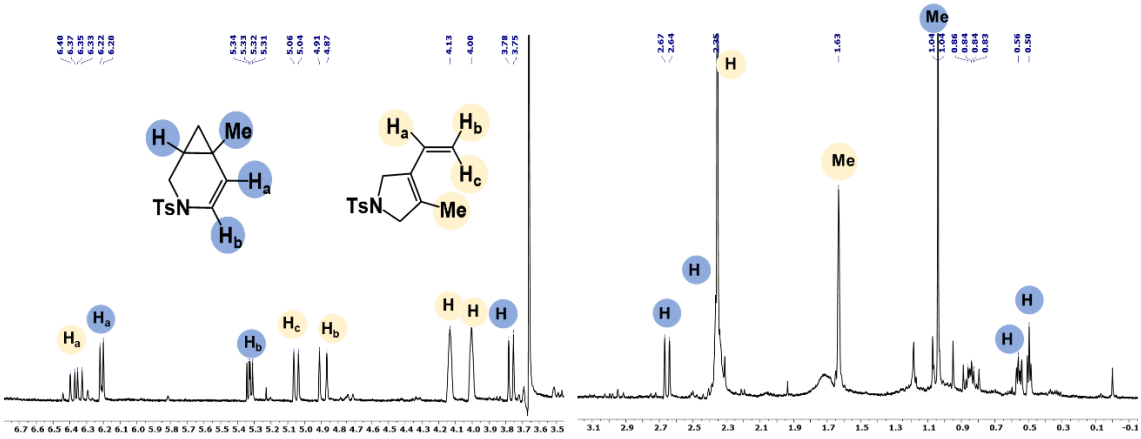

Figure S59. ^{1}H NMR of mixture of compounds **17a** and **17b** in $CDCl_3$.[11]

Loading: **4-4-methyl-N-(3-methylbut-2-en-1-yl)-N-(prop-2-yn-1-yl)benzenesulfonamide** (70 mg, 0.25 mmol), catalyst (18 mg, 5 mol%) in DCE (5 mL). Conversion: 100%, yield(%) of **19a:19b** = 76:24

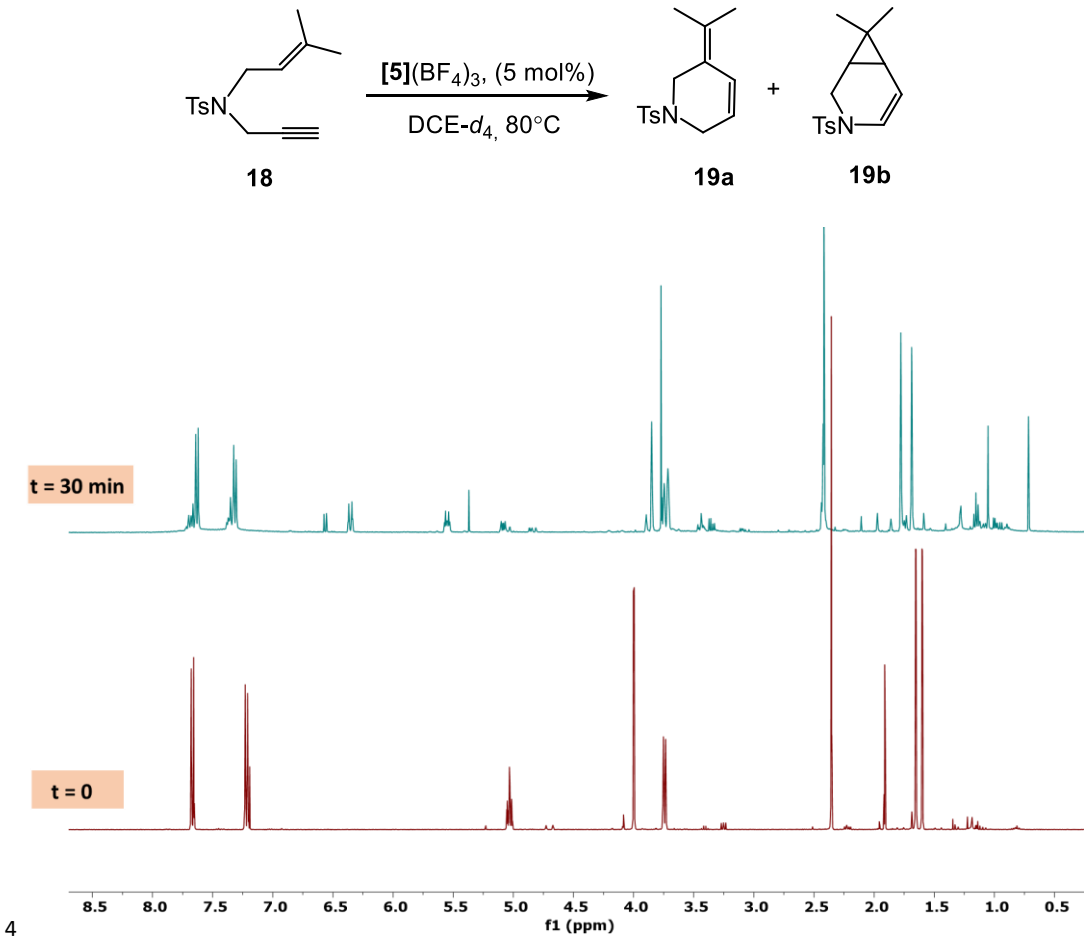

4

Figure S60. ^{1}H NMR spectra collected during cycloisomerization of enyne **18**.

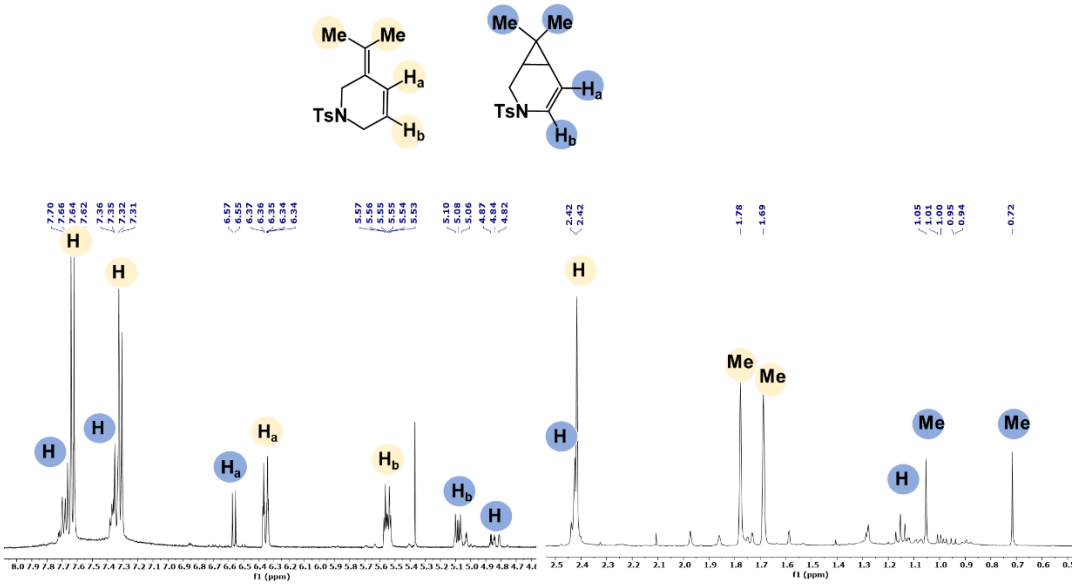

Figure S61. ^{1}H NMR of mixture of compounds **19a** and **19b** in $CDCl_3$.[12]

3. Crystallography

3.1. General crystallographic and refinement details.

Single-crystal X-ray diffraction data collections were performed using Rigaku goniometer diffractometer with graphite mono-chromated Mo Kα radiation (λ = 0.71073 Å). The diffraction intensity details were extracted from the diffraction frames using CrysAlisPro XtalLAB Synergy-S system (version 41.112a) program. The structures were then solved by SHELXT-9740 available in Olex2 crystallographic suite, which located most of the non-hydrogen atoms. Subsequently, least-squares refinements were carried out on F^2 using SHELXL-Version 2018/3 to locate the remaining non-hydrogen atoms. Non-hydrogen atoms were refined with anisotropic displacement parameters. Hydrogen atoms attached to carbon atoms were fixed in calculated positions. All disorders were handled with SADI, SIMU, EADP, SAME and RIGU constraints and restraints. The crystallographic parameters of each structure are given bellow. All structures are deposited to CCDC and their corresponding deposition numbers are listed below:

CCDC: [4](OTf) = 2416301

3.2. Crystallographic parameters.

Table 1. Crystal data and structure refinement for **[4]**(OTf)

Empirical formula	$C_{56.5}H_{49}F_3O_4P_2S_2$
Formula weight	975.01
Temperature/K	200.0(1)
Crystal system	triclinic
Space group	P-1
a/Å	10.0296(3)
b/Å	12.2752(3)
c/Å	22.7212(6)
α/°	80.179(2)
β/°	80.228(2)
γ/°	67.613(3)
Volume/Å^3	2531.68(13)
Z	2
ρ_{calc}g/cm^3	1.279
μ/mm^{-1}	0.225
F(000)	1018.0
Crystal size/mm^3	0.287 × 0.132 × 0.039
Radiation	Mo Kα (λ = 0.71073)
2Θ range for data collection/°	4.422 to 62.034
Index ranges	-14 ≤ h ≤ 12, -17 ≤ k ≤ 17, -32 ≤ l ≤ 30
Reflections collected	34010
Independent reflections	12574 [R_{int} = 0.0360, R_{sigma} = 0.0426]
Data/restraints/parameters	12574/136/678
Goodness-of-fit on F^2	1.038
Final R indexes [I>=2σ (I)]	R_1 = 0.0472, wR_2 = 0.1240
Final R indexes [all data]	R_1 = 0.0657, wR_2 = 0.1322
Largest diff. peak/hole / e Å^{-3}	0.40/-0.33

4. Computational details

4.1. General information

All the molecular structures reported in this study were optimized with the ωB97X-D[13] functional and def2TZVP basis set[14] with the Gaussian-16 program.[15] For Pt atom the dev2TZVP effective core potential and corresponding basis set were used. Frequency calculations were performed on the optimized geometries to confirm that they are local minimum in the potential energy surface. The Natural Bond Order (NBO) were performed on the optimized structures using NBO-5.0 program as it is implemented in QChem-6.02 program.[16] The absolutely localized molecular orbital – energy decomposition analysis (ALMO-EDA)[17] were performed using the QChem-6.02 program with ωB97X-D3[18] functional and def2TZVP basis set. Deformation density plots were visualized using IQmol 3.0 program.[19] XYZ coordinates of optimized structures are given as a separate file.

4.2. Computational data

Table S2. Comparison between the optimized geometries of model complexes **[5*]**$^{3+}$ and **[6*]**$^{3+}$.

	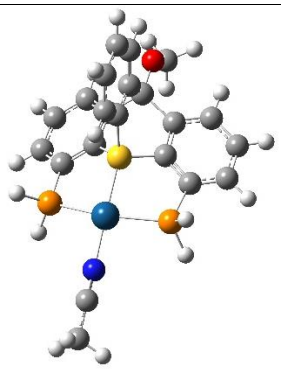 **[5*]**$^{3+}$	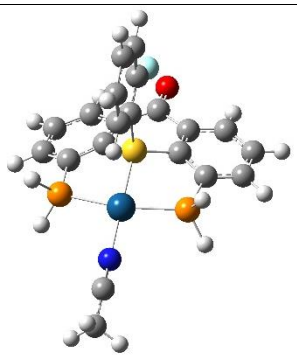 **[6*]**$^{3+}$ (XRD values for complex **[6]**$(BF_4)_3$ are given in brackets)
Bond lengths (Å)		
S-Pt	2.213	2.221 (2.163)[a]
N-Pt	2.006	2.010 (2.020)[a]
P-Pt (av.)	2.377	2.371 (2.346)[a]
Bond angles (°)		
S-Pt-N	176.43	177.72 (178.05)[a]
P-Pt-P	156.74	163.56 (165.49)[a]
S-Pt-P (av.)	83.89	83.00 (83.27)[a]
N-Pt-P (av.)	95.48	96.82 (98.67)[a]

[a] Previously reported computational and experimental data, see ref. S1.

Table S3. Computational data for the model Pt(MeCN) complexes of sulfonium ligands **L1**, **L2**, and **L3**.

		1-st generation sulfonium ligand (**L1**)	2-nd generation sulfonium ligand (**L2**)	3-rd generation sulfonium ligand (**L3**)
		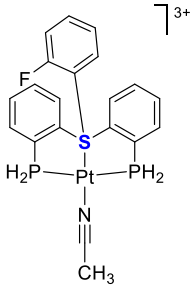	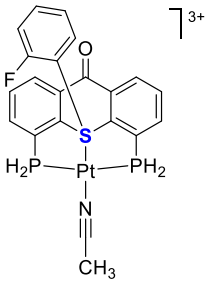	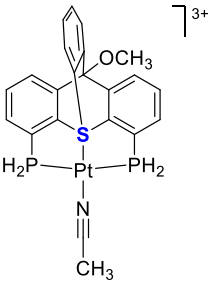
		[7*]$^{3+}$	**[6*]**$^{3+}$	**[5*]**$^{3+}$
NBO calculations				
Wiberg bond indices for the Pt-E[a] bond		0.500	0.520[b]	0.519
NPA charges	Pt	+0.395	+0.407[b]	+0.421
	E[a]	+1.053	+1.110[b]	+1.069
Bonding NLMO composition	Pt (%)	19.9	20.7[b]	16.0
	E (%)[a]	75.5	74.5[b]	77.3
EDA NOCV calculations				
Major Pt-E[a] interactions (kcal/mol)	$\sigma_{L\rightarrow M}$	-86.35	-89.06[b]	-84.53
	$\pi_{M\rightarrow L}$ ($\pi\parallel$+ $\pi\perp$)	-35.48	-36.10[b]	-39.92

[a]E = S or C [b]Previously reported data, see ref. S1.

Table S4: Eigenvalues and orbital energies of the first 20 NOCV pairs obtained from ALMO-EDA calculations for model complexes **[5*]$^{3+}$** and **[7*]$^{3+}$**. NOCV pairs attributed to $\sigma_{L\rightarrow M}$, $\pi\|_{M\rightarrow L}$, and $\pi\perp_{M\rightarrow L}$ interactions are highlighted in grey.

Complex **[5*]$^{3+}$**				Complex **[7*]$^{3+}$**			
$\Delta\rho_n$	**NOCV pair**	**Eigenvalue** ($\|v_n\|$ in *e*)	**ΔE_{orb}** (kcal/mol)	**$\Delta\rho_n$**	**NOCV pair**	**Eigenvalue** ($\|v_n\|$ in *e*)	**ΔE_{orb}** (kcal/mol)
$\Delta\rho_1$	1->1015	1.343	-187.49	**$\Delta\rho_1$**	1->947	1.341	-193.73
$\Delta\rho_2$: $\sigma_{L\rightarrow M}$	2->1014	0.478	-84.45	**$\Delta\rho_2$: $\sigma_{L\rightarrow M}$**	2->946	0.473	-86.27
$\Delta\rho_3$	3->1013	0.385	-22.38	**$\Delta\rho_3$**	3->945	0.387	-24.09
$\Delta\rho_4$: $\pi\perp_{M\rightarrow L}$	4->1012	0.345	-19.63	**$\Delta\rho_4$: $\pi\|_{M\rightarrow L}$**	4->944	0.339	-20.35
$\Delta\rho_5$: $\pi\|_{M\rightarrow L}$	5->1011	0.342	-20.26	**$\Delta\rho_5$: $\pi\perp_{M\rightarrow L}$**	5->943	0.321	-15.10
$\Delta\rho_6$	6->1010	0.281	-12.51	**$\Delta\rho_6$**	6->942	0.287	-11.55
$\Delta\rho_7$	7->1009	0.244	-19.06	**$\Delta\rho_7$**	7->941	0.255	-22.98
$\Delta\rho_8$	8->1008	0.145	-3.56	**$\Delta\rho_8$**	8->940	0.147	-3.66
$\Delta\rho_9$	9->1007	0.142	-3.65	**$\Delta\rho_9$**	9->939	0.141	-3.88
$\Delta\rho_{10}$	10->1006	0.129	-4.72	**$\Delta\rho_{10}$**	10->938	0.133	-3.62
$\Delta\rho_{11}$	11->1005	0.126	-3.17	**$\Delta\rho_{11}$**	11->937	0.124	-4.72
$\Delta\rho_{12}$	12->1004	0.111	-3.89	**$\Delta\rho_{12}$**	12->936	0.112	-3.78
$\Delta\rho_{13}$	13->1003	0.105	-3.65	**$\Delta\rho_{13}$**	13->935	0.102	-2.91
$\Delta\rho_{14}$	14->1002	0.101	-2.79	**$\Delta\rho_{14}$**	14->934	0.102	-2.98
$\Delta\rho_{15}$	15->1001	0.095	-1.12	**$\Delta\rho_{15}$**	15->933	0.098	-2.03
$\Delta\rho_{16}$	16->1000	0.094	-2.46	**$\Delta\rho_{16}$**	16->932	0.095	-1.13
$\Delta\rho_{17}$	17->999	0.093	-2.06	**$\Delta\rho_{17}$**	17->931	0.091	-1.13
$\Delta\rho_{18}$	18->998	0.088	-0.81	**$\Delta\rho_{18}$**	18->930	0.087	-1.68
$\Delta\rho_{19}$	19->997	0.077	-1.32	**$\Delta\rho_{19}$**	19->929	0.083	-2.06
$\Delta\rho_{20}$	20->996	0.065	-0.82	**$\Delta\rho_{20}$**	20->928	0.063	-1.12

Table S5. Selected EDA-NOCV deformation density plots ($\Delta\rho_{1\text{-}10}$) for model complexes **[5*]$^{3+}$** and **[7*]$^{3+}$** (charge depletion and accumulation areas are colored in red and blue, respectively). Plots attributed to $\sigma_{L\rightarrow M}$, $\pi\|_{M\rightarrow L}$, and $\pi\perp_{M\rightarrow L}$ interactions are highlighted in grey.

Model complex	Δρ (iso-values are given in bracket)				
[5*]$^{3+}$	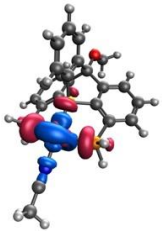 **$\Delta\rho_1$** (0.005)	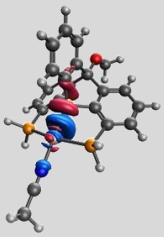 **$\Delta\rho_2$: $\sigma_{L\rightarrow M}$** (0.004)	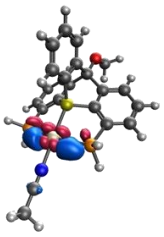 **$\Delta\rho_3$** (0.003)	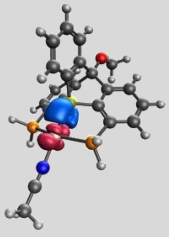 **$\Delta\rho_4$: $\pi\perp_{M\rightarrow L}$** (0.003)	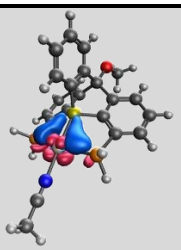 **$\Delta\rho_5$: $\pi\|_{M\rightarrow L}$** (0.003)
	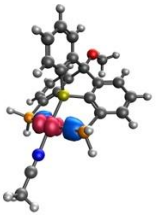 **$\Delta\rho_6$** (0.002)	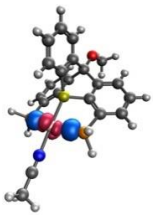 **$\Delta\rho_7$** (0.002)	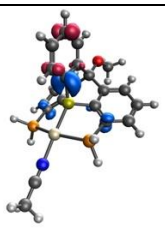 **$\Delta\rho_8$** (0.001)	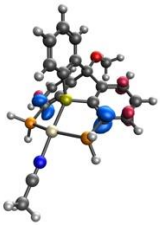 **$\Delta\rho_9$** (0.001)	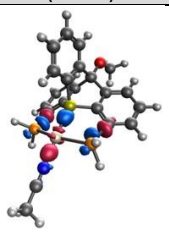 **$\Delta\rho_{10}$** (0.001)
[7*]$^{3+}$	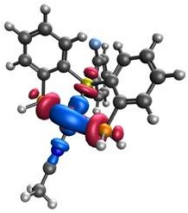 **$\Delta\rho_1$** (0.005)	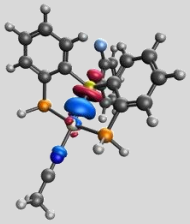 **$\Delta\rho_2$: $\sigma_{L\rightarrow M}$** (0.005)	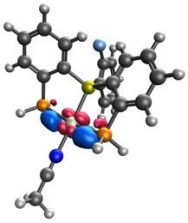 **$\Delta\rho_3$** (0.004)	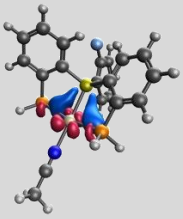 **$\Delta\rho_4$: $\pi\|_{M\rightarrow}$** (0.003)	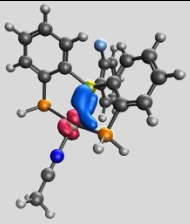 **$\Delta\rho_5$: $\pi\perp_{M\rightarrow L}$** (0.003)
	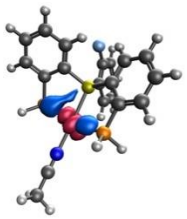 **$\Delta\rho_6$** (0.002)	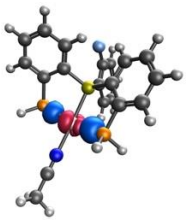 **$\Delta\rho_7$** (0.002)	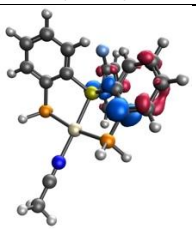 **$\Delta\rho_8$** (0.001)	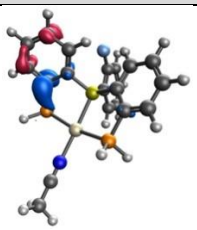 **$\Delta\rho_9$** (0.001)	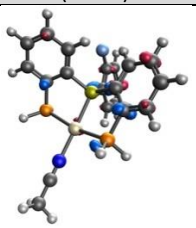 **$\Delta\rho_{10}$** (0.001)

5. References

1. R. Li, M. Zafar, D. Danovich, V. Subramaniyan, F. Tibika and Y. Tulchinsky, *Angew. Chem. Int. Ed.*, 2024, **136**, e202314997.
2. M. P. J. Carreras, W. Thiel and M. Alcarazo, *J. Am. Chem. Soc.*, 2012, **40**, 16753.
3. J. Carreras, G. Gopakumar, L. Gu, A. Gimeno, P. Linowski, J. Petuskova, W. Thiel and M. Alcarazo, *J. Am. Chem. Soc.*, 2013, **135**, 18815-1.
4. M. T. Payne, C. N. Neumann, E. Stavitski and M. Dincă, *Inorg. Chem.* , 2021, **60**, 11764.
5. W. Ji, S. Jing, Z. Liu, J. Shen, J. Ma, D. Zhu, D. Cao, L. Zheng and M. Yao, *Inorg. Chem.*, 2013, **52**, 5786.
6. V. Vallejos González, J. Kahle, C. Hüßler, R. Heckershoff, A. S. K. Hashmi, B. Birenheide, A. Hauser and J. Podlech, *Eur. J. Org. Chem.*, 2023, **26**, e202300545.
7. M. C. Blanco Jaimes, F. Rominger, M. M. Pereira, R. M. B. Carrilho, S. A. C. Carabineiro and A. S. K. Hashmi, *Chem. Commun.*, 2014, **50**, 4937.
8. Y. Qi, L. T. Jesikiewicz, G. E. Scofield, P. Liu and K. M. Brummond, *ACS Catal.*, 2024, **14**, 17065.
9. (a)) J. Carreras, G. Gopakumar, L. Gu, A. Gimeno, P. Linowski, J. Petuskova, W. Thiel and M. Alcarazo, J. Am. Chem. Soc., 2013, 135, 18815-18823; (b) Y. Lu, Y. Qiao, H. Xue and G. Zhou, J. Org. Chem., 2018, 20, 6632-6635.
10. (a) H. Y. D. You, S. Sen and and F. P. Gabbaï, J. Am. Chem. Soc., 2018, 140, 9644–9651; (b) F. Inagaki, C. Matsumoto, Y. Okada, N. Maruyama and C. Mukai, Angew. Chem. Int. Ed., 2015, 54, 818-822.
11. (a) A. Cervantes-Reyes, F. Rominger, M. Rudolph and A. S. K. Hashmi, Adv. Synth. Catal., 2020, 362, 2523-2533; (b) T. Ozawa, T. Kurahashi and S. Matsubara, Org. Lett., 2012, 14, 3008-3011.
12. K. Muratov and F. Gagosz, Angew. Chem. Int. Ed., 2022, 61, e202203452.
13. J.-D. Chai, M. Head-Gordon, *Phys. Chem. Chem. Phys*. 2008, **10**, 6615**.**
14. F. Weigend, *Phys. Chem. Chem. Phys.*, 2006, **8**, 1057.
15. Gaussian 16, Revision B.01, M. J. Frisch, G. W. Trucks, H. B. Schlegel, G. E. Scuseria, M. A. Robb, J. R. Cheeseman, G. Scalmani, V. Barone, G. A. Petersson, H. Nakatsuji, X. Li, M. Caricato, A. V. Marenich, J. Bloino, B. G. Janesko, R. Gomperts, B. Mennucci, H. P. Hratchian, J. V. Ortiz, A. F. Izmaylov, J. L. Sonnenberg, D. Williams-Young, F. Ding, F. Lipparini, F. Egidi, J. Goings, B. Peng, A. Petrone, T. Henderson, D. Ranasinghe, V. G. Zakrzewski, J. Gao, N. Rega, G. Zheng, W. Liang, M. Hada, M. Ehara, K. Toyota, R. Fukuda, J. Hasegawa, M. Ishida, T. Nakajima, Y. Honda, O. Kitao, H. Nakai, T. Vreven, K. Throssell, J. A., Jr. Montgomery, J. E. Peralta, F. Ogliaro, M. J. Bearpark, J. J. Heyd, E. N. Brothers, K. N. Kudin, V. N. Staroverov, T. A. Keith, R. Kobayashi, J. Normand, K. Raghavachari, A. P. Rendell, J. C. Burant, S. S. Iyengar, J. Tomasi, M. Cossi, J. M. Millam, M. Klene, C. Adamo, R. Cammi, J. W. Ochterski, R. L. Martin, K. Morokuma, O. Farkas, J. B. Foresman, D. J. Fox, Gaussian, Inc., Wallingford CT, 2016.
16. E. Epifanovsky, A. T. B. Gilbert, X. Feng, J. Lee, Y. Mao, N. Mardirossian, P. Pokhilko, A. F. White, M. P. Coons, A. L. Dempwolff, Z. Gan, D. Hait, P. R. Horn, L. D. Jacobson, I. Kaliman, J. Kussmann, A. W. Lange, K. U. Lao, D. S. Levine, J. Liu, S. C. McKenzie, A. F. Morrison, K. D. Nanda, F. Plasser, D. R. Rehn, M. L. Vidal, Z-Q. You, Y. Zhu, B. Alam, B. J. Albrecht, A. Aldossary, E. Alguire, J. H. Andersen, V. Athavale, D. Barton, K. Begam, A. Behn, N. Bellonzi, Y. A. Bernard, E. J. Berquist, H. G. A. Burton, A.l Carreras, Kevin Carter-Fenk, Romit Chakraborty, Alan D. Chien, Kristina D. Closser, Vale Cofer-Shabica, Saswata Dasgupta, Marc de Wergifosse, Jia Deng, Michael Diedenhofen, Hainam Do, Sebastian Ehlert, Po-Tung Fang, Shervin Fatehi, Qingguo Feng, Triet Friedhoff, James Gayvert, Qinghui Ge, Gergely Gidofalvi, Matthew Goldey, Joe Gomes, Cristina E. González-Espinoza, Sahil Gulania, Anastasia O. Gunina, Magnus W. D. Hanson-Heine, Phillip H. P. Harbach, Andreas Hauser, Michael F. Herbst, Mario Hernández Vera, Manuel Hodecker, Zachary C. Holden, Shannon Houck, Xunkun Huang, Kerwin Hui, Bang C. Huynh, Maxim Ivanov, Ádám Jász, Hyunjun Ji, Hanjie Jiang, Benjamin Kaduk, Sven Kähler, Kirill Khistyaev, Jaehoon Kim, Gergely Kis, Phil Klunzinger, Zsuzsanna Koczor-Benda, Joong Hoon Koh, Dimitri Kosenkov, Laura Koulias, Tim Kowalczyk, Caroline M. Krauter, Karl Kue, Alexander Kunitsa, Thomas Kus, István Ladjánszki, Arie Landau, Keith V. Lawler, Daniel Lefrancois, Susi Lehtola, Run R. Li, Yi-Pei Li, Jiashu Liang, Marcus Liebenthal, Hung-Hsuan Lin, You-Sheng Lin, Fenglai Liu, Kuan-Yu Liu, Matthias Loipersberger, Arne Luenser, Aaditya Manjanath, Prashant Manohar, Erum Mansoor, Sam F. Manzer, Shan-Ping Mao, Aleksandr V. Marenich, Thomas Markovich, Stephen Mason, Simon A. Maurer, Peter F. McLaughlin, Maximilian F. S. J. Menger, Jan-Michael Mewes, Stefanie A. Mewes, Pierpaolo Morgante, J. Wayne Mullinax, Katherine J. Oosterbaan, Garrette Paran, Alexander C. Paul, Suranjan K. Paul, Fabijan Pavoševi´c, Zheng Pei, Stefan Prager, Emil I. Proynov, Ádám Rák, Eloy Ramos-Cordoba, Bhaskar Rana, Alan E. Rask, Adam Rettig, Ryan M. Richard, Fazle Rob, Elliot Rossomme, Tarek Scheele, Maximilian Scheurer, Matthias Schneider, Nickolai Sergueev, Shaama M. Sharada, Wojciech Skomorowski, David W. Small, Christopher J. Stein, Yu-Chuan Su, Eric J. Sundstrom, Zhen Tao, Jonathan Thirman, Gábor J. Tornai, Takashi Tsuchimochi, Norm M. Tubman, Srimukh Prasad Veccham, Oleg Vydrov, Jan Wenzel, Jon Witte, Atsushi Yamada, Kun Yao, Sina Yeganeh, Shane R. Yost, Alexander Zech, Igor Ying Zhang, Xing Zhang, Yu Zhang, Dmitry Zuev, Alán Aspuru-Guzik, Alexis T. Bell, Nicholas A. Besley, Ksenia B. Bravaya, Bernard R. Brooks, David Casanova, Jeng-Da Chai, Sonia Coriani, Christopher J. Cramer, György Cserey, A. Eugene DePrince III, Robert A. DiStasio Jr., Andreas Dreuw, Barry D. Dunietz, Thomas R. Furlani, William A. Goddard III, Sharon Hammes-Schiffer, Teresa Head-Gordon, Warren J. Hehre, Chao- Ping Hsu, Thomas-C. Jagau, Yousung Jung, Andreas Klamt, Jing Kong, Daniel S. Lambrecht, WanZhen Liang, Nicholas J. Mayhall, C. William McCurdy, Jeffrey B. Neaton, Christian Ochsenfeld, John A. Parkhill, Roberto Peverati, Vitaly A. Rassolov, Yihan Shao, Lyudmila V. Slipchenko, Tim Stauch, Ryan P. Steele, Joseph E. Subotnik, Alex J. W. Thom, Alexandre Tkatchenko, Donald G. Truhlar, Troy Van Voorhis, Tomasz A. Wesolowski, K. Birgitta Whaley, H. Lee Woodcock III, Paul M. Zimmerman, Shirin Faraji, Peter M. W. Gill, Martin Head-Gordon, John M. Herbert, and Anna I. Krylov. *J. Chem. Phys.,* 2021, **155**, 084801.
17. a) P. R. Horn, M. J. Head-Gordon, *Chem. Phys.* 2015, **143**, 114111; b) P. R. Horn, Y. Mao, M. J. Head-Gordon, *J. Chem. Phys.* 2016, **144**, 114107; c) P. R. Horn, Y. Mao, M. Head-Gordon, *Phys. Chem. Chem. Phys.* 2016, **18,** 23067.
18. Y.-S. Lin, G.-D. Li, S.-P. Mao, J.-D. Chai. *J. Chem. Theory Comput.* 2013, **9**, 263.
19. A. Gilbert, IQmol, http://iqmol.org/